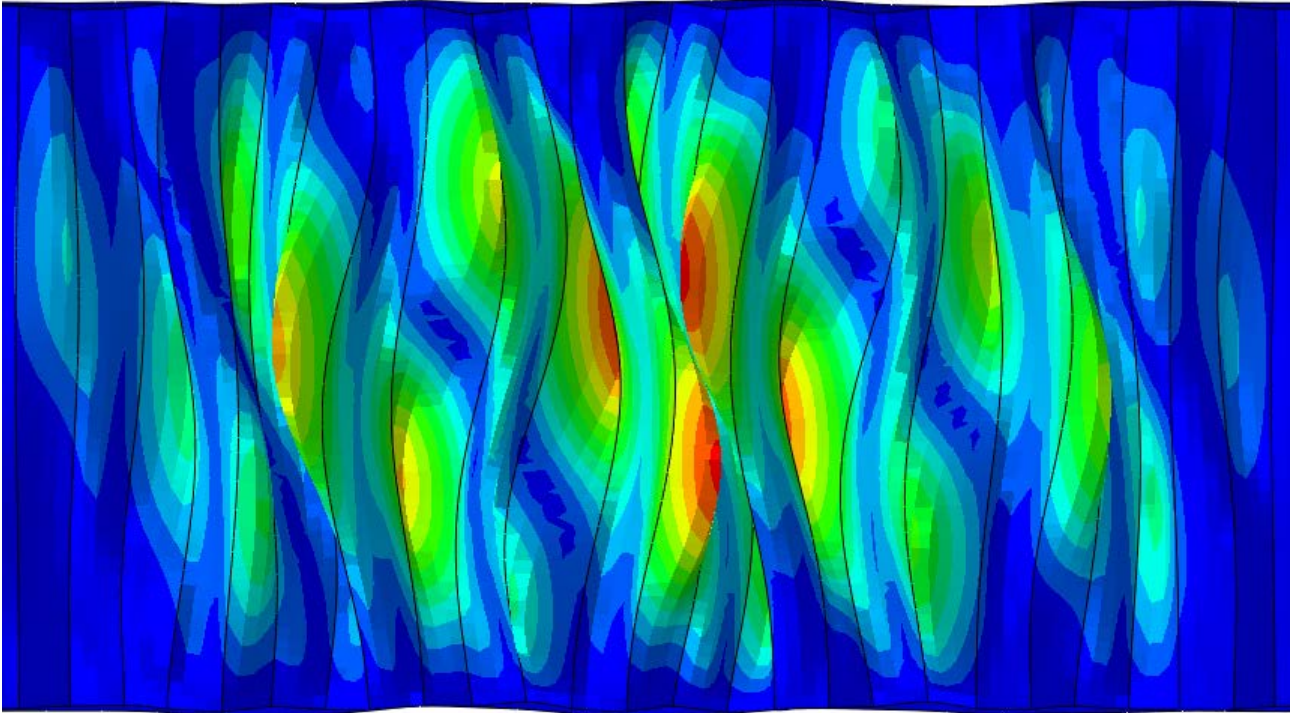




CHALMERS
UNIVERSITY OF TECHNOLOGY



Stainless Steel Bridge Girders with Corrugated Webs

Efficiency, stability and life-cycle cost analysis

Master's Thesis in the Master's Programme Structural Engineering and Building Technology

EMIL KARLSSON

Department of Architecture and Civil Engineering
Division of Structural Engineering
Lightweight Structures
CHALMERS UNIVERSITY OF TECHNOLOGY
Gothenburg, Sweden 2018
Master's Thesis ACEX30-18-27

MASTER'S THESIS ACEX30-18-27

Stainless Steel Bridge Girders with Corrugated Webs

Efficiency, stability and life-cycle cost analysis

Master's Thesis in the Master's Programme Structural Engineering and Building Technology

Emil Karlsson

Department of Architecture and Civil Engineering

Division of Structural Engineering

Lightweight structures

CHALMERS UNIVERSITY OF TECHNOLOGY

Gothenburg, Sweden 2018

Stainless Steel Bridge Girders with Corrugated Webs

Efficiency, stability and life-cycle cost analysis

Master's Thesis in the Master's Programme Structural Engineering and Building Technology

Emil Karlsson

© Emil Karlsson, 2018

Examensarbete ACEx30-18-27/ Institutionen för bygg- och miljöteknik,
Chalmers tekniska högskola 2018

Department of Architecture and Civil Engineering

Division of Structural Engineering

Lightweight structures

Chalmers University of Technology

SE-412 96 Göteborg

Sweden

Telephone: + 46 (0)31-772 1000

Cover:

Interactive buckling mode for a corrugated web, obtained from FE-simulations.

Department of Architecture and Civil Engineering

Gothenburg, Sweden, 2018

Stainless Steel Bridge Girders with Corrugated Webs

Efficiency, stability and life-cycle cost analysis

Master's thesis in the Master's Programme Structural Engineering and Building Technology

Emil Karlsson

Department of Architecture and Civil Engineering
Division of Structural Engineering and Building Technology
Lightweight Structures, Chalmers University of Technology

ABSTRACT

Steel bridge girders are susceptible to corrosion, a consequence of which is the need to maintenance, mainly in form of surveillance, repainting, and replacement, during their service life. The issues associated with corrosion could be significantly minimized by using stainless steel instead of the traditional carbon steel. Stainless steel, however, is more expensive and therefore effective material utilization is highly desirable. In this regard, beams with corrugated webs are highly advantageous as larger material utilization could generally be achieved. This is mainly due to the higher shear capacity of such beams, thanks to the corrugation out-of-plane stiffness, which allows for deeper girders. This technique combined with stainless steel material could lead to more competitive steel bridges considering the whole life-cycle costs.

The purpose of this master's thesis is to investigate the applicability and efficiency of bridge girders with corrugated webs made of stainless steel. This is achieved by performing case studies, life cycle cost analysis and extensive optimization and finite element (FE) simulations. Two case studies are performed where two existing road bridges are redesigned with corrugated webs and stainless steel. FE-simulations and analytical calculations are performed to confirm the results. In addition, the positive effects of stainless steel on the maintenance and operation costs are investigated through life cycle cost (LCC) analysis. Furthermore, parametrical optimization and implementation of stainless steel considering corrugated webs into new reduction factors are addressed in this study.

The results show that stainless steel girders with corrugated webs are not only competitive but in some cases even superior than traditional steel alternatives. The benefits consist of enhancements in both material usage and life-cycle costs. The parametric study highlights some principles that could be followed when deciding on the corrugation shape to maximise the shear capacity. Also, the existing Eurocode design code for the shear capacity of stainless steel beams with corrugated webs are improved by proposing new shear-buckling reduction factors. The proposed design model considers global, local and interactive buckling modes. Further modifications in the existing design models is suggested as a subject for future research.

Key words: Corrugated web, Stainless steel, Steel bridges, Case study, Parametric study, Optimization, Material reduction, LCC study, Design code

Rostfria brobalkar med korrugerade liv
Effektivitet, stabilitet och livscykel-kostnads-studie

Examensarbete inom Masterprogrammet Structural Engineering and Building
Technology

Emil Karlsson

Institutionen för arkitektur och samhällsbyggnadsteknik
Avdelningen för Konstruktionsteknik
Stål- och Träbyggnad
Chalmers tekniska högskola

SAMMANFATTNING

Stålbalkar i broar är känsliga för korrosion, vilket innebär att underhåll är nödvändigt, huvudsakligen i form av inspektioner, rostskyddsmålning och reparationer. De problem som är förknippade med korrosion kan minimeras avsevärt genom att använda rostfritt stål istället för det mer konventionella kolstålet. Rostfritt stål är emellertid dyrare och därför är effektivt materialutnyttjande önskvärt. I detta avseende är balkar med korrugerade liv mycket fördelaktiga eftersom större mindre material kan ge samma bärande egenskaper. Detta beror främst på den högre tvärkraftskapaciteten hos sådana balkar, tack vare den ökade styvheten för deformationer ut ur planet, vilket möjliggör djupare balkar. Denna teknik kombinerad med rostfritt stål kan leda till mer konkurrenskraftiga stålbroar, särskilt med avseende på hela livscykelkostnaden.

Syftet med detta examensarbete är att undersöka användbarheten av brobalkar med korrugerade liv och rostfritt stål. Detta uppnås genom att utföra fallstudier, livscykelkostnadsanalyser och parametriska studier. Två fallstudier utförs där två befintliga broar är omformade med korrugerat liv och rostfritt stål. FE-simuleringar görs sedan för att bekräfta resultaten. Dessutom undersöks de positiva effekterna av rostfritt stål med avseende på underhålls- och driftskostnaderna genom LCC-analys. Vidare utförs parametrisk optimering och implementering av rostfritt stål med hänsyn till korrugerade liv i modifierade reduktionsfaktorer.

Resultaten visar att rostfria stålbalkar med korrugerade liv inte bara är konkurrenskraftiga men i vissa fall även överlägsna traditionella stålalternativ. Fördelarna består av förbättringar i både materialanvändning och livscykelkostnader. Den parametriska studien belyser några principer som kan följas när design av korrugerade geometrier utförs för att maximera tvärkraftskapaciteten. Dessutom förbättras den befintliga designkoden för tvärkraftskapacitet hos rostfria stålbalkar med korrugerade banor genom att föreslå nya skjvningsreduceringsfaktorer. Ytterligare modifikationer i befintliga designmodeller föreslås som ämne för framtida forskning.

Nyckelord: Korrugerat liv, Rostfritt stål, Stålbroar, Fallstudie, Parametrisk studie, Optimering, Materialreduktion, LCC-studie, Designkoder

Contents

ABSTRACT	I
SAMMANFATTNING	II
CONTENTS	III
PREFACE	VII
NOTATIONS	VIII
1 INTRODUCTION	1
1.1 Aim and scope	1
1.2 Approach	2
1.3 Limitations	2
2 THEORY	3
2.1 Corrugated webs in bridge girders	3
2.1.1 Advantages with corrugated webs	3
2.1.2 Sinusoidal webs	4
2.1.3 Trapezoidal webs	4
2.1.4 General design process	5
2.2 Design process of girders with corrugated webs	5
2.2.1 Design parameters for a corrugated web	6
2.2.2 Moment resistance in ULS	7
2.2.3 Shear resistance in ULS	8
2.2.4 Resistance against lateral-torsional buckling in ULS	11
2.2.5 Design against fatigue failure, FLS	13
2.2.6 Design in SLS	14
2.3 Stainless steel	14
2.3.1 Application of stainless steel in infrastructure	14
2.3.2 Mechanical properties of stainless steel	15
2.3.3 Designing for deflection in SLS	16
2.3.4 Partial factors, cross-section classes and shear lag for stainless steel	17
2.4 Modelling corrugated webs with stainless steel in numerical simulations	18
2.4.1 Mesh elements density, shape and non-linear model	18
2.4.2 Modelling initial imperfections	18
2.4.3 Modelling stress-strain curves in FE-models with stainless steel	20
2.5 LCC study for bridge girders	22
3 EXISTING BRIDGES WITH CORRUGATED STEEL WEB	23
3.1 Cross-section parameters of existing bridges with corrugated steel web	23
3.2 Japan	23
3.2.1 Shinkai Bridge, 1993	23
3.2.2 Hondani bridge,	23

3.2.3	Himi Yume Bridge, 2004	24
3.2.4	Yahagigawa Bridge (Toyota arrows bridge), 2005	24
3.3	France	25
3.3.1	Cognac Bridge, 1986	25
3.3.2	Maupre bridge, 1987	26
3.3.3	Dole Bridge, 1993	26
3.3.4	Meaux Viaduct, 2004	27
3.4	Other countries where corrugated steel web has been used in bridge design	27
3.4.1	Altwipfergrund Bridge Germany, 2001	27
3.4.2	Ilsun Bridge Korea, 2007	28
4	SETUP FOR NUMERICAL SIMULATIONS IN ABAQUS	29
4.1.1	Modelling shear buckling in ABAQUS	29
4.1.2	Mesh convergence study	31
4.1.3	Buckling modes in ABAQUS	31
5	SKULNÄS BRIDGE – SIMPLY SUPPORTED ROAD BRIDGE	33
5.1	Previous results and new design	33
5.2	Results numerical simulations for Skulnäs bridge	35
5.3	Life Cycle Cost study	37
5.4	Summary	41
6	NISSAN HIGHWAY BRIDGE – CONTINUOUS ROAD BRIDGE	42
6.1	Previous results and new design	42
6.2	Results numerical simulations for Nissan bridge	43
6.3	Life Cycle Cost study	45
6.4	Summary	46
7	PARAMETRIC STUDY	47
7.1	Influence of initial imperfections	47
7.2	Influence of length/height-ratio	52
7.3	Influence of web thickness and web depth	53
7.4	Influence of a_1 – flat fold length	54
7.5	Influence of α – corrugation angle	56
7.6	Proposal modified reduction factor regarding global and local buckling	57
7.7	Modified reduction factors including the interactive buckling mode	59
7.7.1	Incorporating interactive buckling into local buckling reduction factor	59
7.7.2	Creating a separate interactive buckling factor	61
7.8	Summary	64

8	DISCUSSION	65
8.1	Case studies	65
8.2	Parametric study	66
8.2.1	Buckling curves for global, local and interactive buckling	66
8.2.2	Optimal design regarding corrugation geometry	66
9	CONCLUSIONS	67
10	SUGGESTIONS FOR FURTHER RESEARCH	69
	REFERENCES	70
	APPENDIX A – MATLAB OPTIMIZATION ROUTINE	73
	APPENDIX B – FE-RESULTS REGARDING CASE STUDIES	86
	APPENDIX C – RESULTS FROM LCC STUDIES	88
	APPENDIX D – FE-RESULTS FROM PARAMETRIC STUDIES	92
	APPENDIX E – SHEAR BUCKLING MODES FOR DIFFERENT A_1	95

Preface

This master's thesis was carried out both at WSP bridge department in Gothenburg, Sweden, and at the Division of Structural Engineering, department of Architecture and Civil Engineering at Chalmers University of Technology, Sweden, from January 2018 to June 2018.

First of all, I would like to thank my supervisor Dr. Mohsen Heshmati. Without your invaluable dedication and generosity regarding time I would not have been able to conduct this thesis. I would also like to thank my examiner Associate Professor Mohammad Al-Emrani for his guidance and commitment during long meetings and correspondence throughout this work.

Furthermore, I would like to send my greatest gratitude towards my fiancée Ivana, who supported me through this process and gave me strength when I needed it. Also, I give my thanks to my family for their support during this project and all years I have spent at Chalmers.

Finally, I would like to dedicate this master's thesis to the memory of my friend Adam Hillberg who was supposed to write this together with me.

Emil Karlsson

Notations

Roman upper-case letters

D_x	Parameter calculated for global buckling
D_z	Parameter calculated for global buckling
E	Modulus of elasticity
$E_{s,i}$	Sectional modulus of elasticity used for stainless steel
E_y	Tangent modulus of the stress strain curve at yield strength
G	Shear modulus
L	Longitudinal length of girder
L_e	Length between two points of zero bending moment
M_{cr}	Critical moment of beam when uniform bending
I_z^*	Second moment of area of one corrugation length
I_z	Moment of inertia around the weak axis
I_t	Torsion constant
I_w	Warping constant for corrugated webs
I_w^*	Warping constant for flat webs
I_{y1}	Moment of inertia around the strong axis for the upper flange
I_{y2}	Moment of inertia around the strong axis for the lower flange
K	Stiffness matrix
$R_{p0.05}$	Proof stress for stainless steel
S	Stress stiffness matrix
$V_{b,Rd}$	Shear capacity of a girder
$V_{bw,Rd}$	Web contribution to shear strength
$V_{bf,Rd}$	Flanges contribution to shear strength
W_y	Section modulus

Roman lower-case letters

a_1	Flat fold length in corrugation
a_2	Inclined fold length in corrugation
a_3	Corrugation depth
a_4	Longitudinal length of a_2
b_0	Width of the outstand part of flange
b_1	Width of the flange in compression
b_2	Width of the flange in tension
b_f	Flange width
c_f	Largest outstanding part of the flange
f_y	Yield stress limit
$f_{yf,r}$	Reduced yield stress limit due to transverse moments in flanges
f_{yf}	Yield stress limit in flange
f_{yw}	Yield stress limit in web
h_m	Distance between centroids of flanges
h_w	Web height
s	Unfolded length of one half corrugated web wave
t_1	Thickness of the flange in compression
t_2	Thickness of the flange in tension

t_f	Flange thickness
t_w	Web thickness
ν	Poissons ratio
w	Length of one half corrugated wave

Greek letters

α_{LT}	Imperfection factor for lateral torsional buckling
α	Corrugation angle
ε	Engineering strain
σ	Engineering stress
$\sigma_x(M_z)$	Stress due to the transverse moments in the flange
$\sigma_{i.Ed.ser}$	SLS design stress
σ_{true}	True stress in FE-simulations
ε_{true}	True strain in FE-simulations
ε_{true}^{pl}	Plastic part of the true strain used in FE-simulations
γ_{M0}	Safety factor
γ_{M1}	Safety factor
$\tau_{cr,G}$	Global critical shear stress for a corrugated web
$\tau_{cr,I}$	Interactive critical shear stress for a corrugated web
$\tau_{cr,L}$	Local critical shear stress for a corrugated web
τ_y	Critical yielding shear stress for a corrugated web
χ	Reduction factor for out of plane buckling
$\chi_{c,l}$	Reduction factor due to local buckling
$\chi_{c,g}$	Reduction factor due to global buckling
$\chi_{c,g}$	Reduction factor due to interactive buckling
λ	Eigenvalue regarding buckling
λ_{LT}	Non-dimensional slenderness of beam
$\lambda_{c,L}$	Slenderness regarding local buckling
$\lambda_{c,G}$	Slenderness regarding global buckling
$\lambda_{c,I}$	Slenderness regarding interactive buckling

1 Introduction

Large infrastructural investments are on-going, especially in the city of Gothenburg, Sweden. Many billions of euros will be invested in the coming decades and bridges are involved in many of the projects. Because a bridge in many cases is designed to stand for at least a century it is desirable to make a well thought out investment.

Steel bridges often suffer from issues regarding corrosion and therefore need maintenance during their life cycle, mostly in form of re-painting and surveillance. This is costly for the tax payers and takes resources from new investments. If stainless steel could be used, the negative effects regarding this issue would be reduced. Stainless steel though, is expensive compared to regular steel (carbon steel) and therefore material quantity must be reduced. This would make stainless steel more competitive to use in bridges and therefore increase the demand on stainless steel girders.

One way to do this is to use corrugated webs in bridge girders, which gives a large out-of-plane rigidity and increases shear capacity for webs. This would make it possible to reduce material amount and make it reasonable to use stainless steel instead of conventional carbon steel.

This master's thesis was initiated by Chalmers University of Technology and conducted at WSP's department for bridges in Gothenburg.

1.1 Aim and scope

The aim of this study is to investigate the efficiency and applicability of stainless steel to bridge girders with corrugated webs. This aim was achieved by defining two major objectives presented below.

The first objective is to investigate the usefulness, advantages and disadvantages of using the material stainless steel in existing bridge girders by redesigning them with a corrugated web instead of flat web. Benefits such as material reduction and less life-cycle costs will be examined and presented. The new designs will be compared with the original designs with carbon steel and flat webs.

The second objective is to investigate and draw conclusions regarding influence of different geometrical design-parameters in a corrugated web with stainless steel and if the reduction factors in Eurocode for corrugated webs can be modified to better fit the material stainless steel. Furthermore, it will be investigated if there are possibilities to develop new shear buckling curves regarding stainless steel and corrugated webs. These buckling curves can then be used to improve the accuracy of the existing reduction factors in Eurocode.

These two objectives together will create a better understanding of the subject and provide necessary information for more efficient design of stainless steel bridge girders with corrugate webs.

1.2 Approach

The project will be divided into different stages to reach the objectives. These are:

- A literature study covering previous research, general theories and design processes regarding the subject. Several different existing bridges with corrugated webs will be examined to see if these kinds of bridges have a relevance and are practically doable.
- Case studies will be performed to see if the subject is applicable on existing infrastructure. The approach here will be to choose existing and common bridges in Sweden and then re-model them with stainless steel, different geometries and a corrugated web. Results will be verified with both analytical calculations and FE-simulations. Comparison will be made between original design and new designs both regarding capacities and life cycle costs. LCC studies will therefore be performed for the case studies to investigate the economic aspects of the new concept.
- A parametric study will be performed using results from FE-simulations in ABAQUS 6.13. These simulations will contain many different cross-sections and corrugation geometries. The FE-results will further be used in a regression study to create new shear buckling curves and to modify existing reduction factors in Eurocode.

1.3 Limitations

Limitations for this thesis will be as followed:

- Only load-carrying steel girders in which the design is governed by shear buckling will be analysed in FE-simulations. The rest of the bridge such as deck and other non-steel materials will be excluded.
- No regard to connections, bolts or joints will be done.
- Corrugated webs do not contribute to longitudinal/axial stiffness.
- Flanges contribution to shear strength are neglected in both analytical calculations and numerical simulations.
- Pre-stressing is not considered.
- Welding details will not be analysed regarding moment or shear capacity.
- Only duplex stainless-steel grade 1.4162 will be considered.
- The parametric study will contain certain ranges of investigated parameters. Web thickness t_w is between 2-6mm, web height h_w is between 500-2500mm, corrugation angle α is between 25-45° and flat fold length a_f is between 50-350mm.

2 Theory

There is a lot of previous research conducted for either corrugated webs or the stainless-steel material. However, there is not much done combining these two. This chapter will present theory regarding design of a corrugated web with stainless-steel and how to conduct numerical simulations and LCC studies.

2.1 Corrugated webs in bridge girders

Beam girders with high capacity, often have deep cross-sections which can result in instability problems such as lateral-torsional and shear buckling. To strengthen beams, web stiffeners are used, whose function is to stabilize the web. A different design approach on how to strengthen the beam is to use a corrugated web instead of the conventional flat one. According to previous studies this provides rigidity in the out-of-plane direction and improves buckling stability of the beam (Boutillon, et al., 2015). It also improves the need for web stiffeners while reducing the required web plate thickness, which will result in a reduction of the amount of needed material and welds when constructing a bridge girder. There are mainly two different types of corrugation shapes that can be used; trapezoidal and sinusoidal. These two have generally the same influence on load-bearing capacity of beams but vary in detail.

2.1.1 Advantages with corrugated webs

Some of the main advantages and features regarding corrugated webs in bridge girders are listed below:

- When a corrugated steel web is used in a concrete box girder the self-weight reduces between 10% and 30% compared to a conventional concrete box girder (Boutillon, et al., 2015). If material quantity could be reduced, the possibilities to use new and less maintenance-demanding materials, that are often more expensive than the conventional building materials, in a cost-efficient manner would be increased.
- Accordion effect emerges in a corrugated steel web because of its very low capacity against axial forces. In a conventional girder, not only the flanges can take tensile and compression forces from bending. Also, some of these forces will be resisted by the web. In a steel beam with corrugated web there will be no tensile or compression forces from bending in the web which means that all axial forces will be taken in the flanges, further improving the impact of pre-stressing. This is especially beneficial when designing bridges with large spans (Boutillon, et al., 2015).
- In steel girders with flat webs, web stiffeners are used to prevent shear and lateral buckling. Due to the high out of plane rigidity of corrugated webs, no stiffeners are needed which is a great advantage when producing webs at factory (Boutillon, et al., 2015).

2.1.2 Sinusoidal webs

Sinusoidal webs are created with a circular configuration, see Figure 2.1, instead of plane plates. This way of constructing corrugated webs are not as common in bridges as the case of trapezoidal webs, which can be seen when reviewing existing bridges.

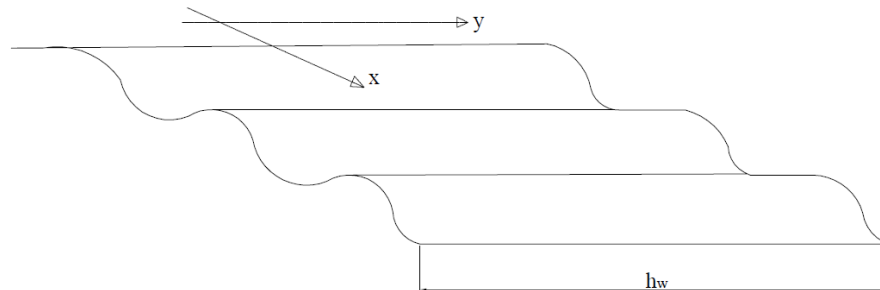


Figure 2.1 Example of a corrugated web with sinusoidal geometry.

Sinusoidal webs are fabricated in an automated process and can be configured in many different geometries and spans to fit transports etc. Therefore, they must be connected on construction site by either welding or bolts, to create long spans. General mechanical properties, compared with trapezoidal webs, can be described as better performance for thicker plates during the ultimate limit stage (Hosseinpour, Baharom, & Yadollahi, 2015). Although sinusoidal webs will not be used in the case and parametric studies in this thesis, the applicable design methods from Eurocode as well as the previous research will be presented in the theory chapter.

2.1.3 Trapezoidal webs

Trapezoidal webs are the most commonly used in bridges which give high ultimate load-bearing capacities with relatively thin web plates. Steel girders with corrugated webs are usually welded in the workshop and assembled in-situ. In case several splices are needed, butt welds are used to connect them on site. Trapezoidal webs are available in different dimensions and can be custom made because of its relatively simple geometry, which can be seen in Figure 2.2.

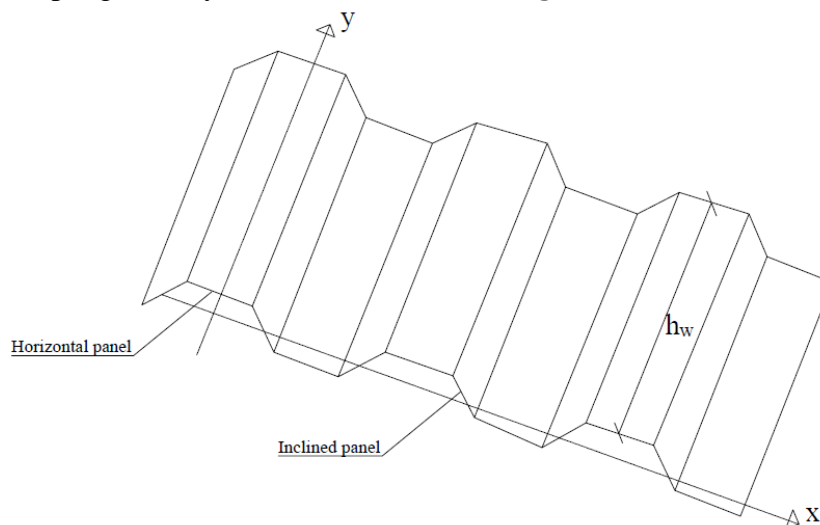


Figure 2.2 Example of a corrugated web with trapezoidal geometry.

General mechanical properties, compared with sinusoidal webs, can be described as better performance for thinner plates with respect to the ultimate load-bearing capacity. Trapezoidal webs are used in this thesis when performing case studies and parametric studies. This is justified by the fact that it is more commonly used in practice compared to the sinusoidal plates, see Section 3.

2.1.4 General design process

The general standards for any structural member of a bridge with a corrugated web is that it must satisfy the criteria of serviceability, ultimate and fatigue limit state given in (EN1990, 2005). Safety factors, such as load factors and partial factors should be taken into consideration when calculating load effects and material strengths.

- The **serviceability limit state** (SLS) concerns criteria such as deflection, displacement, comfort of user etc. These values must be within certain limits during the whole service life of the bridge.
- In the **ultimate limit state** (ULS), bending moments, shear forces, torsional forces, compressive and tensile forces shall be below limited values which will prevent the bridge from collapse or catastrophic consequences.
- The **fatigue-limit state** concerns failure because of fluctuating load scenarios. It should be checked that the bridge is constructed so that it can remain safe from fatigue failure during its life span.

The main principles, regarding bending and shear resistance, when designing a corrugated steel-web, with trapezoidal or sinusoidal shape, are given in (EN1990-1-5, 2006). The calculation procedure in Eurocode regarding sinusoidal webs is conservative because it is not considering the latest test results for beams with this configuration (Pasternak & Kubieniec, 2010). The main behaviour of a beam with corrugated web can be defined by the accordion effect as described in section 2.1.1. Normal force and bending moment are carried by the flanges only and web is affected by shear and lateral-torsional forces.

2.2 Design process of girders with corrugated webs

The design process, presented in this chapter, for ULS regarding corrugated webs with trapezoidal and sinusoidal configurations are gathered from Annex D in (EN1990-1-5, 2006) and (Yazeed Sayed-Ahmed, 1998). These equations are for calculating resistance against bending, shear and lateral-torsional buckling.

The web in a girder is mainly taking care of the shear stresses, however flanges can contribute if they are not fully utilized in bending. The main shear failure modes are local, global and interactive buckling further explained in section 2.2.3. It is these failure modes a web should be able to hold against.

Equations regarding resistance against lateral-torsional buckling can be found in (EN1990-1-1, 2005). These are for flats webs but can be used for corrugated webs by using the equation for critical moment obtained from (Larsson & Persson, 2013).

Pictures of a trapezoidal web and a sinusoidal web with geometric notations used in the design process can be seen in Figure 2.3 and Figure 2.4 respectively.

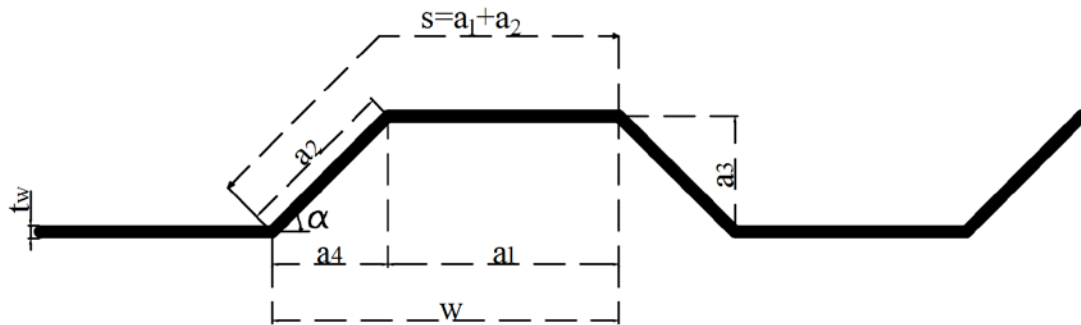


Figure 2.3 Geometric notations for a trapezoidal web.

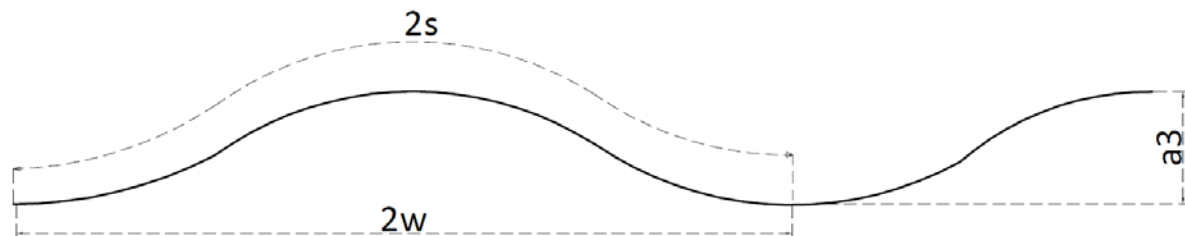


Figure 2.4 Geometric notations for a sinusoidal web.

2.2.1 Design parameters for a corrugated web

The design parameters in this chapter is obtained from experimental and numerical studies and give a hint on how to best design a corrugated web regarding its shear capacity. These tips are assembled from (Yazeed Sayed-Ahmed, 1998) and (Luo & Edlund, 1996) and are summarized in Table 2.1. Generally, it can be stated that after the first shear buckle, the main shear capacity of the girder is drastically reduced by ca. 70-80%. Therefore, it is important to design against shear buckling. The optimal ratio between the maximum allowed design shear stress τ_d and yield shear stress τ_y shall be between 0.8 and 1.0 according to (Yazeed Sayed-Ahmed, 1998). When designing a corrugated web there are four input parameters that would affect the corrugation configuration and in turn, the shear buckling behaviour. These are a_1 , α , h_w and t_w and their influence on shear strength and buckling, gathered from previous research (Luo & Edlund, 1996), are further explained in Table 2.1. Equations in Table 2.1 on how to calculate a_2 , a_3 and a_4 are obtained from (Yazeed Sayed-Ahmed, 1998).

Table 2.1 Summary of design parameters and their effects for corrugated web regarding shear capacity gathered from (Luo & Edlund, 1996).

Cross-section web			
Description	Notation	Effect on shear capacity	Effect on buckling
Thickness web	t_w	Increases when t_w increase, but not linearly.	Increased post-buckling capacity when t_w increase. t_w smaller = More local buckling
Depth web	h_w	Increases proportionally with h_w . Shear capacity not dependent on Length/Depth ratio of a girder.	h_w larger = More interactive buckling
Corrugation web			
Description	Notation	Effect on shear strength	Effect on buckling
Angle	α	Increased α gives somewhat larger shear capacity	30° = More global 45° = More interactive 60° = More local
Flat fold	a_1	Increased a_1 gives less shear capacity	-
Length inclined fold	$a_2 = \frac{a_4}{\cos \alpha}$	-	-
Corrugation depth	$a_3 = a_4 \tan \alpha$	No influence on shear capacity	Increased a_3 = Buckling mode goes from interactive to local
Length inclined fold x-direction	$a_4 = a_1 \cos \alpha$	-	-

2.2.2 Moment resistance in ULS

The moment resistance due to bending is only dependent on the flanges. Equations in this chapter are taken from (EN1990-1-5, 2006). Moment capacity for a girder with corrugated web can be calculated from Equation 1.

$$M_{f,Rd} = \min \left\{ \underbrace{\frac{b_2 t_2 f_{yf,r}}{\gamma_{M0}} \left(h_w + \frac{t_1 + t_2}{2} \right)}_{\text{Tension flange}}; \underbrace{\frac{b_1 t_1 f_{yf,r}}{\gamma_{M0}} \left(h_w + \frac{t_1 + t_2}{2} \right)}_{\text{Compression flange}}; \underbrace{\frac{b_1 t_1 \chi f_{yf,r}}{\gamma_{M0}} \left(h_w + \frac{t_1 + t_2}{2} \right)}_{\text{Compression flange}} \right\} \text{Equation 1}$$

Where χ is the reduction factor for out of plane buckling according to EN 1993-1-1 6.3 and $f_{yf,r}$, see Equation 2, is the value of yield stress reduced due to transverse moments in flanges.

$$f_{yf,r} = f_{yf} f_T \quad \text{Equation 2}$$

$$f_T = 1 - 0.4 \sqrt{\frac{\sigma_x(M_z)}{f_{yf}}} \quad (\text{trapezoidal corrugation}) \quad \text{Equation 3}$$

$$f_T = 1 \quad (\text{sinusoidal corrugation}) \quad \text{Equation 4}$$

Where $\sigma_x(M_z)$ is the stress due to the transverse moments in the flanges.

2.2.3 Shear resistance in ULS

Three modes of buckling failure are related with shear and corrugated webs. These are according to (Yazeed Sayed-Ahmed, 1998):

- Local buckling failure mode (see Figure 2.5), which occurs in one panel of the web during uniform shear. Usually it is this kind of buckling that will initiate the buckling procedure (Luo & Edlund, 1996). The critical shear stress for this mode is calculated using Equation 10.

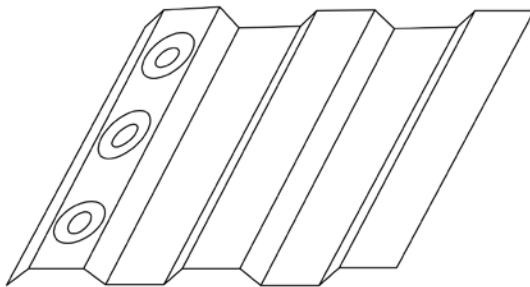


Figure 2.5 Local buckling failure mode for a corrugated web.

- Global buckling failure mode (see Figure 2.6), which occurs diagonally over several panels of the web. Critical global shear stress is calculated using Equation 14.

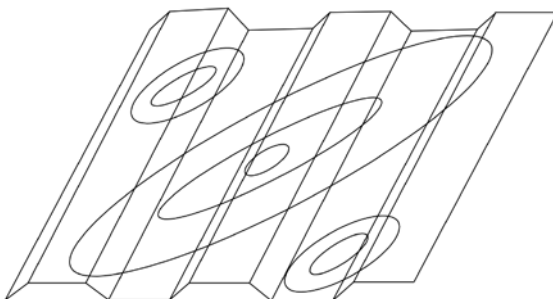


Figure 2.6 Global buckling failure mode for a corrugated web.

- Interactive buckling mode see Figure 2.7, which is based on interaction between local and global buckling modes.

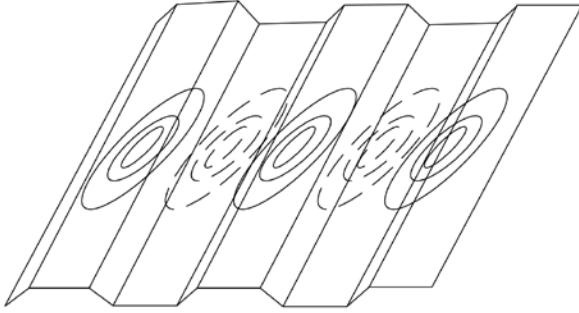


Figure 2.7 Interactive buckling mode.

Interactive critical shear stress is calculated from Equation 5 which is taken from (Tohamy, Abdel-Halim, Saddek, & Hamed, 2016).

$$\frac{1}{\tau_{cr,I}^n} = \frac{1}{\tau_{cr,L}^n} + \frac{1}{\tau_{cr,G}^n} + \frac{1}{\tau_y^n} \quad \text{Equation 5}$$

Where $\tau_{cr,I}$ is the critical interactive shear stress, $\tau_{cr,L}$ the critical local shear stress, $\tau_{cr,G}$ the critical global shear stress and τ_y is the yield stress equal to $\tau_y = \frac{f_y}{\sqrt{3}}$. The value of n is chosen to either increase or decrease the effect of critical interactive shear buckling in design. Interactive buckling has not been considered in Eurocode for design of corrugated webs and therefore there is no standard value of n to choose. However, if n is set equal to 1, the interactive critical shear force will always be less than local, global and yield stress limits. The value of n can be set to a greater value than 1 e.g. 3 or 5 which was used in (Tohamy, Abdel-Halim, Saddek, & Hamed, 2016). For example, when n is set to 5 the interactive critical shear stress is closer to the lowest value of the three limits in Equation 5 than if n is set to a lower value.

The total shear resistance for a girder with corrugated web can be calculated from Equation 6.

$$V_{b,Rd} = V_{bw,Rd} + V_{bf,Rd} \quad \text{Equation 6}$$

Where $V_{bw,Rd}$ is the shear resistance contribution from a trapezoidal corrugated web according to (EN1990-1-5, 2006) and described in Equation 7. $V_{bf,Rd}$ is the shear resistance contribution from the flanges described in Equation 17.

$$V_{bw,Rd} = \chi_c \frac{f_{yw}}{\gamma_{M1}\sqrt{3}} h_w t_w \quad \text{Equation 7}$$

Where f_{yw} is the yield stress limit in the web and χ_c is chosen as the less of local buckling factor $\chi_{c,l}$ or global buckling factor $\chi_{c,g}$.

$$\chi_{c,l} = \frac{1.15}{0.9 + \lambda_{c,l}} \leq 1.0 \quad \text{Equation 8}$$

$$\lambda_{c,l} = \sqrt{\frac{f_{yw}}{\tau_{cr,l}\sqrt{3}}} \quad \text{Equation 9}$$

$$\tau_{cr,l} = 4.83E \left[\frac{t_w}{a_{max}} \right]^2 \quad (\text{trapezoidal corrugation}) \quad \text{Equation 10}$$

Where a_{max} shall be taken as the greater of a_1 and a_2 , see Figure 2.3. For sinusoidal webs the use of Equation 11 is recommended, regarding $\tau_{cr,l}$.

$$\tau_{cr,l} = \left(5.34 + \frac{a_3 s}{h_w t_w} \right) \frac{\pi^2 E}{12(1-\nu^2)} \left[\frac{t_w}{s} \right]^2 \quad (\text{sinusoidal corrugation}) \quad \text{Equation 11}$$

$$\chi_{c,g} = \frac{1.5}{0.5 + \lambda_{c,g}^2} \leq 1.0 \quad \text{Equation 12}$$

$$\lambda_{c,g} = \sqrt{\frac{f_{yw}}{\tau_{cr,g}\sqrt{3}}} \quad \text{Equation 13}$$

$$\tau_{cr,g} = \frac{32.4}{t_w h_w^2} \sqrt[4]{D_x D_z^3} \quad \text{Equation 14}$$

$$D_x = \frac{Et_w^3}{12(1-\nu^2)} \frac{w}{s} = \frac{Et_w^3}{12(1-\nu^2)} \frac{a_1 + a_4}{a_1 + a_2} \quad \text{Equation 15}$$

$$D_z = \frac{EI_z^*}{w} = \frac{Et_w a_3^2}{12} \frac{3a_1 + a_2}{a_1 + a_4} \quad \text{Equation 16}$$

Where I_z^* is the second moment of area of one corrugation of length w , see Figure 2.3. s and I_z^* are related to the actual shape of the corrugation and plates in web are assumed to be hinged at the edges. D_x and D_z can be calculated in two ways where the first expression is useable for sinusoidal corrugations and the second is for

trapezoidal corrugation in Equation 15 and 16 respectively (Johansson, Maquoi, Sedlacek, Muller, & Beg, 2007).

When $M_{Ed} < M_{f,Rd}$, shear resistance contribution from flanges can be considered by using Equation 17.

$$V_{bf,Rd} = \frac{b_f t_f^2 f_{yf}}{c \gamma_{M1}} \left(1 - \left(\frac{M_{Ed}}{M_{f,Rd}} \right)^2 \right) \quad \text{Equation 17}$$

$$c = a \left(0.25 + \frac{1.6 b_f t_f^2 f_{yf}}{t_w^2 f_{yw}} \right) \quad \text{Equation 18}$$

2.2.4 Resistance against lateral-torsional buckling in ULS

Moment resistance against lateral-torsional buckling according to (EN1990-1-1, 2005) is described in Equation 19.

$$M_{b,Rd} = \chi_{LT} W_y \frac{f_y}{\gamma_{M1}} \quad \text{Equation 19}$$

Where

$W_y = W_{pl,y}$	for CRC 1 or 2
$W_y = W_{el,y}$	for CRC 3
$W_y = W_{eff,y}$	for CRC 4

Where χ_{LT} is the reduction factor due to lateral-torsional buckling, see Equation 20.

$$\chi_{LT} = \frac{1}{\Phi_{LT} + \sqrt{\Phi_{LT}^2 - \lambda_{LT}^2}} \quad \text{but } \chi_{LT} \leq 1 \quad \text{Equation 20}$$

$$\Phi_{LT} = 0.5[1 + \alpha_{LT}(\lambda_{LT} - 0.2) + \lambda_{LT}^2] \quad \text{Equation 21}$$

Where α_{LT} is an imperfection factor, see Table 2.2 and Table 2.3.

Table 2.2 Recommended values for imperfection factors for later-torsional buckling curves.

Buckling curve	a	b	c	d
α_{LT}	0.21	0.34	0.49	0.76

Table 2.3 Recommended values for lateral torsional buckling curves for cross-sections.

Cross-section	Limits	Buckling curve
Rolled I-sections	$h/b \leq 2$	a
	$h/b > 2$	b
Welded I-sections	$h/b \leq 2$	c
	$h/b > 2$	d
Other cross-sections	-	d

λ_{LT} is the non-dimensional slenderness, see Equation 22.

$$\lambda_{LT} = \sqrt{\frac{W_y f_y}{M_{cr}}} \quad \text{Equation 22}$$

Where M_{cr} is the critical moment obtained from (Larsson & Persson, 2013), see Equation 23, when the beam is subjected to a uniform bending moment.

$$M_{cr} = \frac{\pi^2 E I_z}{L^2} \sqrt{\frac{I_w}{I_z} + \frac{L^2 G I_t}{\pi^2 E I_z}} \quad \text{Equation 23}$$

Where I_z is the moment of inertia around the weak axis (same as for flat-web-girders). I_t is the torsion constant, also same as for flat-web-girders. I_w is the warping constant regarding corrugated webs described in Equation 24.

$$I_w = I_w^* + c_w \frac{L^2}{E \pi^2} \quad \text{Equation 24}$$

Where I_w^* is the warping constant for a flat web and c_w is defined by Equation 25.

$$c_w = \frac{(2d)^2 h_m^2}{8u_x(a_1+a_4)} \quad \text{Equation 25}$$

$$u_x = \frac{h_m}{2G a_1 t_w} + \frac{h_m^2 (a_1+a_4)^3 (I_{y1}+I_{y2})}{600 a_1^2 E (I_{y1} I_{y2})} \quad \text{Equation 26}$$

Where I_{y1} and I_{y2} are the moment of inertia around the strong axis for the upper and lower flange respectively. For beams with equal flanges, Equation 27 for u_x can be used.

$$u_x = \frac{h_m}{2Ga_1t_w} + \frac{h_m^2(a_1+a_4)^3}{25a_1^2Ebft_f^3} \quad \text{Equation 27}$$

2.2.5 Design against fatigue failure, FLS

A steel bridge construction can experience failure even though it has never reached yield or ultimate limit loads. This is due to long term repetitive cycles of normal and shear stresses leading to small cracks propagating in the material finally leading to a brittle failure. The most important factor when calculating fatigue failure is the number of cycles n_i a construction needs to reach failure with a certain stress range $\Delta\sigma$. This connection between stress ranges and cycles can be seen in a S-N-curve, see Figure 2.8.

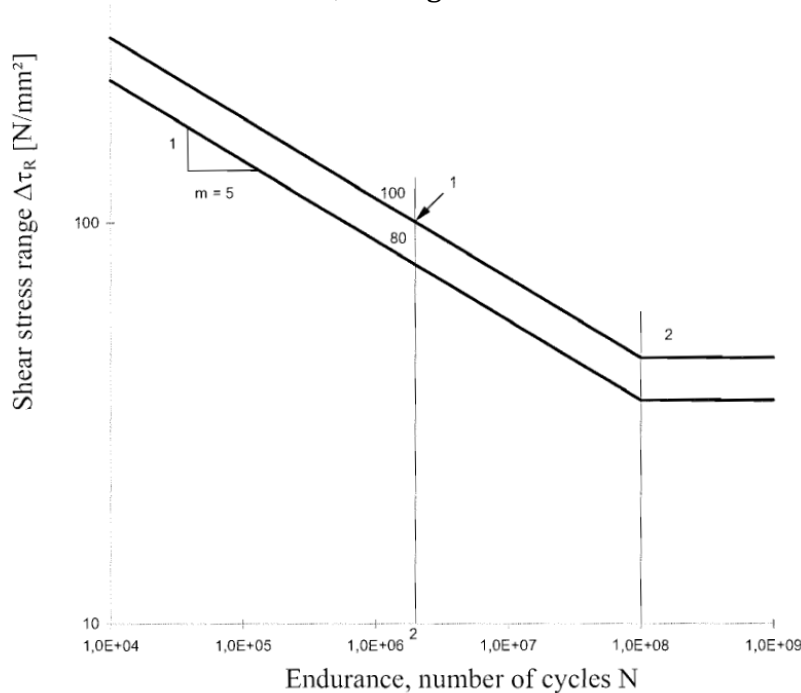


Figure 2.8 Example of S-N-curve where number of load cycles are on the x-axis and stress range is on y-axis, gathered from (EN1993-1-9, 2005).

The number of cycles before failure which can be seen in the above S-N-curve is simplified by using linear relationships at different stress ranges. Basically, the curve describes number of loading cycles for a specific detail before it goes to fatigue failure.

Calculations regarding fatigue can be found in (EN1993-1-9, 2005). Different details in the construction have different behaviour due to fatigue, so therefore different details have different S-N-curves. In Eurocode these are called detail categories or C-class, which can be applied on all critical parts for calculations.

Details can be loaded with normal stress or shear stress, variable stress ranges or constant ones. For welded details and according to EN 1993-1-9, to following rules apply:

- When a detail is subjected to variable amplitude normal stresses, the S-N-curve must be extended to 100 million cycles. The slope is now 3 before 5 million cycles and 5 afterwards.
- When a detail is subjected to shear stresses the S-N-curve slope is constantly 5 until it reaches 100 million cycles.

When evaluating details considering fatigue, the total damage is calculated using either Palmgren-Miner method or the equivalent stress range concept.

2.2.6 Design in SLS

For design in SLS using stainless steel material a modified modulus of elasticity shall be used, see section 2.3.3. The largest deflection of a bridge will be calculated for SLS and compared with the largest allowable deflection.

2.3 Stainless steel

One of the largest issues with carbon steel bridges is corrosion. In a chemical or electrochemical reaction, a metal can be successively destroyed. To avoid this engineers and chemists have invented stainless steel, an alloy of steel and chromium (Forum, 2018), to protect the material. A small layer of oxide is created around the steel and protect it from corrosion. The material is self-repairing, which means that if a damage occurs in the metal, a new layer is created directly to protect the weak part. Stainless steel is therefore very effective against corrosion and can increase the life length of a bridge girder for example.

There are different types of stainless steels and grades that can be used in various environments, situations and locations. Mechanical properties are also something that has been more considered lately, because of higher demand of stainless steel in bearing structures. The main differences of stainless steels are the amount of iron, carbon, chromium, nickel and some other substances. The stainless steels mainly used for infrastructure projects is duplex and austenitic steels, where duplex is used in structurally bearing members. The different compositions of stainless steels can be seen in Table 2.4 and their mechanical properties in Figure 2.9.

Table 2.4 Composition and properties of different stainless-steel types.

	Chromium	Nickel	Molybdenum	Corrosion resistance
Ferritic	12.5-17%	~0%	0	Good
Martensitic	10.5-18%	~0%	0	Moderate
Austenitic	16-26%	6-12%	optional	Very good
Duplex	18-26%	4-7%	0-4%	Very good

2.3.1 Application of stainless steel in infrastructure

Stainless steel is used in several of applications such as infrastructure, architecture, water applications, surgical tools, kitchen tools etc. Some examples of existing bridges with elements made of stainless steel are listed below:

Railway bridge structure in San Sebastian, Spain (Railway Bridge)

Corrosion had damaged a previous railway steel bridge structure, in San Sebastian, beyond repair and made its replacement vital. The local authorities could with the new stainless-steel bridge extend the durability requirement to 130 years with no major maintenance. Duplex stainless steel, which had already performed well in other types of bridges, was used in this bridge. The structure is the first railway bridge fully designed in stainless steel (Worldstainless, Railway bridge structure, 2018).

River delta crossing, Hong Kong, Macau, China (Road Bridge)

River delta crossing is a massive infrastructural project between Hong Kong and Macau with a budget of approximately US\$ 10.6 billion and completion at late 2016. As corrosion damage would be difficult to repair later, duplex stainless steel was used at the outer parts of the reinforcement which may be exposed to cracks and corrosion due to raised chloride levels when the carbonation of the concrete develops (Worldstainless, River delta crossing, 2018).

Both these projects show that stainless steel is applicable in bridge designs. Benefits are less or no need for maintenance during life time and increased life length of the structure.

2.3.2 Mechanical properties of stainless steel

Stainless steel is considered in (EN1990-1-4, 2006). Duplex stainless steel is a combination of the austenitic and ferritic stainless-steel types, which means it has good mechanical strength and corrosion resistance properties. Stainless steel mechanical properties differ from conventional carbon steel because it has no distinctive yielding point. Instead elongation after fracture and proof strength are important properties (Finnås & Olsson, 2018). Stainless steel compared to carbon steel stress-strain behaviour can be seen in Figure 2.9.

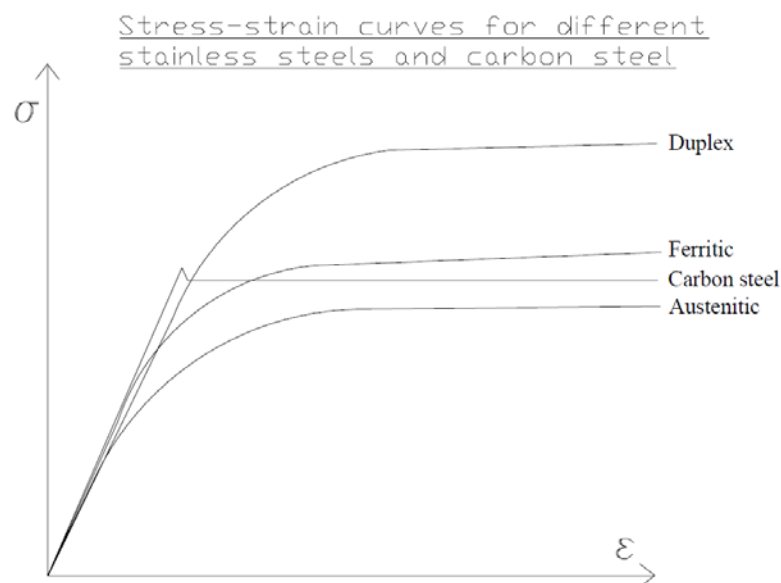


Figure 2.9 Tensile stress-strain curve comparison between stainless steel and carbon steel.

There are tables in (EN1990-1-4, 2006) which helps to select what stainless steel that should be chosen in different locations and environments. For a bridge there can be many different environments, though mostly outside. A summary of stainless-steels that can be used for outdoor bridges with its properties can be seen in Table 2.5. It is stated in Eurocode (EN1990-1-4, 2006) that f_y and f_u should be taken as the minimum specified values for the 0.2% proof strength of stainless steel and that they are varying with thickness of the evaluated member.

Table 2.5 Mechanical properties for stainless steels suitable for outdoor bridges.

Grade	Performance regarding corrosion	Type	Density [kg/m ³]	Poissons ratio ν	Modulus of elasticity [GPa]	f_y [MPa]	f_u [MPa]
1.4301	Moderate	Austenitic	7900	0.3	200	210	520
1.4318	Moderate	Austenitic	7900	0.3	200	330	630
1.4362	Good	Duplex	7800	0.3	200	400	630
1.4401	Good	Austenitic	8000	0.3	200	220	520
1.4462	Very good	Duplex	7800	0.3	200	460	640
1.4162	Very good	Duplex	7800	0.3	200	480	650

Duplex steel grade 1.4162 has good mechanical properties and sufficient resistance against corrosion, therefore this type will be used in this thesis. For specific mechanical properties regarding this stainless-steel type, see Table 2.6.

Table 2.6 Yield and ultimate strength for Duplex stainless-steel grade 1.4162.

	$t \leq 6.4$ mm		6.4 mm $< t \leq 10$ mm		$10 < t$	
Grade	f_y [Mpa]	f_u [Mpa]	f_y [Mpa]	f_u [Mpa]	f_y [Mpa]	f_u [Mpa]
1.4162	530	660	460	660	450	660

The strength of stainless-steel type 1.4162 varies depending on thickness of the specimen. This is because a thicker steel plate has larger possibilities of deformations and instabilities.

2.3.3 Designing for deflection in SLS

When calculating deflections in SLS for stainless steels, a secant modulus of elasticity $E_{s,ser}$ shall be used, considering stresses in the member and orientation of rolling direction. This can be obtained from Equation 28.

$$E_{s,ser} = \frac{(E_{s,1} + E_{s,2})}{2} \quad \text{Equation 28}$$

Where $E_{s,1}$ and $E_{s,2}$ is the secant modulus corresponding to σ_1 and σ_2 in the tension and compression flange respectively. Both these values can be estimated from Equation 29.

$$E_{s,i} = \frac{E}{1 + 0.002 \frac{E}{\sigma_{i,Ed,ser}} \left(\frac{\sigma_{i,Ed,ser}}{f_y} \right)^n} \quad \text{Equation 29}$$

Where $\sigma_{i,Ed,ser}$ is the appropriate SLS design stress. n corresponds to the rolling direction and can be found in Table 2.7 obtained from Annex C of (EN1990-1-4, 2006).

Table 2.7 Values of n .

Steel grade	Coefficient n	
	Longitudinal direction	Transverse direction
1.4003	7	11
1.4016	6	14
1.4512	9	16
1.4301 1.4306 1.4307 1.4318 1.4541	6	8
1.4401 1.4404 1.4432 1.4435 1.4539 1.4571	7	9
1.4462 1.4362	5	5

2.3.4 Partial factors, cross-section classes and shear lag for stainless steel

Partial factors for stainless steel when designing for ULS shall be taken from Table 2.8 according to (EN1990-1-4, 2006).

Table 2.8 Partial factors for stainless steel in ULS.

Resistance of cross-section to excessive yielding including local buckling	γ_{M0}	1.1
Resistance of members to instability assessed by member checks	γ_{M1}	1.1
Resistance of cross-sections in tension to fracture	γ_{M2}	1.25
Resistance of bolts, rivets, welds, pins and plates in bearing	γ_{M2}	1.25

Cross-section classes for stainless steel shall be calculated in the same manner as for carbon steels according to (EN1990-1-3, 2006), with one exception that the overall width-thickness ratio b/t and h/t shall not exceed 400. Cross section classes are divided into 1, 2, 3 and 4. The properties of cross-section class 4 may be obtained by using an effective width for parts in compression.

Shear lag in flanges, both for ULS and SLS, may be ignored if $b_0 < L_e / 50$, where b_0 is the outstand of the flange or half the width of an internal element and L_e is the length

between two points of zero bending moment. When this limit is surpassed, the design process for carbon steel in (EN1990-1-5, 2006) is applicable also for stainless steel.

2.4 Modelling corrugated webs with stainless steel in numerical simulations

To further analyse a stainless steel corrugated web girder, FE-simulations will be conducted in Abaqus. This chapter explains some of the most important things regarding this.

2.4.1 Mesh elements density, shape and non-linear model

Number of elements in a mesh is critical when considering computational power and time consumption. If a finer mesh is used than necessary, it will take more time and power than needed. But instead if a coarser mesh is used, the study might not be reliable. Therefore, a sufficient number of elements, a mesh density, must be found for every type of geometry analysed in a FE-simulation. To make elements quadratically is practical when trying to make an even number of elements on the geometry shape. Best way to decide number of elements is by performing a mesh convergence study. A start value for mesh density should be a sufficient number for the flat web fold and then derive the other number of elements accordingly.

According to (Yong Song, Mei Yu, & Zhang, 2011) eight nodes shell elements shall be used for simulations for girders with corrugated web. Each node has six degrees of freedom, translation in x, y and z directions and rotation around x, y and z axis. As for all non-linear FE-models an iterative process with incrementations are being used, moreover Newton-Raphson solution method can be applied for modelling shear buckling of corrugated webs. When considering large deformations during a non-linear buckling analysis, Von-Mises buckling standard shall be used to analyse damage conditions during complex stresses (Yong Song, Mei Yu, & Zhang, 2011).

2.4.2 Modelling initial imperfections

Corrugated steel web elastic buckling analysis is for non-defect ideal components, but in reality there will be initial imperfection in structures. These imperfections will cause buckling at different buckling modes than when analysing in elastic behaviour. To consider initial imperfections, non-linear finite element analysis must be performed with a predefined initial imperfection (Yong Song, Mei Yu, & Zhang, 2011).

When modelling a corrugated web, initial imperfections location and magnitude must be known in prior. This can be done with a method called Consistent mode imperfection method which is used by (Yong Song, Mei Yu, & Zhang, 2011) to find out the worst distribution mode of initial imperfection. This method's fundamental assumptions are:

- Solving the structural eigenvalue buckling mode will bring the fundamental buckling mode for a structure.
- The eigenvalue problem will give deformations with a minimum potential energy state.

- If initial imperfection distribution is the same as fundamental buckling mode for a structure, this will give worst case of initial imperfection and largest impact on mechanical properties.

First step in this method is to solve eigenvalues for an ideal structure with no defections. The eigenvalue is obtained from Equation 30.

$$([K] + \lambda_i[S])\{\psi\}_i = [0] \quad \text{Equation 30}$$

Where $[K]$ is the stiffness matrix, $[S]$ is the stress stiffness matrix, λ_i are eigenvalues and $\{\psi\}_i$ is character vector of deformation. Eigenvalue buckling is obtained from a linear-elastic FE-simulation in Abaqus, with a non-deformed corrugated web. This will give the critical buckling load and lateral buckling deformations of the structure. The resultant buckling mode obtained from first analysis is then added into the second non-linear model with predefined initial imperfection magnitudes. In previous research from (Yong Song, Mei Yu, & Zhang, 2011) a trapezoidal corrugated web under uniform shear stress is considered for a parametric study where the initial imperfection is simulated for various of magnitudes. The results show that initial imperfections have large impact on shear capacity with reduction of capacity when initial imperfection is increased.

To choose correct magnitude of initial imperfection is the crucial part of initializing initial imperfection into a non-linear FE-modelling of corrugated webs under different load cases. Due to variations in manufacturing processes and quality control from developers, the initial imperfection magnitude can vary from girder to girder (Yong Song, Mei Yu, & Zhang, 2011). A robotic manufactured girder shows less initial imperfections than a hand made one and therefore a big focus on use of corrugated webs should be the manufacture process.

Initial imperfection magnitude – Shear buckling

According to (Driver, Abbas, & Sause, 2006) the imperfection can be taken equal to thickness of web t_w for deeper corrugated webs in bridges. This has proven valid in research when comparing experimental test results with numerical test results. It should be noted that use of t_w as imperfection magnitude gives advantages regarding shear capacity for slender webs according to (Driver, Abbas, & Sause, 2006). Another approach is instead to follow Eurocode (EN1990-1-5, 2006) and use $\frac{h_w}{200}$ as imperfection magnitude (Zevallos, Hassanein, Real, & Mirambell, 2015) and (Hassanein, Elkawas, El Hadidy, & Elchalakani, 2017). The safest of these two approaches would be to use the one with largest imperfection magnitude. However, considering that use of a magnitude equal to t_w already is on the safe side (Driver, Abbas, & Sause, 2006), it might be more reasonable to use the less of $\frac{h_w}{200}$ and t_w . For the case studies performed in this thesis initial imperfection equal to t_w will therefore be used.

Initial imperfection magnitude – Patch loading and flange buckling

When setting up FE-models for patch loading, (Kövesdi & Dunai, 2009) propose to use $\frac{a_1}{200}$ as initial imperfection magnitude.

Models for flange buckling, a magnitude of $\frac{c_f}{50}$ where c_f is the largest outstanding part of the flange, shall be used according to (Jáger, Dunai, & Kövesdi, 2017) which refers to (EN1990-1-5, 2006). This magnitude will result in a conservative design when using stocky flanges with low imperfection sensitivity.

A summary of the initial imperfection magnitudes for different load cases and their validity can be seen in Table 2.9.

Table 2.9 Summary of initial imperfection magnitude for different load cases regarding numerical simulations.

Initial imperfection magnitude for FE-simulations			
	Shear buckling	Patch loading	Flange buckling
Magnitude e	t_w or $\frac{h_w}{200}$	$\frac{a_1}{200}$	$\frac{c_f}{50}$
Validity	Comparative studies with experimental tests and numerical simulations indicates that $e=t_w$ is valid and realistic for larger bridge girders (~1600mm), but that it is conservative approach. $e = \frac{h_w}{200}$ from Eurocode can be used for lower girders.	Verified by comparison between experiments and numerical simulations.	Value from Eurocode.
Sources	(Driver, et al., 2006) (Hassanein, et al., 2017) (EN1990-1-5)	(Kövesdi & Dunai, 2009)	(EN1990-1-5)

2.4.3 Modelling stress-strain curves in FE-models with stainless steel

In nonlinear FE-models the material must be treated as elastic-plastic and damage conditions under complex stress condition shall be defined by Von-Mises criterion (Yong Song, Mei Yu, & Zhang, 2011). Because stainless steel has a different stress-strain behaviour compared to carbon steel, the stress-strain curve needs to be modified in FE-simulations according to Equation 31 and Equation 32 (SCI, 2017).

$$\varepsilon = \frac{\sigma}{E} + 0.002 \left(\frac{\sigma}{E} \right)^n \quad \text{for } \sigma \leq f_y \quad \text{Equation 31}$$

$$\varepsilon = 0.002 + \frac{f_y}{E} + \frac{\sigma - f_y}{E_y} + \varepsilon_u \left(\frac{\sigma - f_y}{f_u - f_y} \right)^m \quad \text{for } f_y < \sigma \leq f_u \quad \text{Equation 32}$$

Where σ is the engineering stress and ε is the engineering strain. E , f_y and f_u are all given in Table 2.5 and Table 2.6 for duplex stainless-steel type 1.4162. n and m are coefficients calculated from Equation 33 and 34.

$$n = \frac{\ln(4)}{\ln\left[\frac{f_y}{R_{p0.05}}\right]} \quad \text{Equation 33}$$

$$m = 1 + 2.8 \frac{f_y}{f_u} \quad \text{Equation 34}$$

Where $R_{p0.05}$ is the 0.05% proof stress and E_y is the tangent modulus of the stress-strain curve at yield strength, see Equation 35.

$$E_y = \frac{E}{1+0.002n\left[\frac{E}{f_y}\right]} \quad \text{Equation 35}$$

Where ε_u is the ultimate strain, corresponding to the ultimate strength f_u , see Equation 36 for duplex steel.

$$\varepsilon_u = 1 - \frac{f_y}{f_u} \quad \text{Equation 36}$$

In FE-simulations σ_{true} , ε_{true} and ε_{true}^{pl} are then used. These values are obtained from Equation 37, 38 and 39.

$$\sigma_{true} = \sigma(1 + \varepsilon) \quad \text{Equation 37}$$

$$\varepsilon_{true} = \ln(1 + \varepsilon) \quad \text{Equation 38}$$

$$\varepsilon_{true}^{pl} = \varepsilon_{true} - \frac{f_y}{E} \quad \text{Equation 39}$$

2.5 LCC study for bridge girders

To evaluate the different designs obtained from this thesis, an LCC-study will be performed. This is to know if it would be beneficial for future investors or companies to invest in this technology.

An LCC study is a way to compare the cost for a construction or product during its whole life cycle time. For a bridge with a life span of 100 years costs could be everything from initial investments to maintenance, repainting and supervision (Javier Veganzones Munoz, Pettersson, Sundquist, & Karoumi, 2016). Also, user costs should be included to show effects on the economy when traffic disturbance will occur during a repair.

For this thesis it will be sufficient to analyse only the steel beams and therefore everything else will be neglected. A carbon steel bridge suffers from corrosion and must be protected with painting at least two times during its life time, except from initial painting. A stainless-steel bridge though, might need a more expensive welding technique and has therefore larger initial costs considering manufacturing. Stainless steel is also approximately three times more expensive (year 2018 prices) compared to carbon steel and therefore a stainless-steel bridge would need less steel volume to be beneficial. In an LCC study also discounting of the money is included which means that all future costs are readjusted to be comparable with the value of today's money (Javier Veganzones Munoz, Pettersson, Sundquist, & Karoumi, 2016).

3 Existing bridges with corrugated steel web

There are many existing bridges using corrugated webs in the world. Mainly Japan and France are in the front of constructing them. This chapter will show application of corrugated web in real bridges.

3.1 Cross-section parameters of existing bridges with corrugated steel web

Example of corrugated steel webs in bridges can be seen in Table 3.1 (Hassanein, Elkawas, El Hadidy, & Elchalakani, 2017). All cross-section data used for design of the webs can be found and some short explanations of each bridge is presented in the following sections.

Table 3.1 Dimension of corrugated webs in existing bridges

Bridge name	a ₁ [mm] Flat panel length	a ₂ [mm]	a ₃ [mm] Corrugation depth	a ₄ [mm]	t _w [mm] Web thickness	h _w [mm] Web Height	s [mm]	w [mm] One length of corrugation wave	α [°] Angle	Described in section
Shinkai	250	250	150	200	9	1183	1000	900	36.9	3.2.1
Matsnoki	300	300	150	260	10	2210	1200	1120	30.0	-
Hondani	330	336	200	270	9	3315	1332	1200	36.5	3.2.2
Cognac	353	353	150	319	8	1771	1412	1344	25.2	3.3.1
Maupre	284	284	150	241	8	2650	1136	1050	31.9	3.3.2
Dole	430	430	220	370	10	2546	1720	1600	30.7	3.3.3
Ilsun	330	386	200	330	18	2292	1432	1320	31.2	3.4.2

3.2 Japan

Theoretical knowledge considering use of corrugated webs in bridges was first developed in Japan and has to date built over 140 bridges with the technology. This section presents some of them.

3.2.1 Shinkai Bridge, 1993

The Shinkai bridge is the first corrugated steel web bridge to be built in Japan year 1993. Construction principles is a single span box girder bridge with a total length of 31m (span is 30m) and a width of 14.8m. This bridge was constructed on site on a fabrication yard and then erected with the launched girder method (Ikeda & Sakurada, 2005).

3.2.2 Hondani bridge,

The third bridge with corrugated steel web built in Japan was Hondani bridge, see Figure 3.2. Construction is made of a three-spanned continuous prestressed concrete box girder. The length of the bridge is 198.2m and width is 11m. Largest span is 97.2m and the bridge was erected with the cantilever method, which greatly reduced the time of construction. The method on how to connect the web with the concrete slabs was embedded connection and single-shear joints between web plates were used. All types of connections were tested and verified before construction (Ikeda & Sakurada, 2005).



Figure 3.1 Hondani bridge Japan, Photo: JSCE

3.2.3 Himi Yume Bridge, 2004

The Himi Yume Bridge is a 3-span continuous extradosed prestressed concrete girder bridge with a centre span of 180 meters and a total length of 365 meters, see Figure 3.3. Because the bridge is extradosed it means that it is a cable-stayed bridge but with a more extensive bridge deck, being stiffer and stronger and allowing the cables to be placed closer to the tower and for the towers to be lower in relation to the span. This is the first bridge in the world to use the extradosed bridge structure. In addition, the bridge is post-tensioned using external prestressing tendons, which will give benefits considering accessibility for maintenance. The bridge was successfully completed in 2004 (Dywidag-Systems, 2018).



Figure 3.2 Picture of Himi Yume Bridge, Photo: sk01, Panoramio

3.2.4 Yahagigawa Bridge (Toyota arrows bridge), 2005

Yahagigawa Bridge is a four-span continuous, hybrid cable-stayed bridge. It is 820 meters long, measures 235 meters for the centre span. It was the first cable-stayed bridge utilizing corrugated webs (Boutillon, et al., 2015). The girder is a 43.8 meters wide, five-cell box structure with trapezoidal corrugated steel webs.



Figure 3.3 Picture of Yahagigawa Bridge, Photo: Tawashi2006, (Wikimedia commons).

3.3 France

Corrugated steel web bridges were, as first country in the world, built in France during 1980s (Ikeda & Sakurada, 2005). Composite bridges had been popular during some time but problems with creep and prestress forces transferred into steel plate webs made a change to corrugated webs interesting (Boutillon, et al., 2015). This section briefly describes some of the bridges constructed in France.

3.3.1 Cognac Bridge, 1986

The first ever built corrugated steel web bridge was Cognac bridge, see Figure 3.5, constructed in France 1986. It is a three-spanned continuous box girder bridge with total length of 105m and maximum span 43m. Erection method was the fixed scaffolding method and external cables are used for prestressing, which makes it possible to maintain or replace them in future (Ikeda & Sakurada, 2005). Cognac bridge proved that it was possible to construct bridges with corrugated webs and is therefore an important bridge for the development of this design method.



Figure 3.4 Cognac Bridge France, Photo: The constructor

3.3.2 Maupre bridge, 1987

Maupre Bridge, see Figure 3.6, was the second bridge that was built with a corrugated steel web, designed by Pierre Thivans, Jacques Combault and Michel Duviard, and completed in 1987. The composite box-girder is triangular and consists of two inclined steel-webs and a horizontal concrete deck, which is transversally prestressed. At the lowest point of the two webs, they are joined on a steel pipe filled with concrete to withstand compression forces (Boutillon, et al., 2015). The bridge is straight 324 meters long and have five spans. The combination of triangular shaped girder and corrugated web makes it possible to remove all diaphragms, a member which resists lateral forces and transfer loads to support.



Figure 3.5 View of Maupre bridge, Photo: J. Mossot, Structurae.net

3.3.3 Dole Bridge, 1993

Forth bridge constructed with a corrugated steel web in France was Dole bridge, see Figure 3.7. The 7-spanned bridge has a length of 497.6m and a maximum span of 80m. Cross-section is a box girder and both external and internal cables were used for prestressing (Ikeda & Sakurada, 2005).



Figure 3.6 Dole Bridge, Photo: Jacques Mossot, *Structuare.net*

3.3.4 Meaux Viaduct, 2004

Meaux Viaduct is a composite structure with two prestressed concrete slabs and a steel web. The steel web properties are like those of corrugated steel web but with a different technology. The web flexibility under compression forces is obtained with a succession of tubes and plate elements.



Figure 3.7 Picture of Meaux viaduct, Photo: V. Le Quéré, *structurae.net*

3.4 Other countries where corrugated steel web has been used in bridge design

Bridges with corrugated steel webs have also been constructed in other countries than Japan and France. Some interesting bridges are described in this section.

3.4.1 Altwipfergrund Bridge Germany, 2001

The first composite bridge with a corrugated web built in Germany is Altwipfergrund Bridge. The bridge consists of three spans, with an end span of 82 meters and a mid-span of 115 meters and was built using the cantilever method (Boutillon, et al., 2015). First the corrugated steel plates were erected and then the upper and lower concrete decks were cast on site. The connections between the upper slab and corrugated steel

web were basically studs with U-shaped square bars to resist transverse bending moments. The jointing between corrugated steel plates was used single or double shear friction connection (Ikeda & Sakurada, 2005).



Figure 3.8 Picture of Altwipfergrund Bridge, Photo: M. Sander, Wikimedia Commons

3.4.2 Ilsun Bridge Korea, 2007

First corrugated steel web bridge constructed in Korea and the longest and widest ever built (Kwanghoe, Kwangsoo, Chungwook, & Jang-Ho, 2010), is Ilsun bridge see Figure 3.10. It is divided into a 12-spanned and 2-spanned continuous box girder bridge with a total length of 801m and width of 30.9m. Maximum span is 60m and construction method was incremental launching method which according to (Kwanghoe, Kwangsoo, Chungwook, & Jang-Ho, 2010) is a rare type of method considering these type of bridges. The concrete parts of bridge were installed after erection of the steel sections. This reduced the self-weight of bridge during construction and therefore made it easier to use the incremental launching method (Ikeda & Sakurada, 2005).



Figure 3.9 Ilsun Bridge, Photo: (Kwanghoe, Kwangsoo, Chungwook, & Jang-Ho, 2010).

4 Setup for numerical simulations in ABAQUS

To verify that the analytical calculations are correct for the case studies, numerical simulations will be performed in ABAQUS. This model will also be used for the parametric study in section 7. The corrugated web is only taking shear load and the flanges are assumed neglectable considering shear capacity and therefore they are not investigated in the FE-studies. The simulations are conducted by acquiring the first shear buckling mode in a linear-elastic buckle analysis and use it as initial imperfection in a non-linear analysis of the girder as described in section 2.4.2. The initial imperfection is set to t_w according to section 2.4.2. To ensure that the actual design is verified and correct, the results from the FE-simulation needs to give larger shear capacity than from analytical calculations with Eurocode. This is because Eurocode formulas are conducted with linear-elastic theory and FE-simulations uses non-linear theory. This should give some extra capacity due to plastic redistribution in the steel material.

4.1.1 Modelling shear buckling in ABAQUS

When modelling non-linear stainless steel in ABAQUS, material behaviour is modelled as described in section 2.4.3. The true stress-strain curves for stainless steel 1.4162 are different depending on thickness of the material. Plastic material behaviours used in this project are presented in Figure 4.1 and in Table 4.1.

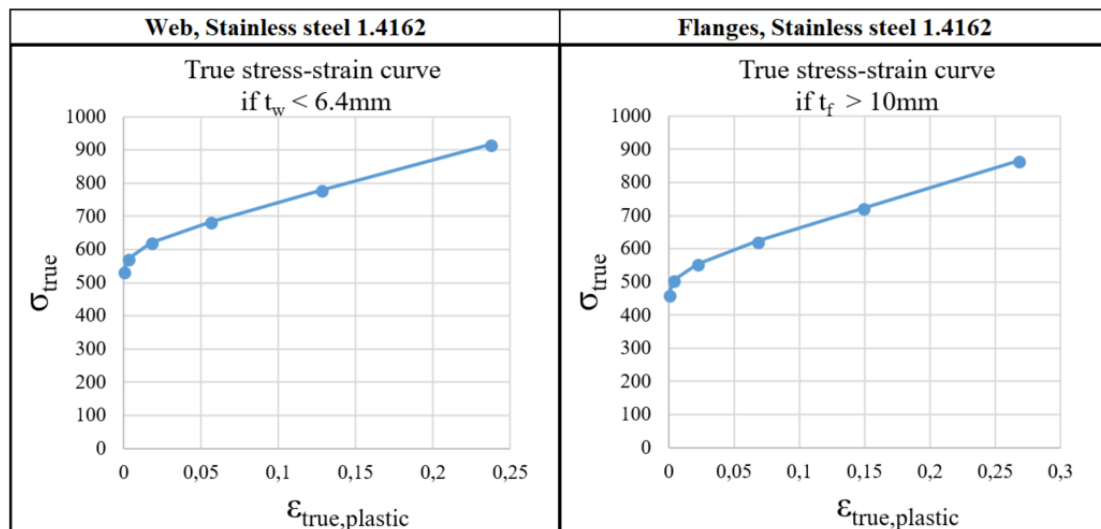


Figure 4.1 True stress-strain curve for stainless steel 1.4162 for web and flanges.

Table 4.1 Input parameters for true stress-strain curve.

True stress-strain Stainless 1.4162			
$t_w < 6.4\text{mm}$		$t_r > 10\text{mm}$	
Sigma true	Epsilon true plastic	Sigma true	Epsilon true plastic
532	0	462	0
572	0,0028	504	0,00367
620	0,01755	554	0,02207
684	0,0561	623	0,06766
779	0,12776	723	0,14879
917	0,2368	866	0,26778

Parts in ABAQUS are constructed as 3D shell elements, web and vertical stiffener as extrusion and flanges as planar. These are later assembled into a larger part which is the actual beam with a corrugated web presented in Figure 4.2.

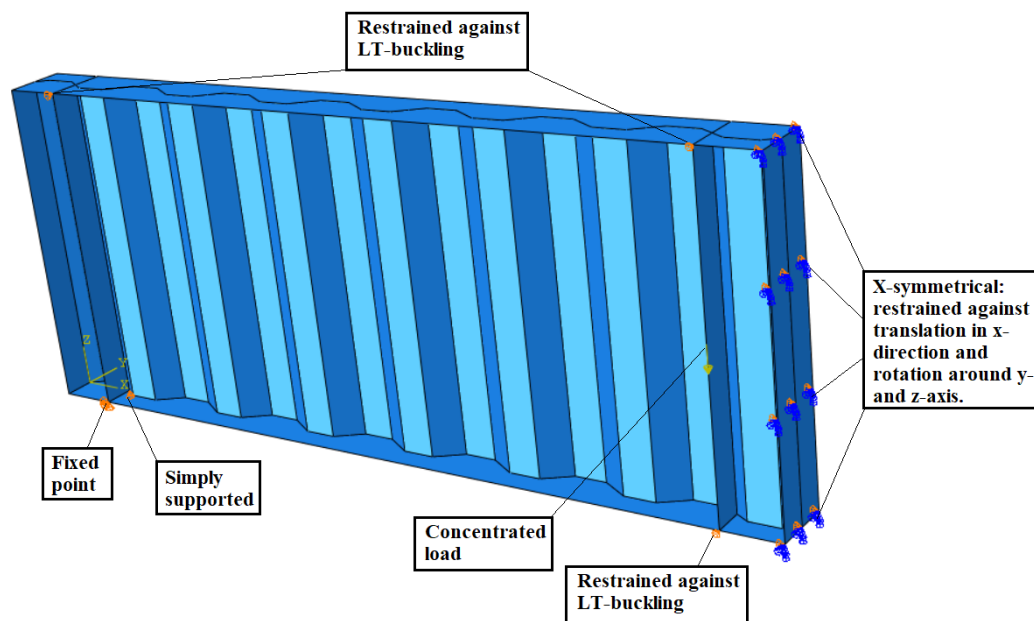


Figure 4.2 ABAQUS model used for shear buckling analysis.

Three different boundary conditions are used. The beam is simply supported at the ends which is modelled as translation restraint in z-direction. One point need to be fixed in all directions so that rigid body motion is avoided. The beam also needs to be restrained against lateral-torsional buckling and therefore points along the flanges are fixed in translation y-direction. The load is concentrated and placed at points on both sides of the vertical stiffener. The beam length is created to achieve the same Length-Height-ratio for all tested specimens.

4.1.2 Mesh convergence study

A mesh convergence study is performed to see if a certain mesh size is valid for the FE-simulations. Several mesh sizes are tested in a linear buckle analysis and the study is converging when the eigenvalue is converging. Element shape used in ABAQUS is quad and elements are freely organized. Results are presented in Figure 4.3.

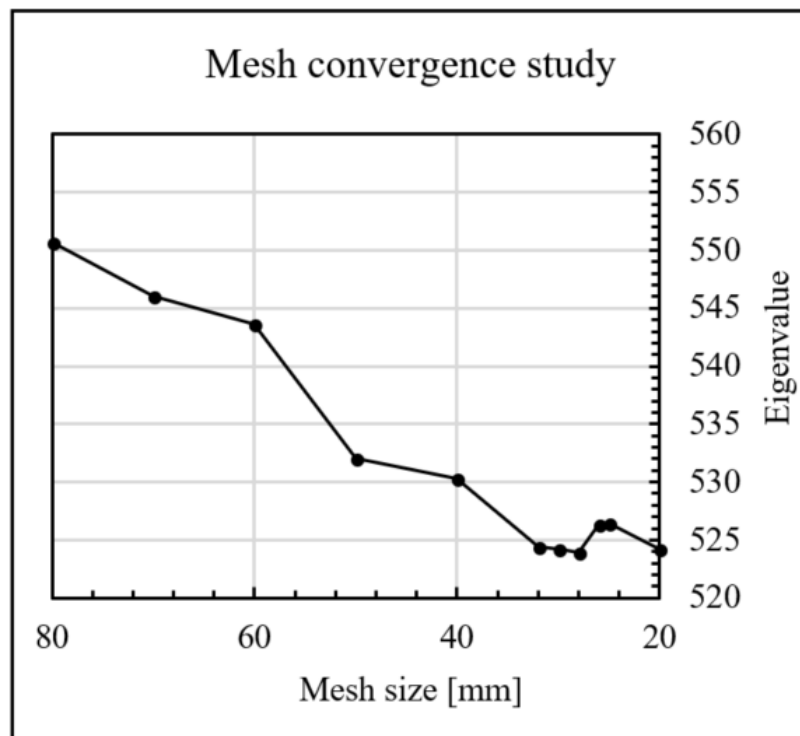


Figure 4.3 Mesh convergence study for a girder with a corrugated web.

It can be concluded from the convergence study that a sufficient mesh size is approximately 30mm because it is where the eigenvalues start to converge. This size will therefore be used in all FE-simulations to ensure that the FEM setup is correct and gives valid results.

4.1.3 Buckling modes in ABAQUS

As described in section 2.2.3 there are three different shear buckling modes for a corrugated web. These are global, interactive and local buckling. To ensure that the FE-model can simulate all three of these ones, different sizes are tested to achieve all buckling modes. The results are presented in Figure 4.4.

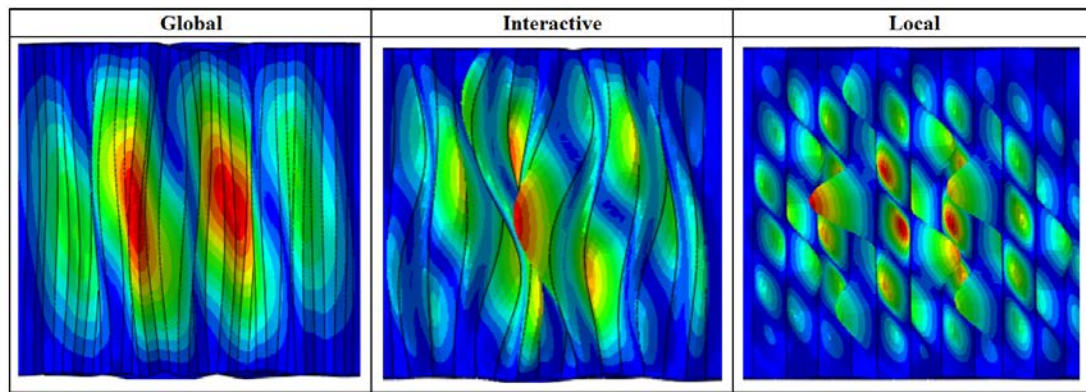


Figure 4.4 Buckling modes achieved for different geometries of corrugated webs, deformed shape.

The buckling modes are well defined in ABAQUS results and easy to differ from each other's. The results do match the theory about buckling modes as described in section 2.2.3 and this ensure that the FE-model can describe all three buckling modes.

5 Skulnäs Bridge – Simply supported road bridge

The first case study in this thesis is about Skulnäs bridge, which is a composite bridge over Swedish E4 European road with a span of 32 meters. It is simply supported and constructed by two steel I-beams and a concrete deck roadway which are in full interaction by welded shear studs. The original design is made of carbon steel S355 and S420 and vertical stiffeners is placed with 8 meters distance. Depth of the steel girder is 1.4 meters and the cross-section is constant along the whole bridge. A principle sketch of the bridge girder can be seen in Figure 5.1. The construction is made to withstand self-weight, wind-load and traffic load presented in report from (Mosiello & Kostakakis, 2013).

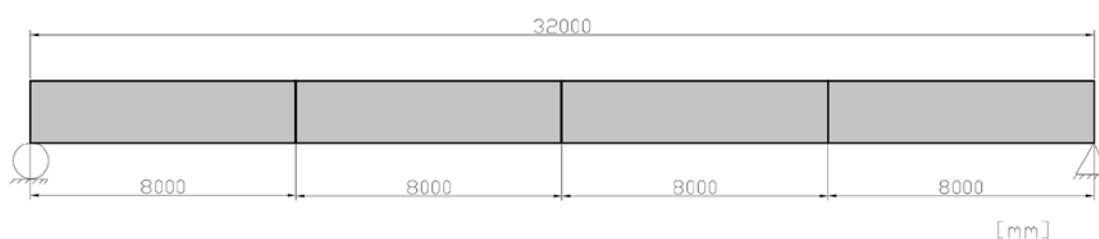


Figure 5.1 Principal sketch of Skulnäs bridge.

Design loads used in calculations are summarized and presented in Table 5.1. These are the loads upon which the bridge shall withstand, and the utilization ratios are calculated from.

Table 5.1 Design load effects for Skulnäs bridge.

Design loads	Value	Unit
M_{ULS}	$12.014 \cdot 10^6$	Nm
V_{ULS}	$1.523 \cdot 10^6$	N
M_{SLS}	$9.673 \cdot 10^6$	Nm
$M_{initial}$	$3.517 \cdot 10^6$	Nm

5.1 Previous results and new design

To make improvements regarding the original design, the approach is to introduce stainless steel as material and to use corrugation in the girder web. Previous calculations and simulations has given cross-section data regarding the carbon steel flat web design, which together with new optimized designs can be seen in Table 5.2. The stainless steel flat web design is made by modifying previous work from (Mosiello & Kostakakis, 2013) with properties and design codes for stainless steel. The new corrugated web designs are obtained by creating a Matlab routine, see Appendix A, which simulates many different designs according to (EN1990-1-5, 2006) and picks to most optimal design. The material used for the design is stainless steel 1.4162 which mechanical properties is described in section 2.3.2.

Table 5.2 Cross-section data for different designs of Skulnäs bridge.

[mm]	Flat web design		Corrugated web design					
	Original design Carbon steel	Stainless steel	Stainless steel			Stainless steel		
h_{web}	1340	1420	1421	α [°]	32	2500	α [°]	31
t_{web}	12	11	4.2	a_1	80	3.68	a_1	220
t_{top}	28	30	29	a_2	80	25	a_2	220
b_{top}	500	400	394	a_3	43	334	a_3	113
t_{bottom}	33	35	45	a_4	68	28	a_4	189
b_{bottom}	610	450	409			388		
Area steel	0.0502m ²	0.0434m ²	0.03624m ²			0.02896m ²		
Reduction	0%	-13.5%	-27.8%			-42.3%		
Design method	Eurocode	Eurocode	Eurocode			Eurocode and FEM (ABAQUS)		

When keeping the flat web but changing the material to stainless steel, the material use is reduced by 13.5% which is related to a higher yield- and ultimate strength of the material. When keeping web depth and changing the flat web to a corrugated web, the material use is reduced even further by 27.8%. This is mainly because a slenderer web can be used and therefore the web thickness is much lower than for the flat web design. The design is further developed by increasing the height of the web to 2500mm. This shows a material reduction of 42.3% which is mainly a result of further reduction of flange dimensions. The latter could only be achieved having deep stable webs which would lead to lower bending stresses in the flanges. To use such deep webs for Skulnäs bridge is only of theoretical significance as limitations with regard to the construction height are often the governing criteria. However, it is interesting to investigate a very slender web because this is where the corrugated web has its largest advantages.

Checks and utilization ratios regarding ULS, SLS and FLS for previous and new designs can be seen in Table 5.3. For the new design considering stainless steel and corrugation, the ratios are obtained from analytical calculations. To ensure that these results are correct numerical simulations will be performed and evaluated in section 5.2.

Table 5.3 Utilization ratios from analytical calculations for the different designs of Skulnäs bridge.

	Check	Flat web design		Corrugated web design	
		Original design Carbon steel	Stainless steel	Stainless steel Hw=1421mm	Stainless steel Hw=2500mm
ULS	Bending	0.78	0.83	1.0	1.0
	Shear	0.65	0.80	1.0	1.0
	Buckling during casting / LT-buckling	0.63	0.99	1.0	1.0
SLS	Deflection	0.90	1.0	0.91	0.62
FLS	Mid span	0.50	0.82	-	-

The first design with carbon steel has a relatively low utilization ratios which indicates that it uses more material than necessary or that some other design parameter was decisive. Also, the flat web with stainless steel, shows some lack in optimization but has higher ratios than the first design. Notable is that FLS calculations is not presented for the corrugated web designs. It is assumed that this will not be critical due to indications from the literature study.

The optimized cross-sections with corrugated webs has high optimized utilization ratios. The only check that does not achieve 1.0 is the SLS deflection check. This is because it is very dependent on the depth of the girder. Therefore, the lower girder has a higher SLS utilization ratio than the deeper.

Buckling during casting and lateral torsional buckling are checked because the girder is not in full interaction with the concrete deck during casting. Therefore, the top flange can buckle due to self-weight of the girder combined with the concrete. After a while, the concrete will cure and get hard and therefore the ULS bending check is only controlled for the bottom flange.

5.2 Results numerical simulations for Skulnäs bridge

To ensure that analytical calculations are valid and correct, numerical simulations in ABAQUS are performed for the new corrugated web designs. The obtained shear buckling modes for both girders can be seen in Figure 5.2.

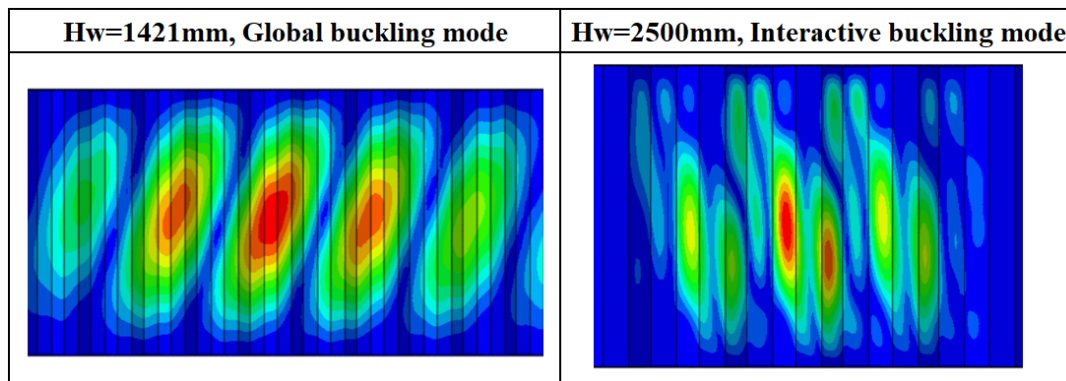


Figure 5.2 Shear buckling modes for the corrugated web designs, non-deformed shape.

The shear buckling mode for the girder with a web depth of 1421mm is global and for web depth of 2500mm the buckling mode is interactive, which is a combination of global and local buckling further explained in section 2.2.3.

The ultimate shear capacities of the two corrugated web designs are presented in Figure 5.3. Initial imperfection is set to be equal thickness of the web for both simulations.

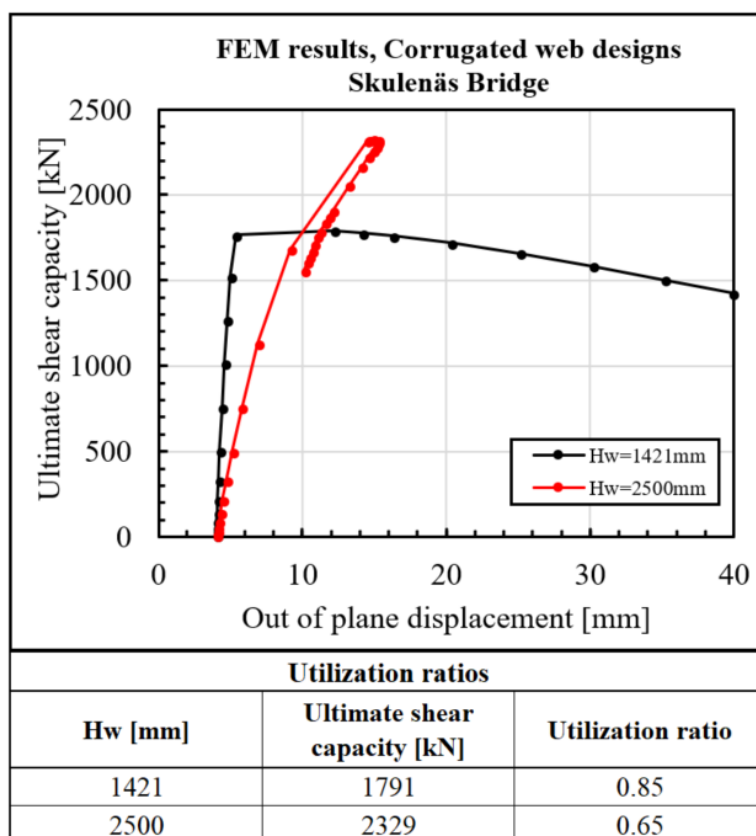


Figure 5.3 FEM results for corrugated web designs and utilization ratios.

There is a large difference between the two girders regarding capacity and post-buckling behaviour. The girder with a lower web shows a ductile stress-strain curve after buckling and the deep girder shows a faster failure. This is further investigated in

the parametric study, see section 7.1. Both designs fulfil criteria's regarding design loads and the utilization ratios are lower than for the checks in the analytical calculations. Especially for the deeper web, the utilization ratio is much lower than analytical calculations. This depends on (EN1990-1-5, 2006) which is not adapted to the material stainless steel in combination with a corrugated web. A proposal on how to change design codes is made in section 7.7. Also, contribution from flanges and other parameters such as choice of initial imperfection can have impact on shear capacity.

For a more detailed list of FE-results regarding Skulnäs bridge, see Appendix B.

5.3 Life Cycle Cost study

An LCC study is performed to compare the different alternatives total cost over a lifetime of 100 years. This is to know if it would be beneficial for future investors or construction companies to use stainless steel in girders and bridges. Everything that does not have a connection with the steel girders are excluded from this analysis. This means that only investments cost will be considered when making LCC for stainless steel bridges, because it lacks any need of repainting or maintenance. A conventional carbon steel bridge needs repainting after some years, were traffic disturbance and user costs will follow. These costs will be larger for a road with more traffic such as highway bridges. Welds is also included in the LCC because it is a bigger cost to weld with stainless steel generally. Though thin webs used for corrugated webs only need to be welded on one side which reduces the cost for these.

Investment costs used in the LCC for Skulnäs bridge can be seen in Table 5.4 where material prices are obtained from BE groups pricelists of 2017 (BEgroup, 2017). It should be noted that prices on different steel and painting materials vary over time.

Table 5.4 Investment costs used in LCC analysis.

	Unit	Price [SEK/unit]
Carbon steel S355	ton	20000
Stainless steel duplex 1.4162	ton	65000
Design and transportation for flat web girders	girder	125000
Design and transportation for corrugated web	girder	150000
Initial painting carbon steel	m ²	1900
Welding material S355	kg	159
Welding material 1.4162	kg	415

During some intervals the bridge needs to be maintained or repaired. Therefore, inspections are being performed for both carbon steel and stainless-steel bridges. The carbon steel bridges though, need more inspections and repairs due to problems with corrosion. A summary of maintenance and inspections can be seen in Table 5.5.

Table 5.5 Maintenance and repair operations used in LCC analysis.

	Interval year	Unit	Price/unit [SEK]	Days	Affected road length [km]
Inspection for carbon steel bridge regarding patch painting	1	-	3240	0.5	0.5
Large inspection all bridge types	6	-	18900	0.5	0.5
Re-painting main girder and cross beam	25	m ²	2100	5	0.5

When the bridge is maintained or repainted there will be disturbance in traffic and therefor costs will follow. These will be larger for a bridge with more traffic or larger speed reductions due to road shut-offs. A summary of user costs used in this LCC is obtained from (Javier Veganzones Munoz, Pettersson, Sundquist, & Karoumi, 2016) and can be seen in Table 5.6.

Table 5.6 User costs used in LCC analysis.

	Value
Percentage of heavy vehicles	10%
Affected road length	0.5 km
Speed reduction	-60 km/h for low ADT -40 km/h for medium ADT -30 km/h for high ADT
Time value heavy vehicles	540 SEK/h
Time value passenger vehicles	145 SEK/h

Results from the LCC study can be seen in Figure 5.4, where ADT is the average daily traffic and yearly interest rate is the rate an investor would be paid if he or she would put the investment somewhere else with a specific rate, for example a bank account or the stock market. There are many ways to vary ADT and yearly interest rates and therefore three different ADT was used for every design to get a hint on what would happen if the bridge was situated in a more trafficked area.

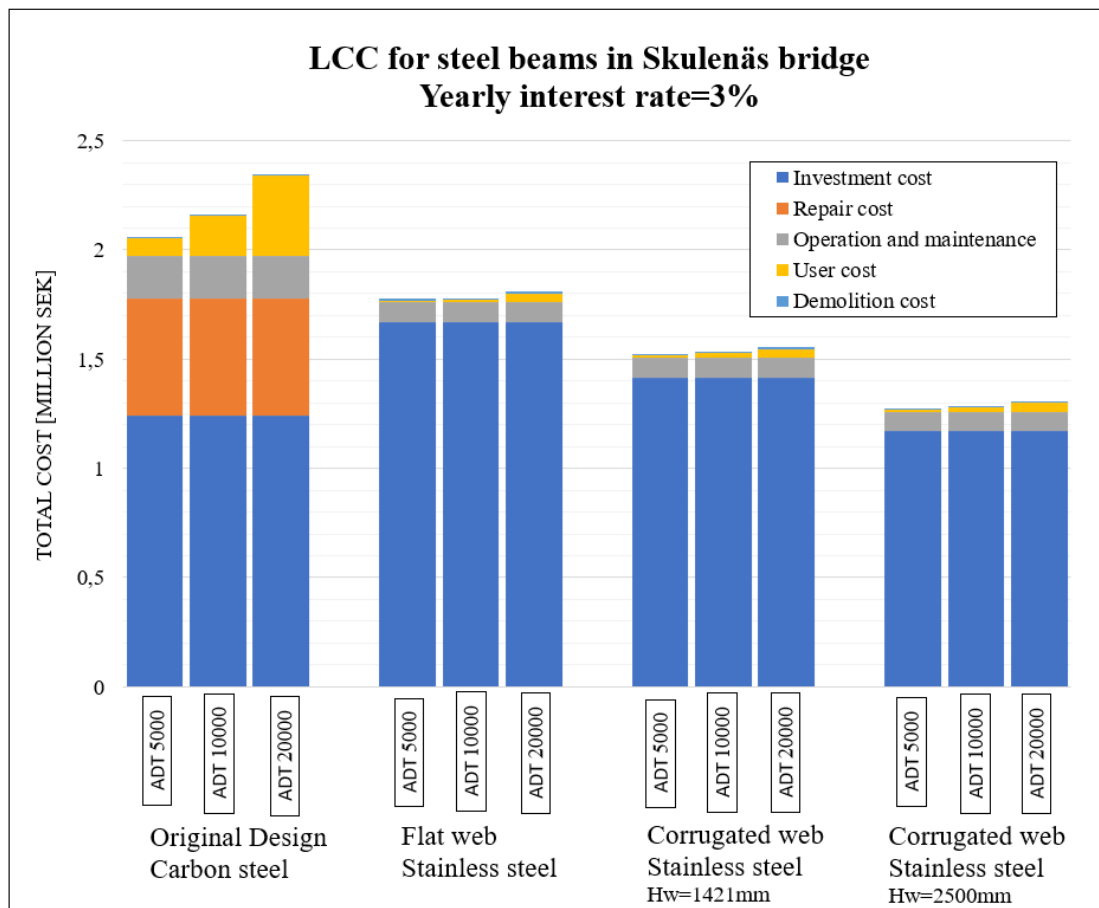


Figure 5.4 LCC study for Skulnäs bridge.

From Figure 5.4 the design with carbon steel is the costliest one during a lifetime of 100 years. It is also clear that the other alternatives have lower costs when the material use is reduced and therefore the design with the deep girder has the lowest overall cost. The investment costs are higher for all stainless-steel materials which is because of an approximately three times higher price on stainless steel. The main difference between the carbon steel bridge and the stainless-steel alternatives is the repair, maintenance and user costs which depends on repainting and more inspections. The change of ADT has largest influence on the carbon steel bridge for the same reasons. A detailed list of results from LCC analysis regarding Skulnäs bridge designs can be found in Appendix C.

There are many factors that can be changed in a LCC analysis and one of them is the yearly interest rate which is the interest rate an investor would get if putting the

investment somewhere else. A sensitivity analysis regarding interest rate can be seen in Figure 5.5.

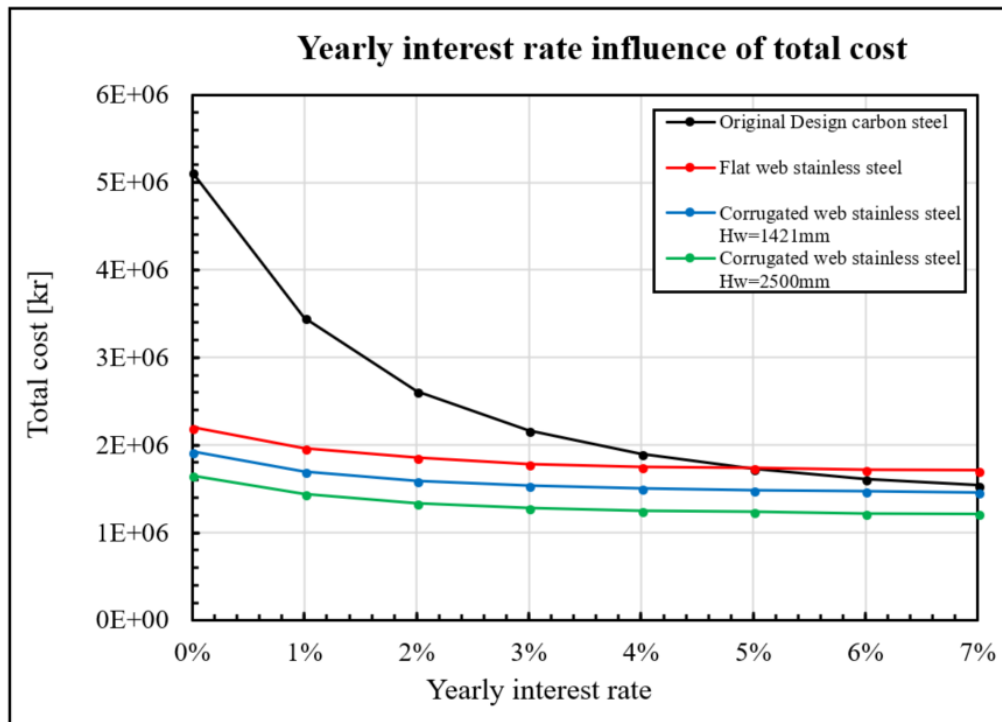


Figure 5.5 Sensitivity analysis regarding yearly interest rate and LCC for Skulnäs bridge designs.

As seen in Figure 5.5 the yearly interest rate has a major impact for the carbon steel bridge. This is because a lot of the costs are in the future. When the yearly interest rate is around 5%, the carbon steel bridge has the same lifetime cost as the flat web stainless steel design. It should be noted that the cost for the carbon steel girder is higher even at a rate of 7%.

The LCC analysis shows that it is very likely that use of stainless steel in bridge girders would reduce total costs for an investor. If lifetime was expanded the benefits of stainless steel would be even more. When introducing a corrugated web design, the total costs reduces with -29% for the same web height and -41% for a deeper girder. Except from economic benefits, there can be environmental reasons to not do extra bridge maintenance or use steel painting. These matters however, needs to be investigated in further life cycle analysis focusing on environmental impacts.

5.4 Summary

This section summarizes the results from the investigations regarding Skulnäs bridge and its steel girder. A summary of all design alternatives regarding material reduction and total lifetime costs can be seen in *Table 5.7*.

Table 5.7 Summary of new designs for Skulnäs bridge regarding material use and total cost.

	Material use reduction	Total cost reduction
Carbon steel original design	0%	0%
Stainless steel flat web design	-13.5%	-17,5%
Stainless steel corr. web, Hw=1421mm	-27.8%	-29,2%
Stainless steel corr. web, Hw=2500mm	-42.3%	-40,6%

There is a clear relationship between change of design and reduction of material and total costs. The reduction of material is because of higher yield strength in the stainless-steel material and ability to construct more slender girders because of corrugation. The reduction of materials in the girder is clearly related with the web height and therefore it can be an advantage to be able to construct as deep girders as possible when using corrugated webs.

6 Nissan Highway Bridge – Continuous road bridge

Nissan highway bridge is a continuous highway bridge crossing the river Nissan, Sweden, see Figure 6.1. The existing bridge is obtained from (Mosiello & Kostakakis, 2013) and will be improved by using stainless steel with flat web and corrugated web. The span lengths are 13m, 11m and 13m and distance between vertical stiffeners is 8m.

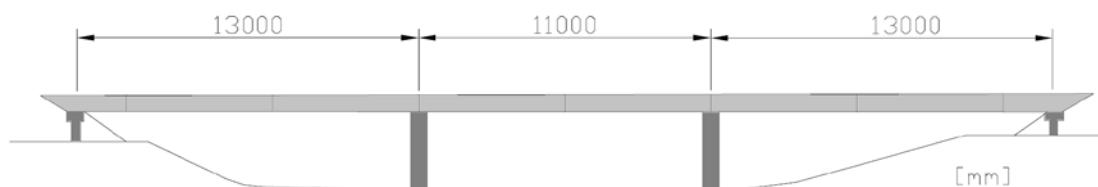


Figure 6.1 Longitudinal view of continuous highway bridge over Nissan, Sweden.

The bridge contains a concrete cast-in-situ deck on top of two steel girders, continuously supported over columns. There is full composite action between the deck and girders. The original bridge is made in steel class S355 and the stainless steel used for the new designs is Duplex 1.4162.

The design loads used in the design can be seen in Table 6.1. The largest moment is obtained in the largest span and the largest shear force is from support.

Table 6.1 Design loads for Nissan bridge.

Design loads	Value	Unit
M_{ULS}	$3.67 \cdot 10^6$	Nm
V_{ULS}	$1.52 \cdot 10^6$	N
M_{SLS}	$1.16 \cdot 10^6$	Nm
$M_{initial}$	$0.589 \cdot 10^6$	Nm

6.1 Previous results and new design

Cross-section variables for existing bridge and new designs with stainless steel and a corrugated web, can be seen in Table 6.2. The same approach is used as for Skulnäs bridge, see section 5.1, when obtaining new designs.

Table 6.2 Overview of all cross-section designs regarding Nissan bridge.

[mm]	Original design carbon steel	Stainless steel flat web	Stainless steel corrugated web Hw=500mm			Stainless steel corrugated web Hw=1525mm		
h_{web}	510	495	500	α [°]	31	1500	α [°]	31
t_{web}	16	14	10.9	a_1	71	4.1	a_1	72
t_{top}	25	20	24	a_2	71	25	a_2	72
b_{top}	400	400	309	a_3	37	204	a_3	37
t_{bottom}	45	35	46	a_4	61	28	a_4	62
b_{bottom}	400	400	353			202		
Area steel	0.036m ²	0.028m ²	0.02962m ²			0.01744m ²		
Reduction	0%	-22.2%	-17.7%			-51.6%		

The new cross-sections with stainless steel shows reductions regarding material use. For the girder with flat web the reduction is 22.2% and for the corrugated web girder it is 17.7% and 43.6% respectively. Utilization ratios regarding ULS, SLS and FLS for the cross-sections can be seen in Table 6.3. Ratios are obtained from analytical calculations with formulas from (EN1990-1-5, 2006).

Table 6.3 Utilization ratios for all Nissan bridge designs, analytical calculations.

	Check	Original design carbon steel	Stainless steel flat web	Stainless steel corrugated web Hw=500mm	Stainless steel corrugated web Hw=1500mm
ULS	Bending	0.87	0.92	1.0	1.0
	Shear	0.91	0.95	1.0	1.0
	Buckling during casting / LT-buckling	-	-	1.0	0.99
SLS	Deflection	0.51	0.97	0.72	0.55
FLS	Detail 1: Mid span	0.18	-	-	-

The new corrugated web designs show high utilization ratios on all parameters except SLS deflection. Especially the girder with a deep web shows low ratios regarding SLS deflection. This is because a deep girder has larger resistance against deflection.

6.2 Results numerical simulations for Nissan bridge

Nonlinear numerical simulations are performed to ensure that results from the analytical calculations are valid. For Nissan highway bridge the simulations were made regarding shear buckling capacity and the same approach was used as for Skulnäs bridge in section 5. The first shear buckling mode can be seen in Figure 6.2.

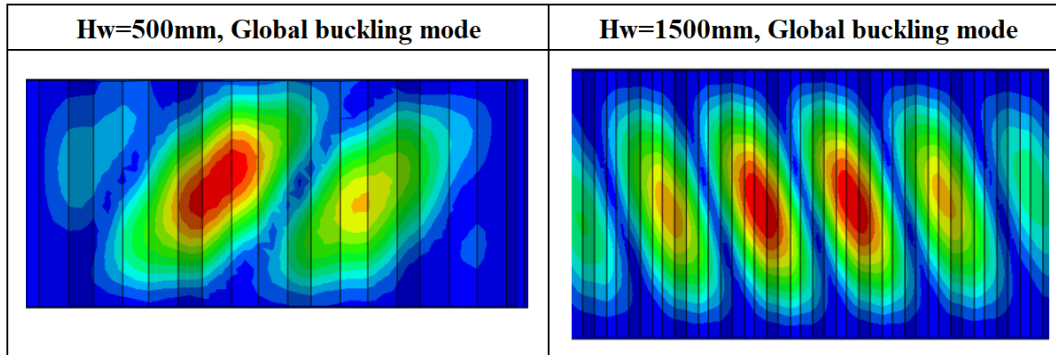


Figure 6.2 First shear buckling mode from FE-simulations for both corrugated web girders, non-deformed shape.

The buckling mode for both girders are global buckling which was also obtained from analytical calculations. The initial imperfection is set to t_w for each girder. The nonlinear analyse gives ultimate shear capacities which can be found in Figure 6.3.

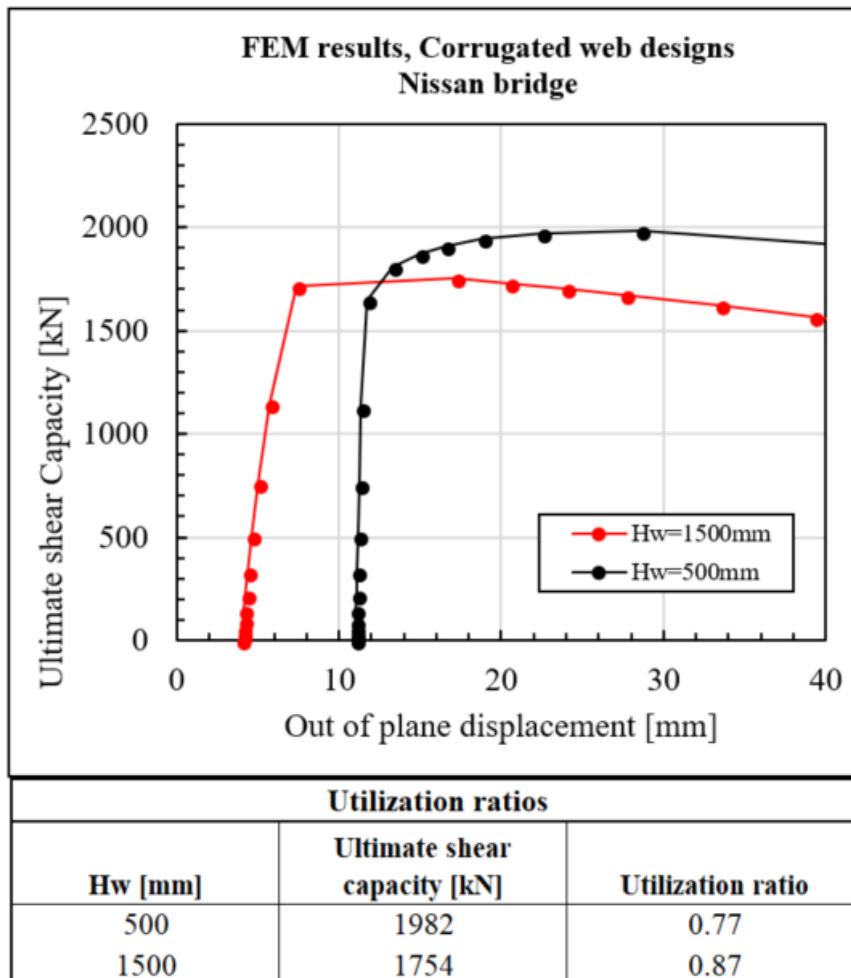


Figure 6.3 Results from FE-simulations regarding ultimate shear capacity for corrugated web designs.

The ultimate shear capacities obtained from the FE-simulations fulfils the requirements of which the girder was designed and gives validity regarding analytical calculations.

For a more detailed list of FE-results regarding Nissan bridge, see Appendix B.

6.3 Life Cycle Cost study

An LCC study is performed for the three alternatives with the same conditions as for Skulnäs bridge in section 5.3. The only difference for this study is that the allowed speed limit for the road is increased to 110km/h and that this will give a larger cost when maintenance works are performed, and speed limits needs to be reduced. The result from the LCC study can be seen in Figure 6.4.

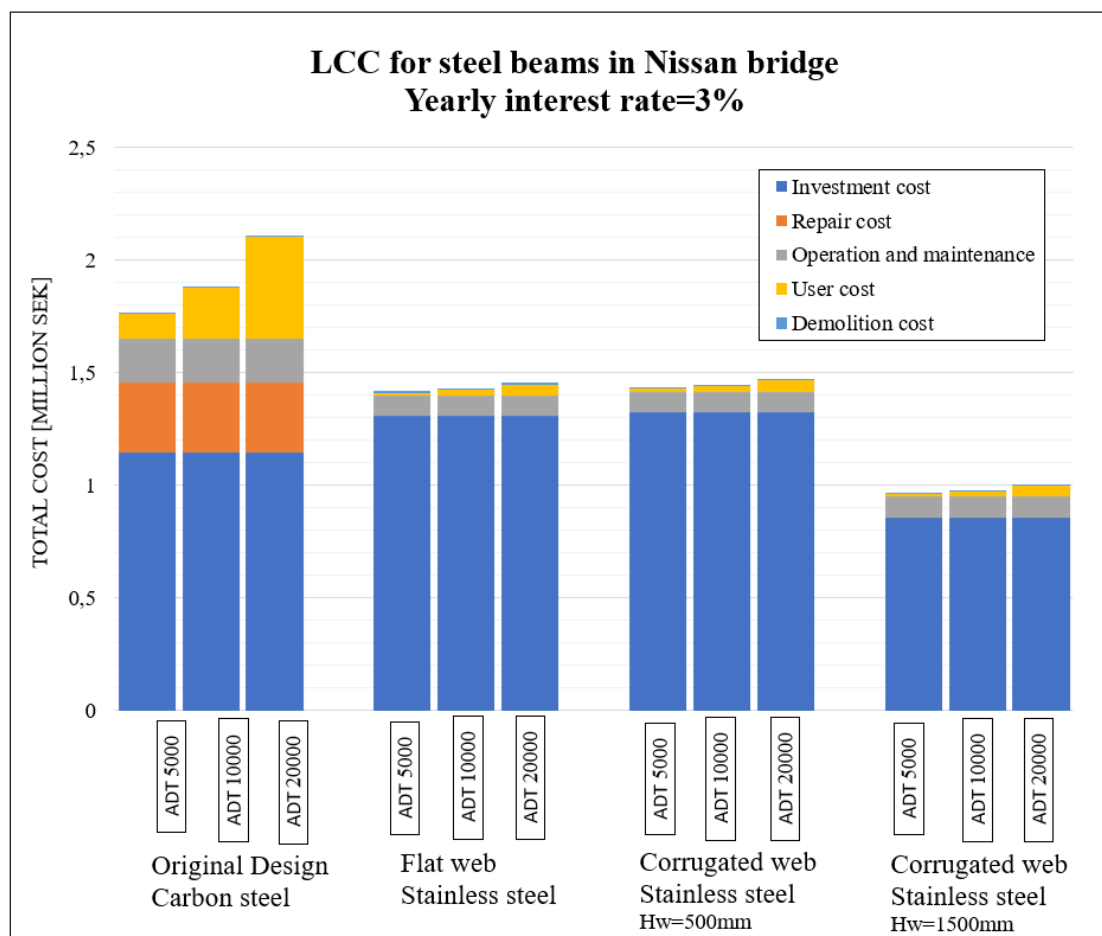


Figure 6.4 LCC study for all alternatives regarding Nissan bridge.

All alternatives with stainless-steel show a lower cost during a lifetime of 100 years for the bridge. Especially the alternative with stainless steel, deeper web and a corrugated web shows much lower costs. This is because large reduction of material uses and no maintenance costs due to traffic disturbance. A detailed list of results from LCC analysis regarding Nissan bridge designs can be found in Appendix C.

6.4 Summary

A summary of all designs for Nissan bridge can be seen in Table 6.4.

Table 6.4 Summary for Nissan bridge regarding material use and total cost.

	Material use reduction	Total cost reduction
Carbon steel original design	0%	0%
Stainless steel flat web design	-22.2%	-31.1%
Stainless steel corr. web, Hw=500mm	-17.7%	-30.2%
Stainless steel corr. web, Hw=1500mm	-51.6%	-52.5%

Results indicates that use of stainless steel will reduce total cost and material use for a bridge girder. Also, if the girder can be deep it will have large influence on material use. Nissan highway bridge girder is relatively small, 500mm, and therefore a change to corrugated web with the same web height will not use less material than if the web is kept flat.

7 Parametric study

To investigate the influence of different parameters on the shear capacity of a corrugated web, a parametric study is performed. The main purpose is to expand our knowledge on how to optimize the shape of a corrugated web by adjusting different inputs, but also to see if there is enough correlation between analytical calculations from Eurocode (EN1990-1-5, 2006) and FE-simulations in ABAQUS. The designs are kept the same for most studies to be more comparable and make it easier to draw conclusions. Four different web heights are considered, and the two initial imperfection magnitudes are in accordance with section 2.4.2. Same FE-model as presented in section 4 is used for the parametrical study. The material used is stainless steel 1.4162 with the true stress-strain curve presented in Figure 4.1. The approach used when modelling is to achieve the first positive eigenvalue and buckling mode in a linear buckle analysis, performed in ABAQUS, and use this to model a nonlinear simulation with initial imperfection.

Further this section will investigate how shear buckling reduction factors can be modified for the purpose to model stainless steel with corrugated webs, of which there is no good approach in Eurocode today. This is achieved by doing regression studies of many FE-simulations and summarize these into shear buckling curves for Stainless steel.

Detailed results from the parametric study regarding all investigated parameters can be found in Appendix D and shear buckling modes when changing flat fold length can be seen in Appendix E.

7.1 Influence of initial imperfections

As seen in previous studies for corrugated webs with carbon steel, initial imperfection has a large impact on the ultimate shear capacity. However, there has not been much research regarding corrugated webs with stainless steel. Four girder designs with the same cross-sections except web height, were studied for five different initial imperfections in ABAQUS. Web thickness is kept to 4mm, corrugation angle is 32 degrees and flat fold length is 100mm. Results can be seen in Figure 7.1.

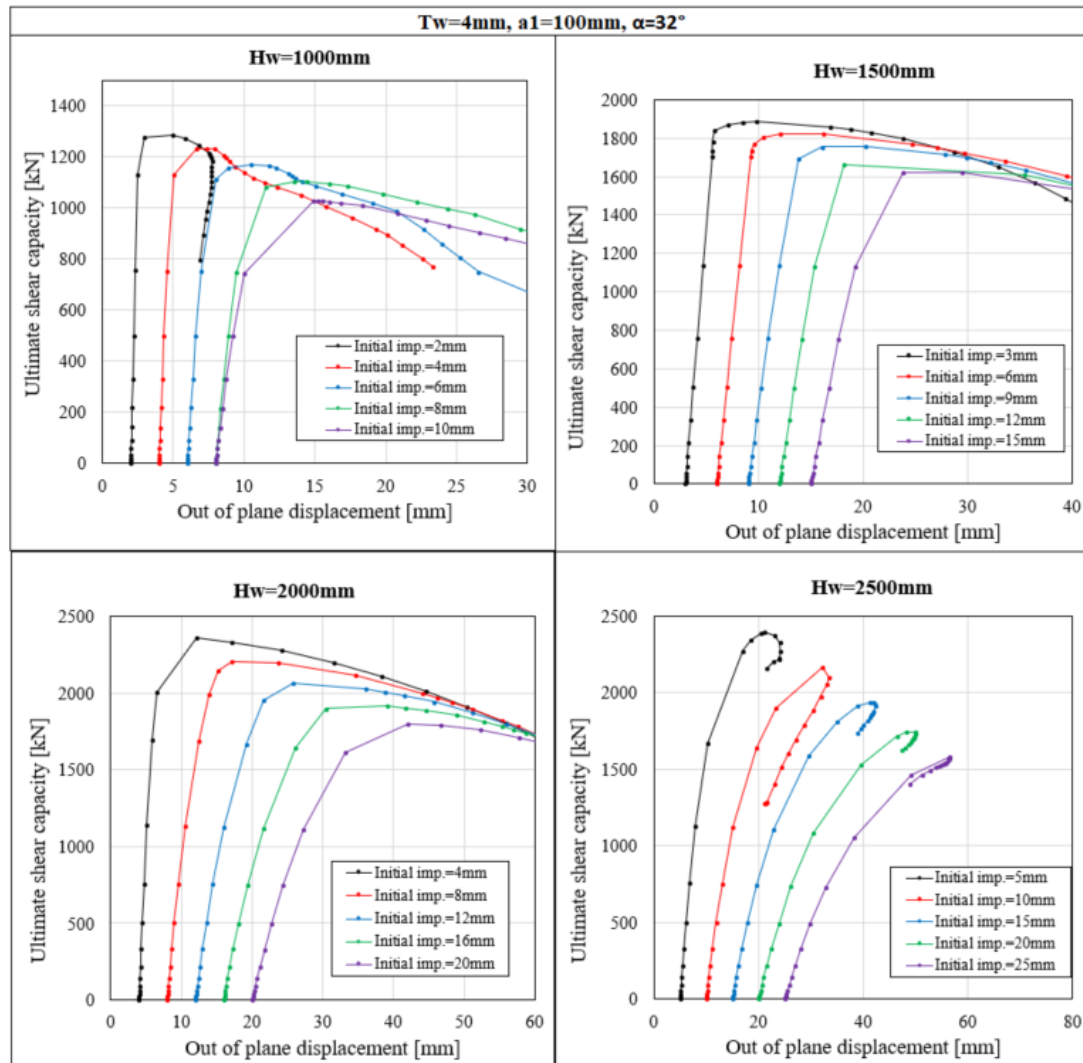


Figure 7.1 Influence of initial imperfection for corrugated webs regarding shear capacity.

The ultimate shear capacity of the girders reduces when the initial imperfection is increased in magnitude. The results follow what has been confirmed in previous research for corrugated webs. The post-buckling behaviour is different for the design with the deepest web with a web height of 2500mm. This web shows a faster reduction in capacity which indicates column buckling behaviour, compared with the other girders with lower webs which has a more ductile post-buckling behaviour. The smallest girder shows interactive buckling mode and the three larger shows global buckling modes. Therefore, it can be stated that the buckling mode does not affect how initial imperfection affects shear capacity or behaviour of the shear strength-displacement curve.

To further investigate the difference between the changed web height and influence of initial imperfection, a comparison regarding initial imperfection as part of web height

and ultimate shear capacity, is performed. Same web designs as in Figure 7.1 are compared and the results be seen in Figure 7.2.

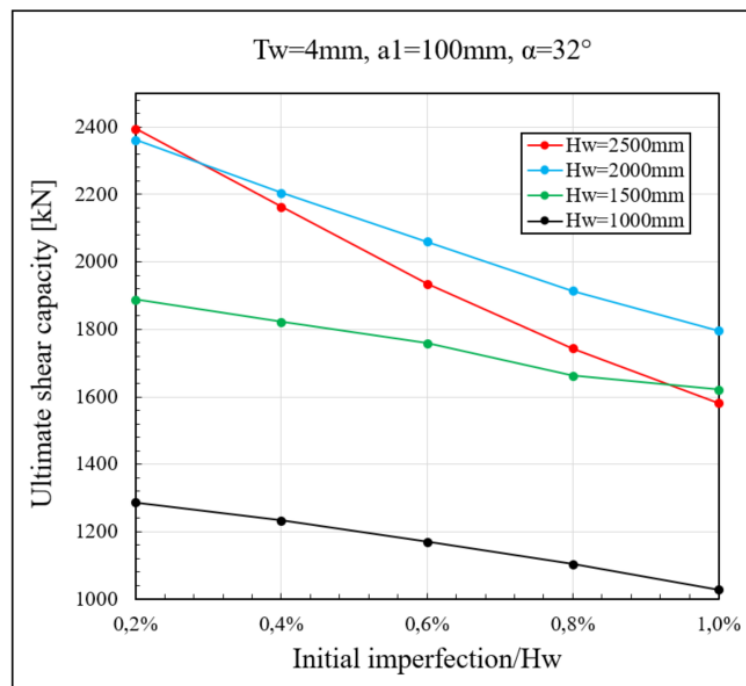


Figure 7.2 Initial imperfection as part of web depth and its corresponding ultimate shear capacity for corrugated webs.

All girders show a reduction-behaviour when comparing them. However, the deepest girder, with a different failure behaviour, shows a larger shear capacity reduction when initial imperfection is increased. This means that the deepest girder is more sensitive than the smaller girders when increasing initial imperfection as part of web height. One of the recommendation from previous research is that initial imperfection should be set to $h_w/200$ which means that deep girders would lose capacity more adversely compared with the others. This recommendation corresponds to Initial imperfection/ $h_w=0.5\%$ in Figure 7.2. However, it should be noted that different corrugation geometries in combination with web cross section parameters give different optimized girders, which in this case makes it difficult to compare the tested girders in Figure 7.2. The other recommendation was to set initial imperfection equal to t_w which in this investigation would give more favourable outcome for the deeper girder.

The three smaller girders which have the same post buckling behaviour show a similar shear capacity reduction slope. The initial imperfections are to account for both geometrical defects and residual stresses, e.g. welding work. To further investigate the post buckling behaviour of the different girders in Figure 7.1, two of them with web height of 1500mm and 2500mm are compared regarding yield stress distribution during loading. For stainless steel the yield stress corresponds to a certain proof strength, see section 2.3.2. The yield stress distribution for web height of 1500mm with the same cross section as in previous tests and initial imperfection magnitude of 6mm can be seen in Figure 7.3. The yield stress is set to 532 MPa which is according to the proof strength of stainless steel 1.4162 with a web thinner than 6mm. The ultimate capacity is 660 MPa. The plot in Figure 7.3 is set to only

show Von Mises-stresses larger than the yield stress, i.e. the grey areas are experiencing stresses less than the yield stress.

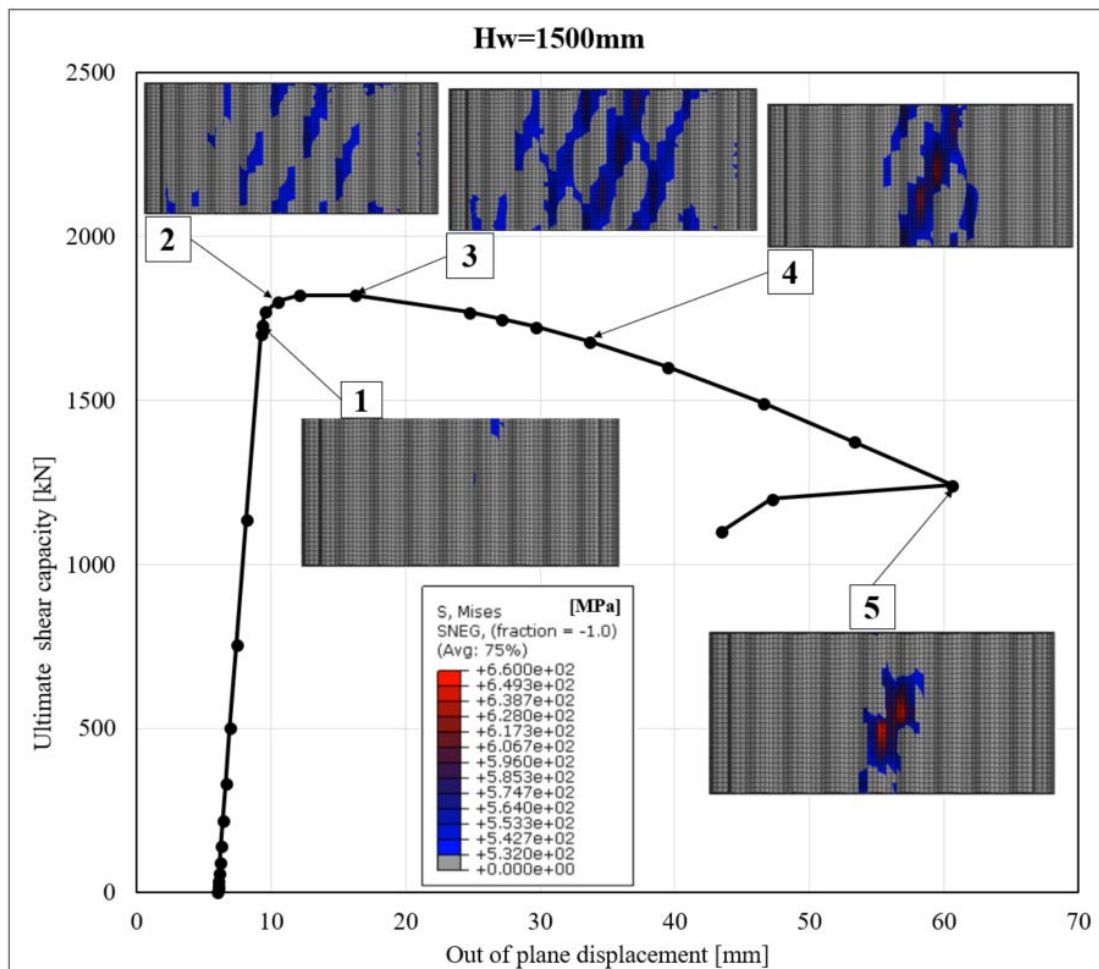


Figure 7.3 Yield stress distribution during shear stress buckling failure for a web height of 1500mm and initial imperfection of 6mm.

Yielding clearly starts at point 1 and 2 where some small yielding areas appear in the web and thereafter distribute in larger parts. The allocation is then, in point 3 spread over a larger area and this is where the ultimate shear capacity is reached. It can be stated that this girder utilizes plastic redistribution which means that when load is increased, the material gets softer and redistributes stresses to other parts which has not yet reached its yield stress capacity yet. Therefore, a material can take more load than the elastic yield capacity and further shows a more ductile behaviour until failure. In point 4 and 5, the stress clearly gets more concentrated into the central parts of the web which in point 5 gives a collapse of the structure. The concentration of stresses in the centre of the web clearly corresponds to a larger out of plane displacement which gives large imperfections and stresses. However, it should be noted that the girder shows relatively low out of plane displacements at ultimate loading. This states that the girder has low ductility before maximum load is reached.

The largest girder, with a web height of 2500mm in Figure 7.1, showed a different buckling behaviour than the other girders. This is further investigated in Figure 7.4.

The web cross section is the same as in previous simulations in this section and initial imperfection is set to 10mm. Noted should be that the initial imperfection does not affect the failure behaviour and therefore the magnitude could be any of the previous investigated.

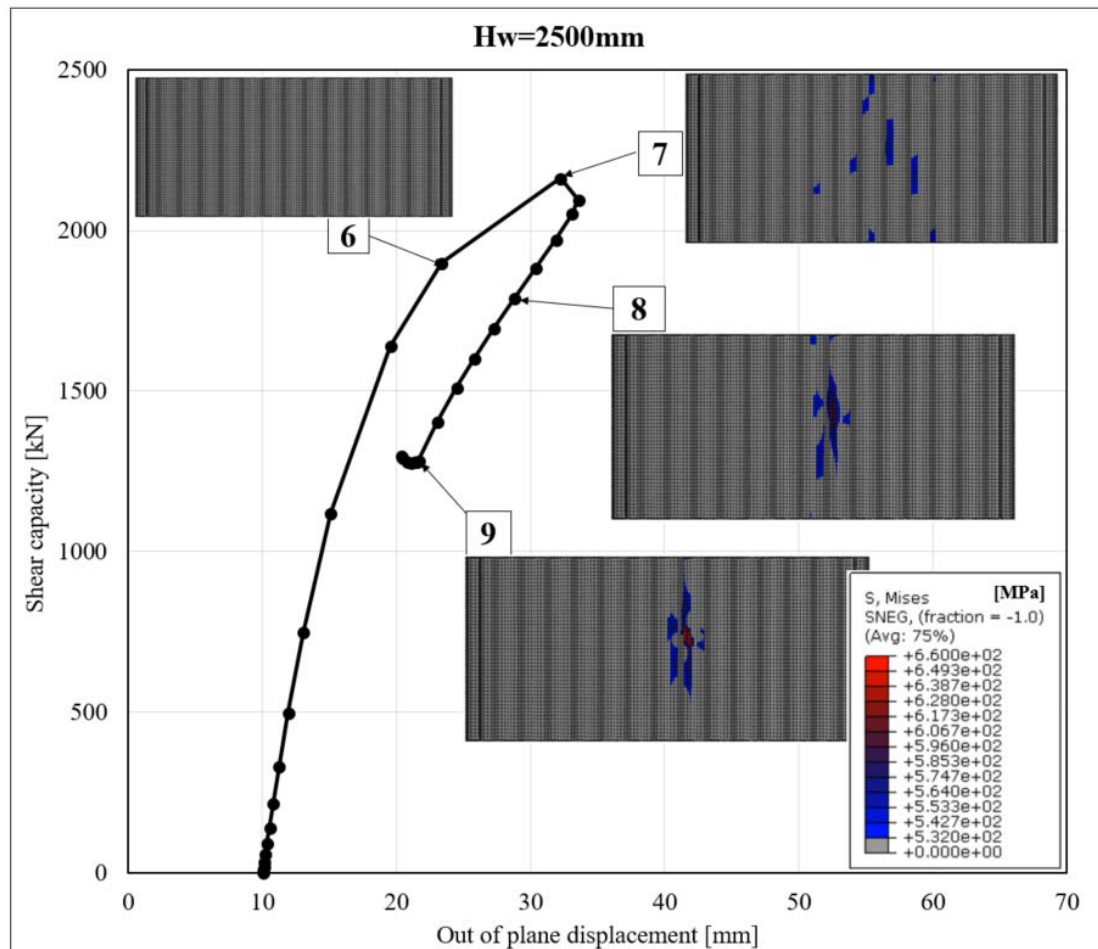


Figure 7.4 Yield stress distribution during shear stress buckling failure for a web height of 2500mm and initial imperfection of 10mm.

Between point 6 and 7 there is none or very little yield stresses in the web. The out of plane displacement of the web however is increased from 10mm to 33mm which means that the girder shows large ductility before reaching ultimate shear load. It can also be stated that the girder does not utilize plastic redistribution in the same manner as the lower girder, when shear load is increased. At point 7 where the ultimate capacity is reached, there is little yield stress distribution and in point 8 where the capacity has been decreased the Von Mises-stresses is concentrated to the centre of the web. At point 9, where collapse occurs, the stresses are large and concentrated to the centre of the web. The failure procedure seems to be fast which indicates that the web is more slender and sensitive of imperfections. This means that these types of deeper girders with a thin web will not utilize plastic redistribution and suffer from fast failure compared to the girder with a web height of 1500mm.

7.2 Influence of length/height-ratio

It was found from previous research that length of a beam divided by its web height will not affect shear capacity (Luo & Edlund, 1996). To ensure that this is correct, two different web heights, with initial imperfection set to t_w are tested in FE-simulations. Different lengths for the specimen are used to model the length-height ratio. Results from this investigation can be seen in Figure 7.5.

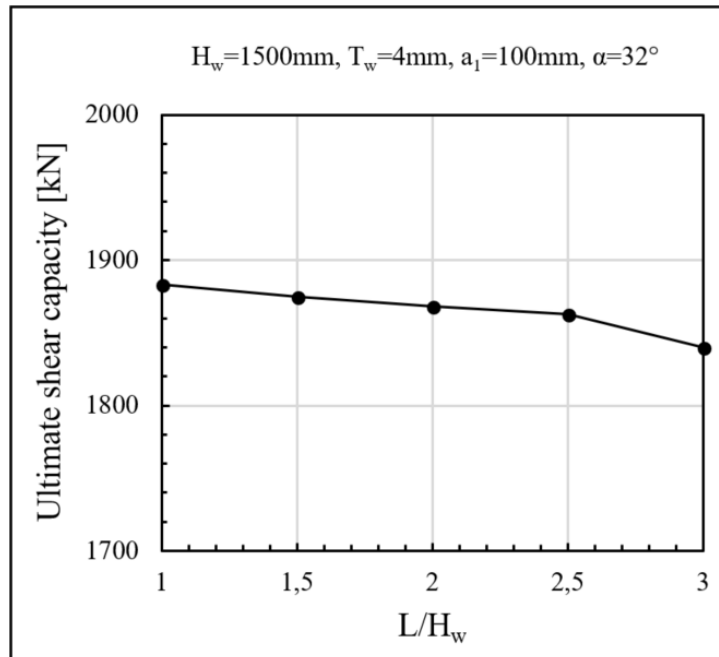


Figure 7.5 Influence of Length/Height-ratio regarding two designs and initial imperfections. Results from FE-simulations in ABAQUS.

Results show that the length of the specimen has low or neglectable influence on the girder. The difference between ratio=1 and ratio=3 is 43kN(2.3%) which is relatively low. The small change in capacity however can originate from other effects such as shear capacity contribution from flanges which are more utilized (i.e. less contribution to shear capacity) for beams with larger spans. It is therefore favourable to keep this in mind when modelling beams in ABAQUS. If the length of the specimen is large, flange buckling often becomes the governing failure mode which is not desirable in this context. See Appendix D for detailed FE-results regarding L-H-ratio.

7.3 Influence of web thickness and web depth

To investigate how web thickness would influence the ultimate shear capacity of beams with corrugated webs made of stainless steel, FE-simulations are performed for a girder with a web height of 1500mm. Flat fold length a_1 is 100mm, corrugation angle is 32 degrees and the initial imperfections are set to t_w . Results can be seen in Figure 7.6.

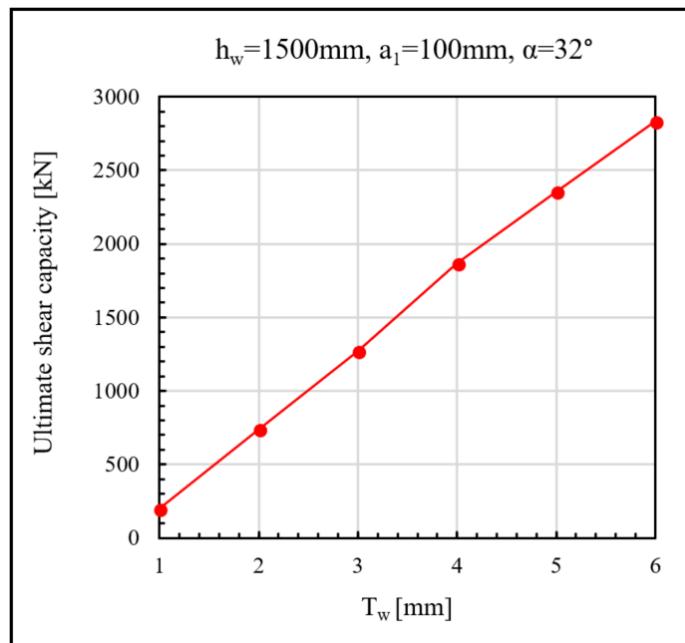


Figure 7.6 Ultimate shear capacity for two different web depths and various web thicknesses, values from analytical calculations with Eurocode and FE-simulations in ABAQUS.

Generally, it can be stated that the shear capacity increases linearly with increasing web thickness. Furthermore, a change of web thickness seems to have influence on the shear buckling mode. According to FE-simulations for the tested specimen, the shear buckling mode changes from interactive to global when t_w is increased.

The same approach was conducted for the influence of web depth on the shear capacity and the result is presented in Figure 7.7. Initial imperfections considered to be as large as t_w .

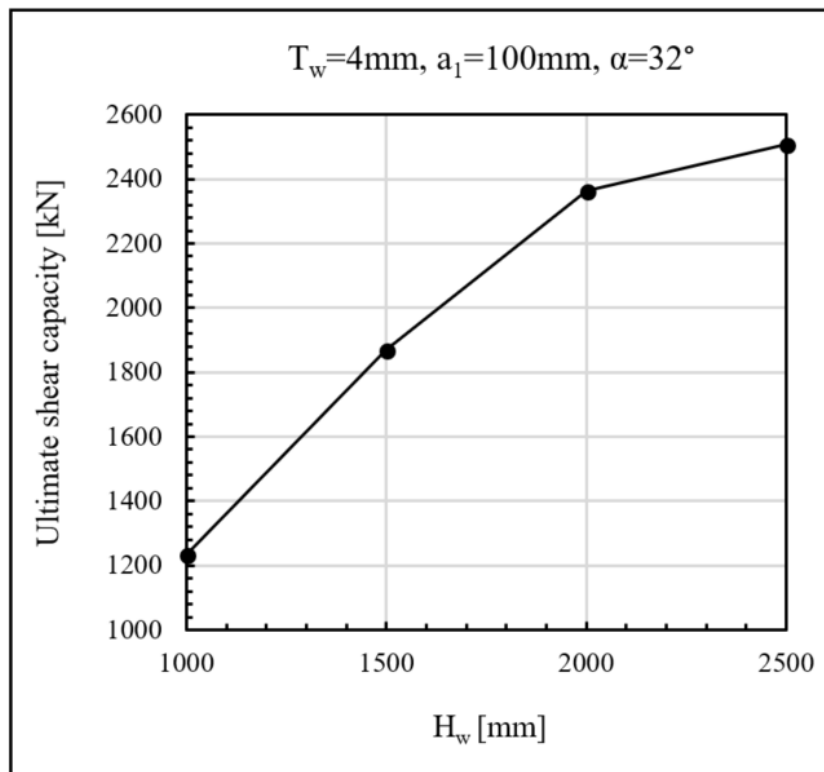


Figure 7.7 Influence of web depth regarding shear capacity.

The result shows that when the web height is increased, the ultimate shear capacity does increase as well, and the buckling mode goes from interactive to global for the studied case. The behaviour, however, is not linear which means that the gain of capacity is not large between a web depth of 2000mm and 2500mm. Further investigations about this phenomenon is done later in this chapter.

See Appendix D for detailed FE-results regarding influence of web thickness and depth for a corrugated web with stainless steel.

7.4 Influence of a_1 – flat fold length

It is difficult to intuitively understand the features of the corrugation geometry parameters in a trapezoidal corrugated web. For this thesis the main inputs regarding the corrugation is the flat fold length a_1 and corrugation angle α . The other parameters for the corrugation geometry are derived from these two factors. Therefore, an investigation is made to find out their influence on the shear capacity. Also, a comparison is made between results from Eurocode calculations and FE-simulations in ABAQUS to see how well the design code in (EN1990-1-5, 2006) fits.

In previous research and studies, increased length of a_1 is reported to reduce shear capacity of a corrugated web. It would therefore be good to have the flat fold as short as possible to reach high shear capacity. A comparison between analytical calculations with existing (EN1990-1-5, 2006) and FE-simulations for 4 different web depths can be seen in Figure 7.8. The girder has a web thickness of 4mm, flat fold length a_1 is varied, corrugation angle is set to 32 degrees and the initial imperfection is

equal to web thickness for all specimens. The material is Duplex stainless steel 1.4162.

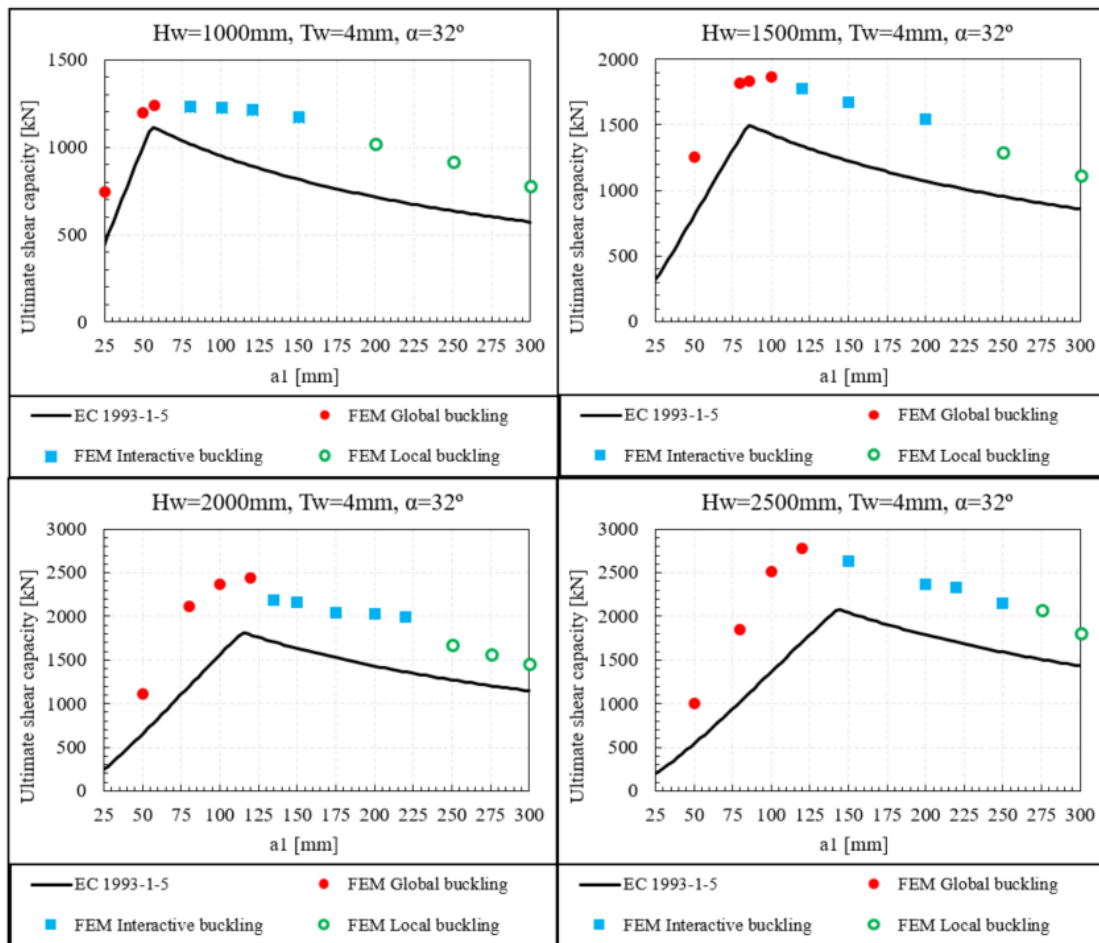


Figure 7.8 Flat fold length a_1 influence on ultimate shear capacity for different web depths and steel materials, comparison between Eurocode and FE-simulations.

The results, in Figure 7.8, clearly show that there is no evidence saying that the shear capacity would decrease if a_1 is increased. It is more reasonable to say that there is an optimal value for a_1 regarding shear capacity and different web depth designs. Similarly, results obtained from FE-simulations confirms that there are an optimal a_1 for every girder design to achieve the most optimal configuration regarding ultimate shear capacity. It is also clear that the existing Eurocode does not comply well with the stainless-steel material. For this reason, the possibilities to improve the existing design models are explored in section 7.6 and 7.7.

When changing the length of a_1 it influences the shear buckling mode, see Appendix E. A smaller value of a_1 gives global buckling and when it is increased the buckling mode varies first to interactive and then to local modes. This means that with a large a_1 the stability of the flat folds would govern the ultimate capacity while with smaller a_1 the corrugated web would buckle in a similar manner to that of beams with flat webs. It should also be noted that for specimens with a small flat-fold length, a_1

approximately 50mm, the failure mode seems to be more like a flat web. Therefore, the corrugation would not be efficient for small a_1 values.

See Appendix D for FE-results regarding flat fold length influence considering a corrugated web with stainless steel. Appendix E, furthermore, contains pictures of obtained buckling modes.

7.5 Influence of α – corrugation angle

In previous research it is suggested that an increase of corrugation angle α and corrugation depth a_3 , which correlates to the corrugation angle, will give somewhat larger shear capacity and change the buckling modes. To investigate the influence of the corrugation angle regarding shear capacity, 9 different angles is simulated in ABAQUS for one specific web design with a web height of 1500mm, web thickness of 4mm, a_1 equals 86mm and the initial imperfection is set to same as web thickness. The reason why a_1 is chosen to be 86mm is because this is where the optimal a_1 is obtained for this web according to Figure 7.8. Results are then compared with (EN1990-1-5, 2006) and presented in Figure 7.9. The material used is as in previous studies Duplex stainless steel 1.4162.

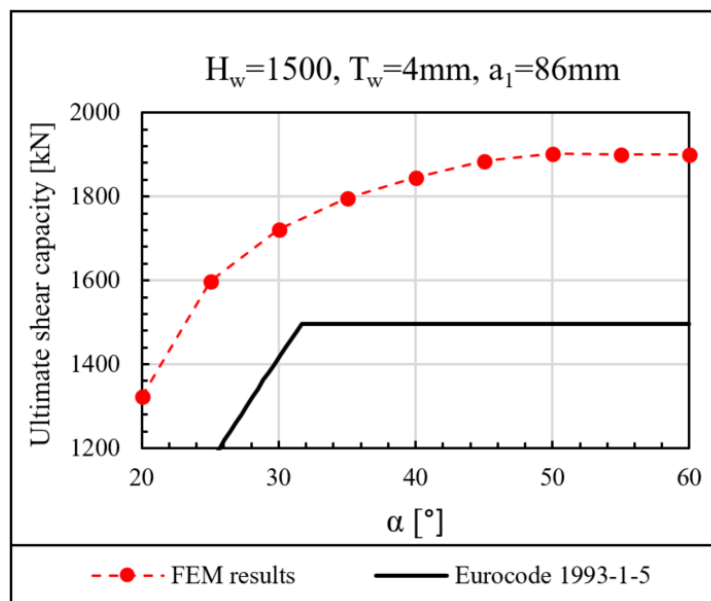


Figure 7.9 FEM results and Eurocode for corrugation angles between 20-60 degrees for a corrugated web with stainless steel 1.4162.

Results show that the shear capacity of the girder increases when α is increased, but to a certain point where the increase of angle is not giving any further increase in capacity. This specific angle can clearly be seen from the Eurocode curve to be somewhat about 32 degrees, for this girder. From the FE-simulations it can be seen that the capacity stops to increase after the corrugation angle has reached around 50 degrees. Also, the difference in capacity between Eurocode and FE-simulations gives reasons, in accordance with section 7.4, to further investigate a modification of the reduction factors in Eurocode regarding corrugated webs with stainless steel. See Appendix D for detailed FE-results regarding this section.

7.6 Proposal modified reduction factor regarding global and local buckling

Previous results show that the existing (EN1990-1-5, 2006) is not well adapted to the stainless-steel material and therefore a modification is needed. A regression study regarding FE-results is performed. New buckling curves for global and local buckling modes of corrugated webs with duplex stainless steel 1.4162 are obtained and presented in Figure 7.10.

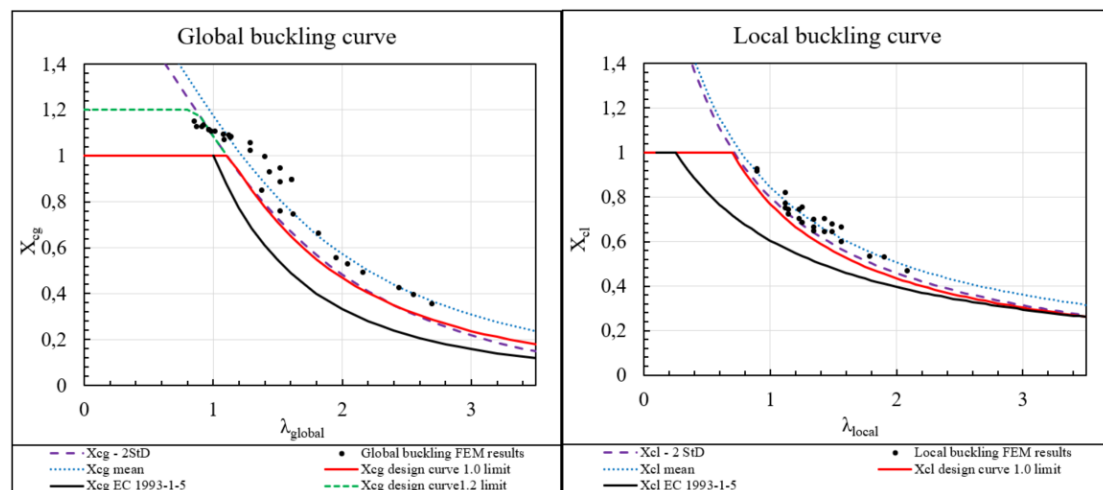


Figure 7.10 Buckling curves for global and local buckling modes regarding Duplex stainless steel 1.4162 and a corrugated web.

The new buckling curves contain approximately 30 results each, from FE-simulations, where the ultimate shear load in combination with material properties and cross section parameters give a value for the shear buckling reduction factor. Cross section constants in combination with corrugation geometry and material properties give the global and local slenderness. Only global buckling modes are evaluated in the buckling curve for global buckling and only local buckling modes for the buckling curve with local buckling. The relation between the buckling reduction factor and slenderness is presented in Figure 7.10 with a mean curve and a lower bound curve which is the 5%-fractile of the results, i.e. a confidence limit of the obtained results or mean values minus two standard deviations. This curve is the design curve and is further used when proposing the modifications to the Eurocode for stainless steel. The new buckling curves clearly seem to fit the FE results more accurately than (EN1990-1-5, 2006) which is intended to be used for carbon steel.

The larger limit, 1.2, that seems to occur for the global buckling curve in Figure 7.10 can emerge from contribution from flanges. For this thesis the limit for global buckling will be set to 1.0 which is in accordance with the Eurocode.

The new relation between slenderness and the buckling reduction factor obtained from the design curve can now be integrated into (EN1990-1-5, 2006) which is presented in Equation 40 and Equation 41. These can be compared with existing reduction factors, see Equation 12 and Equation 8 respectively.

$$X_{cg} = \frac{2.41}{1.14 + \lambda_{global}^2} \quad \text{Equation 40}$$

$$X_{cl} = \frac{1.0}{0.3 + \lambda_{local}} \quad \text{Equation 41}$$

Equation 40 and Equation 41 are used to obtain more accurate results for global and local buckling. These equations with modified factors are used to obtain new shear capacities for the same girders as in Figure 7.8, and the results can be seen in Figure 7.11. The results for the new design codes are compared with (EN1990-1-5, 2006) as well.

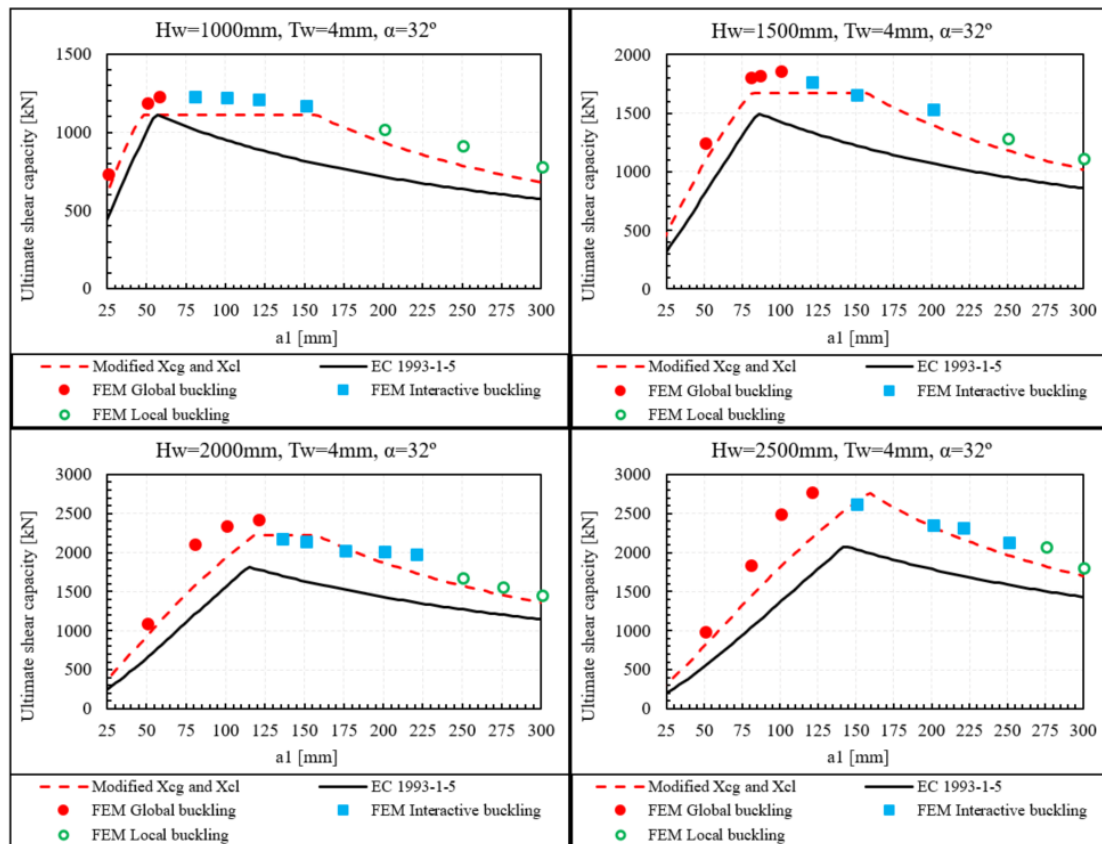


Figure 7.11 Flat fold length a_1 influence on ultimate shear capacity for different web depths and steel materials, comparison between new equations with modified X_{cg} and X_{cl} , Eurocode and FE-simulations.

The results for the modified reduction factors seen in Figure 7.11 show greater ultimate shear capacities for all girders except the one with a web height of 1000mm. The new equations seem to fit the data well for the case of local and global buckling modes. However, there seems to be an overestimated capacity for zones where interactive buckling occurs. When acquiring the relation between local slenderness

and buckling, only local buckling modes were considered which means that effects from interactive buckling will be missed. This is further investigated in section 7.7.

7.7 Modified reduction factors including the interactive buckling mode

The existing Eurocode only includes reduction factors for global and local buckling modes. However, another buckling mode called interactive buckling mode can emerge. As highlighted in the previous section, there is an obvious need to integrate interactive buckling in the calculations as this could result in unsafe designs, see Figure 7.11. Two proposals on how to approach this problem will be presented in this section.

7.7.1 Incorporating interactive buckling into local buckling reduction factor

The first approach is to incorporate interactive buckling modes into the local buckling curve and modify this into a more fitted equation. As can be seen from Figure 7.11, both the reduction rate and trend of beams with interactive buckling mode seem to be similar to that of beams that experience local buckling of the web. Therefore, the same approach as in section 7.6 is performed and the results for the new local buckling curve can be seen in Figure 7.12.

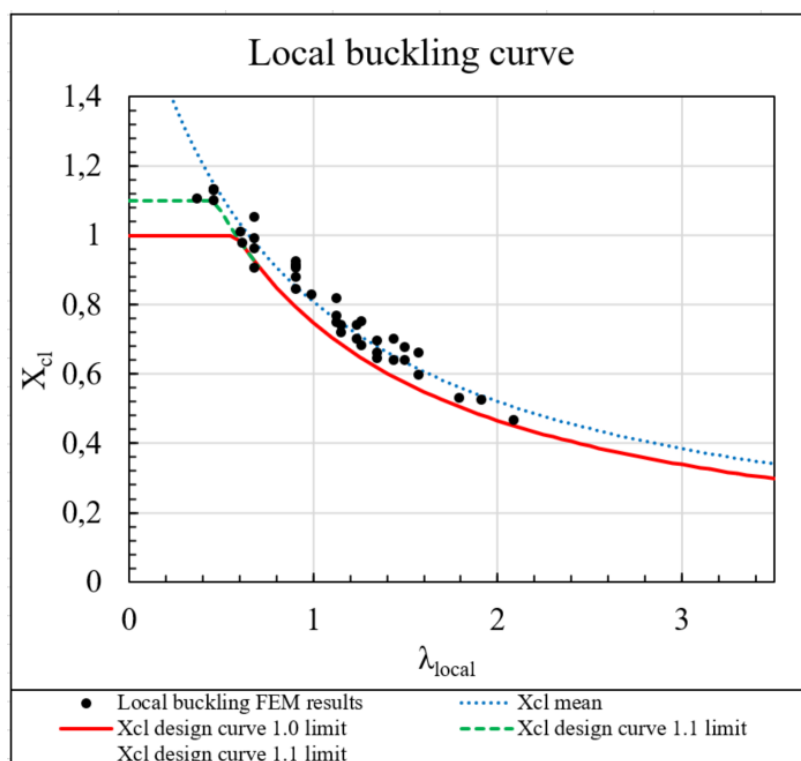


Figure 7.12 Local buckling curve for corrugated web with stainless steel 1.4162 including interactive buckling modes.

The new local buckling curve is used to produce a new relation between local slenderness and the local buckling reduction factor which is presented in Equation 42. This equation is derived from the design curve which is the 5%-fractile of all FE-

results with local and interactive buckling modes. There seems to be an availability to use a larger limit than 1.0 for the local reduction factor. This can occur from contribution from flanges or other effect regarding corrugation and stainless steel. For this buckling curve, however, the limit of 1.0 will be used, which is conservative. This modified local reduction factor can be compared with the existing reduction factor from (EN1990-1-5, 2006), see Equation 8.

$$X_{cl} = \frac{1.24}{0.66 + \lambda_{local}} \quad \text{Equation 42}$$

This new relation for local buckling which incorporates interactive buckling is compared with previous results and (EN1990-1-5, 2006). See Figure 7.13 for the outcome. Same geometries and materials are used as for girders in Figure 7.8 and Figure 7.11 and initial imperfection is set to t_w . X_{cl} with interactive buckling is obtained from Equation 42.

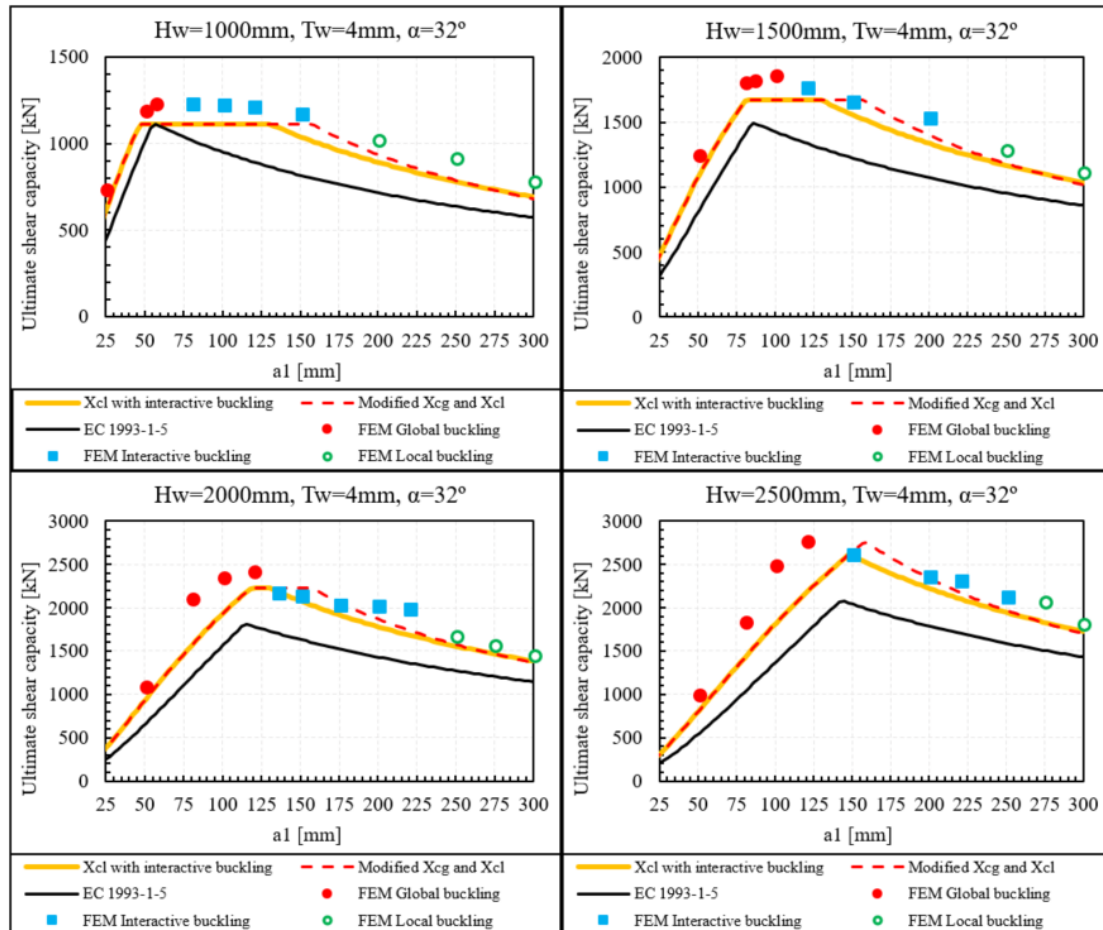


Figure 7.13 a_1 influence on shear capacity for 4 different web heights when interactive buckling is incorporated into X_{cl} .

The new equation for local buckling which is seen in Figure 7.13 clearly fits better than the previous equation for X_{cl} and cuts the peaks where the shear capacity earlier was overestimated. Now the results are on the safe side compared with FE-

simulations for all tested girders. There is also an increase in capacity compared with (EN1990-1-5, 2006) and a larger variety of optimal a_1 that can be chosen.

7.7.2 Creating a separate interactive buckling factor

The second approach performed is to create a separate interactive reduction factor based on the same principals as the global and local reduction factors. However, when calculating the slenderness for a web in interactive buckling, Equation 5 is used to obtain the critical shear stress. Two different values regarding n is used to produce two separate interactive buckling factors which can be seen in Figure 7.14.

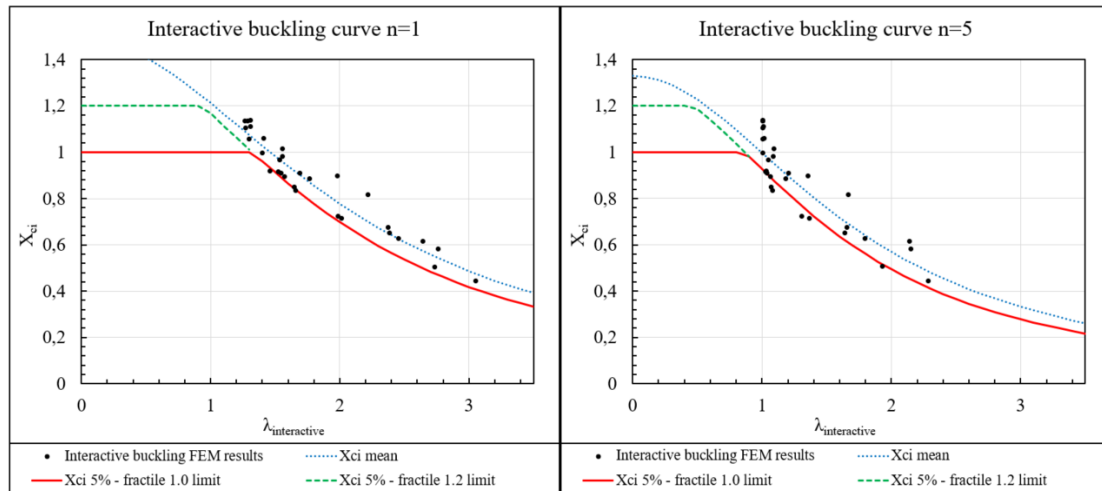


Figure 7.14 Interactive buckling curve for $n=1$ and $n=5$.

When using $n=1$ the critical shear stresses reaches a lower value than $n=5$ for every tested point and therefore creates a larger reduction factor. FE-simulations show results that gives larger values than 1.0 for the reduction factors for some specimens which means that there is an ability to increase the limit to 1.2 for the reduction factor. However, for this case the limit is set to 1.0 because of the uncertainty. The proposals

for new equations regarding interactive buckling reduction factors can be seen in Equation 43 and 44. These are created from the lower bound curve in Figure 7.14.

$$X_{ci} = \frac{5.21}{3.46 + \lambda_{interactive}^2} \text{ if } n = 1 \quad \text{Equation 43}$$

$$X_{ci} = \frac{3.18}{2.43 + \lambda_{interactive}^2} \text{ if } n = 5 \quad \text{Equation 44}$$

The proposed interactive reduction factor is incorporated into Eurocode and the used condition for analytical calculations when picking reduction factors for corrugated webs with stainless steel can be seen in Equation 45.

$$X_c = \min[X_{cG}, X_{cL}, X_{ci}, 1.0] \quad \text{Equation 45}$$

Results regarding a comparison of the new modification and results from section 7.6 are presented in Figure 7.15. Same geometries, materials and initial imperfections are used as in previous sections. Results including X_{ci} is obtained from Equation 40 and

Equation 41 for X_{cg} and X_{cl} in combination with Equation 43 and Equation 44 respectively.

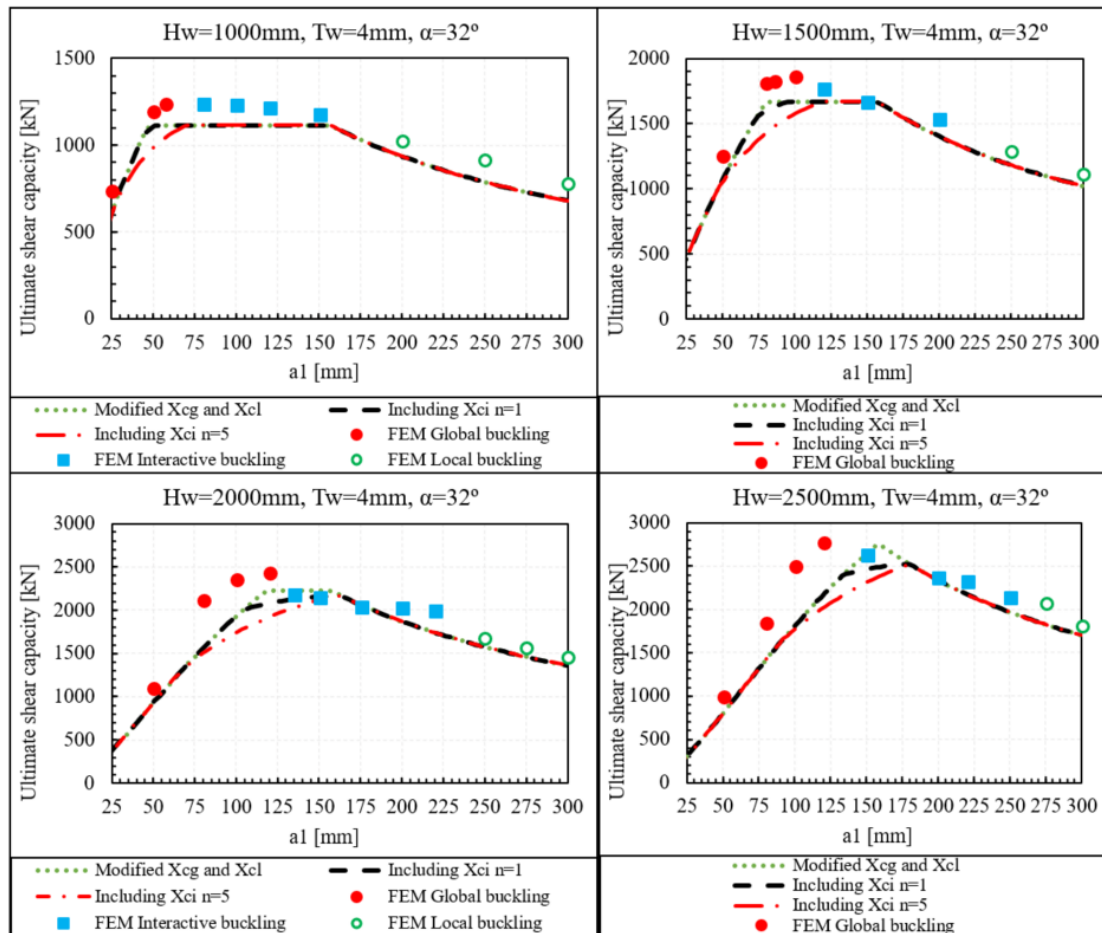


Figure 7.15 Comparison between results with an interactive buckling reduction factor X_{ci} , FE-simulations and with no regard to interactive buckling.

When using an interactive buckling factor, it seems as the peaks from previous results are cut which is the aim of incorporating interactive buckling. However, the new curves show a slightly overestimated shear capacity, compared with FE-simulations, for some of the girders at single points. When using $n=5$ the results seem more conservative than when using $n=1$ which is something that was anticipated. It should also be noted that the interactive buckling factor seems to have more influence on zones where global buckling occurs than zones where interactive buckling occurs.

7.8 Summary

The parametric study has given new insights regarding design of corrugated webs with stainless steel and a summary can be seen in Table 7.1.

Table 7.1 Summary of the parametric study combined with previous knowledge from research. New information marked with green.

Cross-section web			
Description	Notation	Effect on ultimate shear capacity	Effect on buckling mode
Thickness web	t_w	Increases when t_w increase.	Increased web thickness=Buckling goes from local to interactive to global
Depth web	h_w	Increases with h_w . Shear capacity not dependent on Length/Depth ratio of a girder.	Increased web height=Buckling goes from local to interactive to global
Corrugation web			
Description	Notation	Effect on shear strength	Effect on buckling
Angle	α	Increased α gives larger shear capacity, but the increase of capacity is less after a certain point.	Testes specimen goes from global to interactive buckling when corrugation angle is increased.
Flat fold	$a_1 = \frac{h_w}{H_w/a_1}$	There is a optimal a_1 to be found for a specific web design which gives max. shear cap.	Small a_1 =Global buckling Medium a_1 =Interactive buckling Large a_1 =Local buckling
Length inclined fold	$a_2 = \frac{a_4}{\cos \alpha}$	-	-
Corrugation depth	$a_3 = a_4 \tan \alpha$	Same as for α because they are correlated.	Same as for α because they are correlated.
Length inclined fold x-direction	$a_4 = a_1 \cos \alpha$	-	-

The most important information from the parametric study is that:

- There is an optimal value for a_1 and α for every unique cross section investigated in this study.
- Choice of a_1 has large influence on what buckling mode will occur. Less a_1 length gives global buckling, medium length gives interactive and longer a_1 gives local buckling.
- There is no obvious optimal buckling mode to choose when designing corrugated webs according to results from this study. However, for the tested girders the maximum capacity occurs in global and interactive buckling.
- Corrugation angle α and corrugation depth a_3 has influence on the shear buckling mode to a certain limit, where they no longer influence.
- New buckling curves and buckling reduction factors, for corrugated webs with stainless steel, are created and presented. These have greater accuracy than previous design codes. When interactive buckling is incorporated into the local buckling reduction factor it seems to be useful and practical in design.

8 Discussion

This thesis is divided into two main subjects. The first is to investigate in which way the material stainless steel and a corrugated web can influence material use and costs if existing bridges would have been built accordingly. The other subject was to go deeper into the behaviour of a corrugated web with stainless steel, analyse how the different parameters are affecting shear capacity and suggest new relations between reduction buckling factors and slenderness. This discussion chapter will discuss accuracy in measurements if results are significant and mainly if the research provided new insights and answered the aim.

8.1 Case studies

The case studies were made with both analytical calculations and numerical simulations. The analytical calculations were made with optimization Matlab routine, see Appendix A, and numerical simulations were done in ABAQUS, see section 4. When creating the Matlab routine, the existing (EN1990-1-5, 2006) was used which is not adapted to stainless steel but have design codes for corrugated webs. The accuracy of the calculations was validated by comparison with FE-simulations and show that the results regarding capacities are valid. The nonlinear FE-simulations can always be affected by small changes and mistakes in settings, therefore many simulations were performed considering different cross sections and corrugation geometries. Also, a mesh convergence study was performed. The true stress-strain curve is used to make sure that the material stainless steel is handled correctly. When doing a small number of case studies, it is always a problem because of the variety of bridge types and geometries and this has effect on the overall significance.

The LCC study however, is more difficult to estimate accuracy and if it is significant. There are many variables, especially prices on maintenance and material is varying from time to time. Therefore, it is important to do sensitivity analysis in connection with the LCC to show what will happen if parameters are changed. In the case studies performed in this thesis this was done regarding average daily traffic and yearly interest rate which gives some insights into the problem. Other parameters that would be interesting to investigate which has a large impact on the LCC would be steel prices. It is not unreasonable to think that the price for stainless steel would increase if demand increase or reversed.

One of the aims of the study was to investigate benefits with the new design and this is well answered in the thesis. It is also interesting to see how the depth of the girder when constructing corrugated webs has a large influence on cost and material use. There are many previous researches done regarding corrugated webs and carbon steel, but not much done when combining this with stainless steel. Therefore, the topic is hard to compare with previous research and to make statements regarding validity based on this.

Overall it can be stated that there is probability to suggest that corrugated webs with stainless steel can reduce material use and costs for investors and society. More case studies with varying geometries and types of bridges need to be performed to see if this can be a general design technique for future constructions.

8.2 Parametric study

The parametric study was based on approximately 120 FE-simulations in total. These were made with varying cross-sections and corrugation geometries. However, it is important to state that there are infinite combinations of girders and therefore the number of simulations somehow needs to be limited.

8.2.1 Buckling curves for global, local and interactive buckling

When creating new buckling curves for stainless steel and corrugated webs it is important to be aware of the significance in the study. Therefore, statistically evaluations were made of all mean curves regarding normal distribution. The standard deviation is then used, taken from the normal distribution, to create a lower bound design curve. This will give a larger validity for the proposed design equations and is also used in most literature and design guides when describing buckling curves. In this case the 5%-fractile was used for the design curves, which means that the probability that the suggested equations are correct, according to the results in this study, is 95%. To use a smaller fractile would have effect on material use and a larger fractile will have effect on the safety. However, it would be of advantage to further investigate the subject with a larger number of FE-simulations with more varying geometries to get a more accurate regression study.

Modifying the global and local buckling curves gave no accurate results without incorporating the interactive buckling mode. It can be argued easier to use only global and local reduction factors because this is already used in (EN1990-1-5, 2006) and therefore it seems advantageable to incorporate the interactive buckling into the local reduction factor, which was made in section 7.7.1, than to use a separate interactive buckling reduction factor.

8.2.2 Optimal design regarding corrugation geometry

The results from the parametric study clearly show some problems in previous research. One of the main discoveries is that there is an optimal design for every unique girder regarding cross-sections and corrugation geometry. This was seen both for stainless steel, carbon steel, original Eurocode and Eurocode with modified reduction factors. Further investigations on this subject should be done because of the large impact on shear capacity and material use. Also, the parametric study in this thesis overall should be supplemented with more FE-simulations and results. This is to validate the proposed design codes or to improve them.

One other major issue for the FE-simulations in this project is about how to handle the initial imperfections considering shear buckling. Because imperfections have a large influence on slender webs that show a column buckling behaviour it must be handled carefully. In this thesis initial imperfections were set to the same size as t_w for most of the parametric studies. The validity for this magnitude is that it is mentioned in previous research and because it shows reasonable results in analysis. However, further research should be done on this subject to create a value for initial imperfections considering corrugated webs with stainless steel in shear buckling.

9 Conclusions

This chapter contains conclusions for the different studies performed.

- The corrugated webs have been widely used in many bridges. In Japan there has been constructed more than 140 bridges of this type and Europe also has many examples. The idea of corrugated webs in bridge girders has been seen applicable in engineering and therefore makes the introduction of the new material stainless steel interesting and reliable.
- The case studies where two existing bridges were re-designed and optimized with corrugation and stainless-steel showed that there can be great rewards regarding material use. For Skulnäs bridge the material reduction was 27.8% for the original web depth and 42.3% for a larger web depth. For Nissan bridge these values are 17.7% and 51.6% respectively. The main conclusion from the case studies is that corrugated web girder is very effective when they are deep. This is because these girders get larger moment resistance from smaller flanges without increasing web thickness. The FE-results regarding shear capacity for the girders show that utilization ratios are lower than for analytical calculations which means that further optimization with modified reduction factors is possible.
- The cost reduction over a life cycle of 100 years for Skulnäs bridge, according to the LCC study, is 29.2% for the original web depth and 40.6% for the larger web depth. For Nissan bridge the values are 30.2% and 52.5% respectively. This is mainly because of less material use, no need for initial painting and less maintenance. It should be noted that if the stainless-steel girder is made deeper than the original bridge it can even achieve the same initial cost as for the carbon steel bridge.
- The parametric study gave insights into the optimization of a corrugated web. There is an optimal flat fold length a_1 for every unique cross section and corrugation angle α . This is something that should be carefully considered when designing these types of girders, even when using carbon steel. The reduction in capacity can be largely affected by even small deviations from the optimal flat fold length.
- The design process regarding corrugated webs is more complicated than conventional girders. Therefore, it is suggested to begin the design process by first choosing a desirable cross-section with respect to h_w and t_w . The next step would be to choose the corrugation shape. This is to get the most out of the material and save costs, further to make the concept more attractive.

- New modified reduction factors were obtained and presented in section 7.6 and 7.7. Also, new buckling curves which correspond to these factors are presented in these sections. The results for the obtained design equations show that it is sufficient to use Equation 40 for the global reduction buckling factor and Equation 42 for the local reduction buckling factor. The later equation incorporates interactive buckling which makes it more reliable in application.
- A separate interactive buckling reduction factor was proposed and presented in Equation 43 and 44 for different values of n in Equation 5. These equations shall be used in combination with Equation 40 and 41. It can be stated that a larger n value is more on the safe side and that this new reduction factor helps to reduce some peaks that were on the unsafe side in previous calculations. The separate interactive reduction factor is a subject for further investigations.

10 Suggestions for further research

The main topics for further research are summarized in this chapter.

- Further research regarding the concept of corrugated webs in combination with stainless steel materials for bridge girders is shown in this study to be advantageous. Before this conclusion could be generalised, other types of bridges and load scenarios need to be investigated.
- Further LCC studies that focus on bridges in other countries with climates different than Sweden could be of interest mainly due to different costs and maintenance demands.
- A larger parametric study with more results would in further investigations give more validity to a change of design codes. This is desirable for stainless steel in combination with corrugated webs.
- More research should be done to investigate the influence and magnitude of initial imperfections for corrugated webs with respect to ultimate shear capacity. There is no consensus in previous research on how to account for this parameter in numerical simulations.

References

- BEgroup. (2 November 2017). <http://www.begroup.com>. Gathered from http://www.begroup.com/upload/Sweden/Prislistor/Rostfritt/Prislista%20rostfritt%20st%c3%a5l%202017-11-02_rev.pdf 11 April 2018
- Boutillon, L., Combault, J., Ikeda, S., Imberty, F., Mori, T., Nagamoto, N., . . . Kimio, S. (2015). *Corrugated-steel-web bridges*. Federation internationale du beton.
- Driver, R. G., Abbas, H. H., & Sause, R. (2006). Shear Behavior of Corrugated Web Bridge Girders. *Journal of structural engineering*, 132, 195-203.
- Dywidag-Systems. (25 01 2018). *Dywidag Systems*. Gathered from www.dywidag-systems.com: <https://www.dywidag-systems.com/projects/project-details/article/himi-yume-bridge-japan.html>
- EN1990. (2005). *Eurocode 3, EN1990, Basis of structural design*. CEN.
- EN1990-1-1. (2005). *Eurocode 3: Part 1.1 Design of steel structures*. CEN.
- EN1990-1-3. (2006). *Eurocode 3: Part 1.3 Design of steel structures*. CEN.
- EN1990-1-4. (2006). *Eurocode 3: Part 1.4 Supplementary rules for stainless steel*. CEN.
- EN1990-1-5. (2006). *Eurocode 3: Part 1.5 Plated structural elements*. CEN.
- EN1991-2. (2003). *Eurocode 3: Part 2 Traffic loads on bridges*. CEN.
- EN1993-1-9. (2005). *Eurocode 3: Part 1.9 Fatigue*. CEN.
- Finnås, A., & Olsson, A. (19 01 2018). *Rostfria stål i bärande konstruktioner*. Gathered from www.stalbyggnadsinstitutet.se: <http://www.stalbyggnadsinstitutet.se/uploads/source/files/Artiklar/Rostfria%20stal%20i%20barande%20konstruktioner.pdf>
- Forum, I. s. (19 01 2018). *Worldstainless*. Gathered from www.worldstainless.org: <http://www.worldstainless.org/Files/issf/non-image-files/PDF/TheStainlessSteelFamily.pdf>
- Hassanein, M., & Kharoob, O. (2013). Behavior of bridge girders with corrugated webs: (II) Shear strength and. *Engineering structures*, 57, 544-553.
- Hassanein, M., Elkawas, A., El Hadidy, A., & Elchalakani, M. (2017). Shear analysis and design of high-strength steel corrugated web girders. *Engineering structures*, 146, 18-33.

- Hosseinpour, E., Baharom, S., & Yadollahi, Y. (2015). *Evaluation of Steel Shear Walls Behavior with Sinusoidal and Trapezoidal Corrugated Plates*. Hindawi Publishing Corporation.
- Ikedo, S., & Sakurada, M. (2005). Development of hybrid prestressed concrete bridges. Singapore: CI-Premier PTE LTD.
- Jáger, B., Dunai, B., & Kövesdi, B. (2017). Flange buckling behavior of girders with corrugated web Part II: Numerical. *Thin-walled structures*, 118, 238-252.
- Javier Veganzones Munoz, J., Pettersson, L., Sundquist, H., & Karoumi, R. (2016). Life-cycle cost analysis as a tool in the developing. *Structure and infrastructure engineering*.
- Johansson, B., Maquoi, R., Sedlacek, G., Muller, C., & Beg, D. (2007). *Commentary and worked examples to EN 1993-1-5 plated structural elements*. JRC - ECCS.
- Kwanghoe, J., Kwangsoo, K., Chungwook, S., & Jang-Ho, K. (2010). Verification of Incremental Launching Construction Safety for the Ilsun Bridge: The World's Longest and Widest Prestressed Concrete Box Girder with Corrugated Steel Web Section. *Journal of bridge engineering*, 16.
- Kövesdi, B., & Dunai, L. (2009). Determination of the patch loading resistance of girders with corrugated webs. *Computers and Structures*.
- Larsson, M., & Persson, J. (2013). *Lateral-torsional buckling of steel girders with trapezoidally corrugated webs*. Gothenburg: Chalmers University of Technology.
- Luo, R., & Edlund, B. (1996). *Shear capacity of plate girders with trapezoidally corrugated webs*. Gothenburg: Chalmers university of Technology.
- Mosiello, A., & Kostakakis, K. (2013). *The benefits of post weld treatment for cost efficient and sustainable bridge design*. Gothenburg: Chalmers University of Technology.
- Pasternak, H., & Kubieniec, G. (2010). Plate girders with corrugated webs. *Journal of civil engineering and management*.
- SCI. (2017). *Design manual for structural stainless steel* (4 uppl.). Ascot: The Steel Construction Institute.
- Sudeok, S., Sangwook, J., & Seungjae, L. (2017). *Minimum weight design of sinusoidal corrugated web beam using real-coded genetic algorithms*. Hindawi.

- Tohamy, S., Abdel-Halim, A., Saddek, A., & Hamed, A. (2016). Interactive shear buckling of corrugated webs. *Minia journal of engineering and technology*, 35.
- Worldstainless. (19 01 2018). *Railway bridge structure*. Gathered from [www.worldstainless.org: http://www.worldstainless.org/Files/issf/non-image-files/PDF/Infrastructure/Railway_bridge_structure.pdf](http://www.worldstainless.org/Files/issf/non-image-files/PDF/Infrastructure/Railway_bridge_structure.pdf)
- Worldstainless. (19 01 2018). *River delta crossing*. Gathered from [www.worldstainless.org: http://www.worldstainless.org/Files/issf/non-image-files/PDF/Infrastructure/River_Delta_Crossing.pdf](http://www.worldstainless.org/Files/issf/non-image-files/PDF/Infrastructure/River_Delta_Crossing.pdf)
- Worldstainless. (19 01 2018). *Tables of technical properties*. Gathered from www.worldstainless.com: http://www.worldstainless.org/Files/issf/non-image-files/PDF/Euro_Inox/Tables_TechnicalProperties_EN.pdf
- Yadollahi, Y., Pakar, I., & Bayat, M. (2015). Evaluation and comparison of behavior of corrugated steel plate shear walls. *Latin american journal of solids and structures*.
- Yazeed Sayed-Ahmed, E. (1998). *Corrugated steel web plate/box girders: Bridges of the 21st century*. Cairo: University of Cairo.
- Yong Song, J., Mei Yu, Y., & Zhang, S. (August 2011). Initial imperfection simulations and effect on shear buckling of corrugated steel webs - song. *Advanced material research*, ss. 2463-2470.
- Zevallos, E., Hassanein, M., Real, E., & Mirambell, E. (2015). Shear evaluation of tapered bridge girder panels with steel corrugated. *Engineering structures*, 113, 149-159.

Appendix A – Matlab optimization routine

Main routine for choosing inputs

```
clc
close all
clear all
```

Input

```
% 10^4 simulations, set iteration=10
% 100^4 simulations set iteration=100
iteration=10;
% Corrugation input ranges
alpha=linspace(30, 60, iteration);

a1=linspace(50, 300, iteration)*10^-3;

% Cross section input ranges
tw=linspace(2, 11, iteration)*10^-3;

hw=linspace(500, 2500, iteration)*10^-3;

% Flanges and deck input ranges
t1=linspace(20, 50, iteration)*10^-3;
b1=linspace(200, 400, iteration)*10^-3;
t2=linspace(20, 50, iteration)*10^-3;
b2=linspace(200, 400, iteration)*10^-3;

% Concrete deck geometry
h_deck=0.265;
b_deck=2.5;

L=33; % Span length
Lcr=8; %Distance between vertical stiffeners
%%-----

% Design loads
VULS=1.523*10^6;
MULS=12.014*10^6;

MULS_initial=3.517*10^6;

MSLS=9.673*10^6;
VSLS=1.226*10^6;

%Point load from traffic with partial factor 0.9
Q1=0.9*300*10^3;

q1=0.9*9*10^3*b_deck;

q_selfweight=22.895*10^3;
q_windbridge=6*10^3;
```

```

qSLS=q_sel fwei ght+q_wi ndbri dge+q1;

% Material properties
fyw=530*10^6;
fyf=460*10^6;
YMO=1. 1;
YMI=1. 1;
E=200*10^9;
Ec=35*10^9;          %Modulus of elasticity for concrete
v=0. 305;           %Poissons ratio stainless steel

```

Calling optimization function

```

[ALPHA, TW, HW, A1, A2, A3, A4, VRD, MRD, X_Shear, Xcl, Xcg, Utilization_Shear, ...
 Utilization_Moment_final, Utilization_Moment_initial, ...
 Utilization_Moment_LT, T1, B1, T2, B2, Volume_Web, Volume_Flange, ...
 Volume_Total, Position_Min_Volume, SW_RATIO, SLS_RATIO]...
= EVERYTHING_IN_ONE(Ec, alpha, a1, tw, hw, v, VULS, MULS, fyw, fyf, YMO, YMI, E, ...
 t1, b1, t2, b2, h_deck, b_deck, L, iteration, MSLS, VSLS, qSLS, Q1, MULS_initial, Lcr);

```

Presenting results

```

if Utilization_Shear==0 || Utilization_Moment_final==0 ...
    || Utilization_Moment_initial==0 || SLS_RATIO==0
    txt = sprintf('\nNo solution!!! \n');
    disp(txt)
    formatSpec = 'Shear ULS: %4.2f\n';
    fprintf(formatSpec, full(Utilization_Shear))
    formatSpec = 'Moment ULS: %4.2f\n';
    fprintf(formatSpec, full(Utilization_Moment_final))
    formatSpec = 'Moment during casting: %4.2f\n';
    fprintf(formatSpec, full(Utilization_Moment_initial))
    formatSpec = 'Moment LT-buckling: %4.2f\n';
    fprintf(formatSpec, full(Utilization_Moment_LT))
    formatSpec = 'SLS deflection: %4.2f\n\n';
    fprintf(formatSpec, full(SLS_RATIO))

else if Utilization_Shear>0 & Utilization_Moment_final>0 &...
    Utilization_Moment_initial>0 & SLS_RATIO>0

    txt = sprintf('\nShear and moment resistance according to Eurocode \n');
    disp(txt)
    formatSpec = 'Web thickness is %4.2f mm\n';
    fprintf(formatSpec, TW)
    formatSpec = 'Web height is %4.2f mm\n\n';
    fprintf(formatSpec, HW)

    formatSpec = 'a1 is %4.1f mm\n';
    fprintf(formatSpec, A1)
    formatSpec = 'a2 is %4.2f mm\n';
    fprintf(formatSpec, A2)
    formatSpec = 'a3 is %4.2f mm\n';
    fprintf(formatSpec, A3)
    formatSpec = 'a4 is %4.2f mm\n\n';
    fprintf(formatSpec, A4)

```

```

formatSpec = 'Top flange thickness T1 is %4.1f mm\n';
fprintf(formatSpec, T1)
formatSpec = 'Top flange width B1 is %4.2f mm\n';
fprintf(formatSpec, B1)
formatSpec = 'Bottom flange thickness T2 is %4.2f mm\n';
fprintf(formatSpec, T2)
formatSpec = 'Bottom flange width B2 is %4.2f mm\n';
fprintf(formatSpec, B2)

formatSpec = 'Alpha is %4.1f degrees\n\n';
fprintf(formatSpec, ALPHA)

formatSpec = 'Shear capacity is %4.2f MN\n';
fprintf(formatSpec, full(VRD))
formatSpec = 'Moment capacity is %4.2f MNm\n\n';
fprintf(formatSpec, full(MRD))

txt = sprintf('Utilization ratios: ');
disp(txt)
formatSpec = 'Shear ULS: %4.2f\n';
fprintf(formatSpec, full(Utilization_Shear))
formatSpec = 'Moment ULS: %4.2f\n';
fprintf(formatSpec, full(Utilization_Moment_final))
formatSpec = 'Moment during casting: %4.2f\n';
fprintf(formatSpec, full(Utilization_Moment_initial))
formatSpec = 'Moment LT-buckling: %4.2f\n';
fprintf(formatSpec, full(Utilization_Moment_LT))
formatSpec = 'SLS deflection: %4.2f\n\n';
fprintf(formatSpec, full(SLS_RATIO))

formatSpec = 'Total volume per meter is %4.5f m^3\n\n';
fprintf(formatSpec, Volume_Total)
Web_part=(Volume_Web/Volume_Total);
formatSpec = 'Web part of cross section is %4.3f\n';
fprintf(formatSpec, Web_part)
Flange_part=(Volume_Flange/Volume_Total);
formatSpec = 'Flange part of cross section is %4.3f\n\n';
fprintf(formatSpec, Flange_part)

formatSpec = 'SW ratio is %4.5f\n';
fprintf(formatSpec, SW_RATIO)

formatSpec = 'Reduction factor X shear is %4.5f\n';
fprintf(formatSpec, X_Shear)
disp('-----')
disp('Coordinates for one corrugation')
coord1=[0, 0];
coord2=[A4/2, A3/2];
coord3=[(A4/2)+A1, A3/2];
coord4=[(A4/2)+A1+A4, -A3/2];
coord5=[(A4/2)+A1+A4+A1, -A3/2];
coord6=[A4+A1+A4+A1, 0];

g=sprintf('%4.1f ', coord1);
fprintf('Coordinate 1: %s\n', g)

g=sprintf('%4.1f ', coord2);
fprintf('Coordinate 2: %s\n', g)

```

```

g=sprintf('%4.1f ', coord3);
fprintf(' Coordinate 3: %s\n', g)

g=sprintf('%4.1f ', coord4);
fprintf(' Coordinate 4: %s\n', g)

g=sprintf('%4.1f ', coord5);
fprintf(' Coordinate 5: %s\n', g)

g=sprintf('%4.1f ', coord6);
fprintf(' Coordinate 6: %s\n', g)

    end
end

```

Optimization sub-function

```

function [ALPHA, TW, HW, A1, A2, A3, A4, VRD, MRD, X_Shear, Xcl, Xcg, ...
    Utilization_Shear, Utilization_Moment_final, ...
    Utilization_Moment_initial, Utilization_Moment_LT, T1, B1, T2, B2, ...
    Volume_Web, Volume_Flange, Volume_Total, Position_Min_Volume, ...
    SW_RATIO, SLS_RATIO] = EVERYTHING_IN_ONE(Ec, alpha, a1, tw, hw, v, ...
    VULS, MULS, fyw, fyf, YMO, YMI, E, t1, b1, t2, b2, h_deck, b_deck, L, iteration, ...
    MSLS, VSLS, qSLS, Q1, MULS_initial, Lcr)

```

Geometry corrugation

```

% Trigonometry from alpha
cosal pha=cosd(al pha);
sin al pha=sind(al pha);
tan al pha=tand(al pha);

% Calculating corrugation dimesions from a1 and alpha
for i=1:iteration
    for j=1:iteration
        a4(j,i)=a1(i)*cosal pha(j);    %Inclined fold length in x-direction
        a2(j,i)=a4(j,i)/cosal pha(j);  %Inclined fold length
        a3(j,i)=a4(j,i)*tan al pha(j); %Corrugation depth
        if a1(i)>=a2(j,i)                %Picking largest of a1 and a2
            amax(j,i)=a1(i);
        else if a1(i)<a2(j,i)
            amax(j,i)=a2(j,i);
        end
    end
    w(j,i)=a1(i)+a4(j,i);                %One corrugation length in x-direction
    s(j,i)=a1(i)+a2(j,i);                %One corrugation length
    end
end

%-----

```

Shear capacity

This part calculates the shear capacity, according to Eurocode, for an interval of dimensions considering t_w , h_w , a_1 and α .

```
% Allocating space for matrices
Xcl=zeros(iteration*iteration);
Xcg=zeros(iteration*iteration);
X_shear=zeros(iteration*iteration);
Vrd=zeros(iteration*iteration);

for i=1:iteration
    for j=1:iteration
        for k=1:iteration
            for m=1:iteration

% Initiating process bar
if i==1 & j==1 & k==1 & m==1
h = waitbar(0, 'Step 1 of 4: Shear capacity calculation');
end

if j==1 & k==1 & m==1
waitbar(i/100, h, 'Step 1 of 4: Shear capacity calculation')
end

x=(k*iteration)-iteration+m;
y=(i*iteration)-iteration+j;

% Local reduction factor regarding shear
taocr1=4.83*E*(tw(i)/amax(m,j))^2; %Critical shear stress
lambdacl=sqrt((fyw)/(taocr1*sqrt(3))); %Slenderness
Xcl(x,y)=(1.15)/(0.9+lambdacl); %Local reduction factor

% Global reduction factor
Dx=((E*tw(i)^3)/((12*(1-v^2))))*(w(m,j)/s(m,j));
Dz=((E*tw(i)*a3(m,j)^2)/12)*((3*a1(i)+a2(m,j))/(a1(i)+a4(m,j)));
taocr2=(32.4/((tw(i)*hw(k)^2)))*((Dx*(Dz^3))^(1/4)); %Critical shear stress
lambdacg=(fyw/(taocr2*3^(1/2)))^(1/2); %Slenderness
Xcg(x,y)=(1.5)/(0.5+(lambdacg^2)); %Global reduction factor

% Picking lowest the lowest reduction factor
if Xcl(x,y)<Xcg(x,y)
    X_shear(x,y)=Xcl(x,y);
else if Xcl(x,y)>Xcg(x,y)
    X_shear(x,y)=Xcg(x,y);
end
end

if X_shear(x,y)>1
    X_shear(x,y)=1;
end

% Calculating shear resistances for every possible cross-section design.
Vrd(x,y)=X_shear(x,y)*((fyw)/(Ym1*sqrt(3)))*hw(k)*tw(i);

                end
            end
        end
    end
end
```

```

end

close(h)    %Close process bar

%-----

```

Moment resistance

This part calculates moment resistances, according to Eurocode. For moment resistance in ULS and SLS: self-weight, wind load and traffic load are considered. For moment resistance during casting and LT-buckling: only self-weight from girders and the concrete deck is considered.

```

% Allocating space for matrices
Atop=zeros(iteration*iteration);
Abottom=zeros(iteration*iteration);
Mrd_ULS=zeros(iteration*iteration);
Mrd_initial=zeros(iteration*iteration);
Mrd_LT=zeros(iteration*iteration);
Disp_max=zeros(iteration*iteration);
CT=zeros(iteration*iteration);

for i=1:iteration
    for j=1:iteration
        for k=1:iteration
            for m=1:iteration

% Initiating process bar
if i==1 & j==1 & k==1 & m==1
h = waitbar(0, 'Step 2 of 4: Moment capacity and SLS calculation');
end

if j==1 & k==1 & m==1
waitbar(i/100, h, 'Step 2 of 4: Moment capacity and SLS calculation')
end

x=(k*iteration)-iteration+m;
y=(i*iteration)-iteration+j;

% Calculating cross section class demands if CSC < CSC4
epsilon=0.698;
ctop=(b1(j)-tw(i))/2;    %Outstanding top flange distance
cttop=ctop/t1(i);
cbottom=(b2(m)-tw(i))/2;    %Outstanding bottom flange part
ctbottom=cbottom/t2(k);

% Picking cross sections that are lower than CRC 4
if cttop<11*epsilon & ctbottom<11*epsilon
    CT(x,y)=1;    %Less than CRC4
else if cttop>11*epsilon || ctbottom>11*epsilon
    CT(x,y)=0;    %CRC4
end
end

n=E/Ec;
% Areas for top and bottom flange
Atop(x,y)=t1(i)*b1(j);
Abottom(x,y)=t2(k)*b2(m);
Adeck=(h_deck*b_deck)/n;

```

```

% Distance from lower edge to gravity center of every member
ztop=t2(k)+hw(k)+t1(i)/2;
zbottom=t2(k)/2;
zdeck=t2(k)+hw(k)+t1(i)+h_deck/2;

% Calculating global gravity center for girder+concrete deck
ygc=((Atop(x,y)*ztop+Abottom(x,y)*zbottom+Adeck*zdeck)/(Atop(x,y)+...
    Abottom(x,y)+Adeck));

% Distance from each members gravity center to global gravity center
atop=ztop-ygc;
abottom=ygc-t2(k)/2;
adeck=zdeck-ygc;

% Second moment of area for total section
Itot=((b1(j)*t1(i)^3)/12)+Atop(x,y)*atop^2+((b2(m)*t2(k)^3)/12)+...
    Abottom(x,y)*abottom^2+((b_deck*(h_deck/n)^3)/12)+Adeck*adeck^2;
W=Itot/ygc;
Mrd_ULS(x,y)=(W*fyf)/YMO;

% Calculating moment resistance in ULS. Only tension flange will be
%considered because the top flange is restrained.

%-----

```

Moment capacity during casting

During casting the top flange will not be restrained and therefore both flanges needs to be checked.

```

% Areas for top and bottom flange
Atop(x,y)=t1(i)*b1(j);
Abottom(x,y)=t2(k)*b2(m);

% Distance from lower edge to gravity center of every member
ztop=t2(k)+hw(k)+t1(i)/2;
zbottom=t2(k)/2;

% Calculating global gravity center for only girder = no concrete deck.
ygc_initial=((Atop(x,y)*ztop+Abottom(x,y)*zbottom)/(Atop(x,y)+Abottom(x,y)));

% Distance from each members gravity center to global gravity center
adistop_initial=ztop-ygc_initial;
adibottom_initial=ygc_initial-t2(k)/2;

% Second moment of area for total section
Itot_initial=((b1(j)*t1(i)^3)/12)+Atop(x,y)*adistop_initial^2+...
    ((b2(m)*t2(k)^3)/12)+Abottom(x,y)*adibottom_initial^2;

Ncr_initial=(pi^2*E*Itot_initial)/Lcr^2; %Critical normal force
lambda_initial=sqrt((Atop(x,y)*fyf)/Ncr_initial); % Slenderness
alpha_phi=0.49;
phi_initial=0.5*(1+alpha_phi*(lambda_initial-0.2)+lambda_initial^2);

% Reduction factor for flange buckling in compression flange
X_initial=1/(phi_initial+sqrt(phi_initial^2-lambda_initial^2));

```

```

% Picking values lower than 1
if X_initial >= 1
    X_initial = 1;
end

Mrdt_initial = ((b2(m) * t2(k) * fyf) / YMO) * (hw(k) + ...
    (t1(i) + t2(k)) / 2); %Tension flange
Mrdc1_initial = ((b1(j) * t1(i) * fyf) / YMO) * (hw(k) + ...
    (t1(i) + t2(k)) / 2); %Compression flange
Mrdc2_initial = ((b1(j) * t1(i) * X_initial * fyf) / YM1) * ...
    (hw(k) + (t1(i) + t2(k)) / 2); %Compression flange

% Obtaining moment capacity during casting
if Mrdt_initial <= Mrdc1_initial
    mrd1 = Mrdt_initial;
else if Mrdt_initial > Mrdc1_initial
    mrd1 = Mrdc1_initial;
end

if mrd1 <= Mrdc2_initial
    Mrd_initial(x, y) = mrd1;
else if mrd1 > Mrdc2_initial
    Mrd_initial(x, y) = Mrdc2_initial;
end

%-----

```

Lateral torsional buckling capacity during casting

```

%LT-buckling is consider for initial moment without contribution from
%concrete section

alpha_LT = 0.49; %According to Eurocode 1993-1-4 section 5.4.2.1 stiff axis
lambda_OLT = 0.2;

I_top_LT = (b1(j) ^ 3 * t1(i)) / 12; %Second moment of area in y-direction

Ncr_LT = (pi ^ 2 * E * I_top_LT) / Lcr ^ 2; %Critical buckling load
lambda_LT = sqrt((A_top(x, y) * fyf) / Ncr_LT); %Slenderness
phi_LT = 0.5 * (1 + alpha_LT * (lambda_LT - lambda_OLT) + lambda_LT ^ 2);
XLT = 1 / (phi_LT + sqrt(phi_LT ^ 2 - lambda_LT ^ 2)); %LT-buckling reduction factor

if XLT >= 1 %Reduction factor shall be less than or 1
    XLT = 1;
end

% Calculating moment resistance regarding LT-buckling
Mrd_LT(x, y) = ((b1(j) * t1(i) * XLT * fyf) / YM1) * (hw(k) + (t1(i) + t2(k)) / 2);

%-----

```

SLS deflection calculations

Moment resistance regarding SLS is calculated regarding deflection in the mid span of the girder.

```
n=E/Ec;
Adeck=(h_deck*b_deck)/n; %Effective area for concrete deck

% Distance from lower edge to concrete deck local gravity center
zdeck=t2(k)+hw(k)+t1(i)+h_deck/2;

% Global gravity center
ygc=((Atop(x,y)*ztop+Abottom(x,y)*zbottom+Adeck*zdeck)/(Atop(x,y)+...
    Abottom(x,y)+Adeck));

% Distance from each members gravity center to global gravity center
adi stop=ztop-ygc;
adi sbottom=ygc-t2(k)/2;
adeck=zdeck-ygc;

% Second moment of area for total section
Itot=((b1(j)*t1(i)^3)/12)+Atop(x,y)*adi stop^2+((b2(m)*t2(k)^3)/12)+...
    Abottom(x,y)*adi sbottom^2+((b_deck*h_deck^3)/12)+Adeck*adeck;

htot=t1(i)+t2(k)+hw(k)+h_deck; %Total depth of section
si gma_c_ser=(MSLS/Itot)*(htot-ygc); %Pressure in compression flange
si gma_t_ser=(MSLS/Itot)*(-ygc); %Pressure in tension flange

% Calculating secant modulus of elasticity for stainless steel
nser=8;
E1=E/(1+0.002*(E/si gma_c_ser)*(si gma_c_ser/fyf)^nser);
E2=E/(1+0.002*(E/abs(si gma_t_ser))*(abs(si gma_t_ser)/fyf)^nser);
E_ser=(E1+E2)/2;

% Displacement due to self-weight, wind and distributed traffic
Di sp_sw=(5*qSLS*L^4)/(384*E_ser*Itot);

% Displacement due to point load traffic
Di sp_traffi c=(Q1*L^3)/(48*E_ser*Itot);

% Total displacement
Di sp_max(x,y)=Di sp_sw+Di sp_traffi c;

end
end
end
end
close(h) %Close process bar

%- -----
```

Calculating utilization ratios for all checks

```
% Allocating space for matrices
Ut_shear=zeros(iteration*iteration);
Ut_moment_final=zeros(iteration*iteration);
Ut_moment_initial=zeros(iteration*iteration);
Ut_moment_LT=zeros(iteration*iteration);
```

```

SLS_ratio=zeros(iteration*iteration);
Max_def=L/400;

for i=1:iteration
    for j=1:iteration
        for k=1:iteration
            for m=1:iteration

if i==1 & j==1 & k==1 & m==1
h = waitbar(0, 'Step 3 of 4: Calculating Utilization ratios');
end

if j==1 & k==1 & m==1
waitbar(i/100, h, 'Step 3 of 4: Calculating Utilization ratios')
end

x=(k*iteration)-iteration+m;
y=(i*iteration)-iteration+j;

% Shear utilization
if VULS/Vrd(x, y)>1
    Ut_shear(x, y)=0;
else if VULS/Vrd(x, y)<=1
    Ut_shear(x, y)=VULS/Vrd(x, y);
end
end

% Moment utilization final
if MULS/Mrd_ULS(x, y)>1
    Ut_moment_final(x, y)=0;
else if MULS/Mrd_ULS(x, y)<=1
    Ut_moment_final(x, y)=MULS/Mrd_ULS(x, y);
end
end

% Moment utilization initial
if MULS_initial/Mrd_initial(x, y)>1
    Ut_moment_initial(x, y)=0;
else if MULS_initial/Mrd_initial(x, y)<=1
    Ut_moment_initial(x, y)=MULS_initial/Mrd_initial(x, y);
end
end

% Moment utilization LT
if MULS_initial/Mrd_LT(x, y)>1
    Ut_moment_LT(x, y)=0;
else if MULS_initial/Mrd_LT(x, y)<=1
    Ut_moment_LT(x, y)=MULS_initial/Mrd_LT(x, y);
end
end

% SLS utilization
if Disp_max(x, y)/Max_def>1
    SLS_ratio(x, y)=0;
else if Disp_max(x, y)/Max_def<=1
    SLS_ratio(x, y)=Disp_max(x, y)/Max_def;
end
end

```

```

        end
    end
end
end

close(h)

%-----

```

Calculations to get lowest steel volume

This section picks the lowest volume for all designs that fulfils checks

```

% Allocating space for matrices
Volume_total=zeros(iteration*iteration);
imatrix=zeros(iteration*iteration);
jmatrix=zeros(iteration*iteration);
kmatrix=zeros(iteration*iteration);
mmatrix=zeros(iteration*iteration);
Volume_shear=zeros(iteration*iteration);
Volume_moment=zeros(iteration*iteration);
swratio=zeros(iteration*iteration);

MIN=10;
for i=1:iteration
    for j=1:iteration
        for k=1:iteration
            for m=1:iteration

if i==1 & j==1 & k==1 & m==1
h = waitbar(0, 'Step 4 of 4: Picking lowest volume');
end

if j==1 & k==1 & m==1
waitbar(i/100, h, 'Step 4 of 4: Picking lowest volume')
end

x=(k*iteration)-iteration+m;
y=(i*iteration)-iteration+j;

% Calculating web and flange volume for all designs
swratio(x, y)=s(m, j)/w(m, j); %Length of corrugation per meter girder
Volume_shear(x, y)=tw(i)*hw(k)*swratio(m, j); %Volume web
Volume_moment(x, y)=A_top(x, y)+A_bottom(x, y)*1; %Volume flanges

%Find lowest volume
if Ut_moment_final(x, y)==0 || Ut_shear(x, y)==0 || SLS_ratio(x, y)==0 || ...
    Ut_moment_initial(x, y)==0 || Ut_moment_LT(x, y)==0 || CT(x, y)==0
    Volume_total(x, y)=5;
else if Ut_moment_final(x, y)>0 & Ut_shear(x, y)>0 & SLS_ratio(x, y)>0 & ...
    Ut_moment_initial(x, y)>0 & Ut_moment_LT(x, y)>0
    Volume_total(x, y)=Volume_moment(x, y)+Volume_shear(x, y);
end
end
% if Volume_total(x, y)==0
%     Volume_total(x, y)=5;
% end

```

```

if MIN>Volume_total(x,y)
    MIN=Volume_total(x,y);
end

%Create i, j, k, m matrices to find cross-section parameters
imatrix(x,y)=i;
jmatrix(x,y)=j;
kmatrix(x,y)=k;
mmatrix(x,y)=m;
    end
end
end

close(h)
clear Abottom Atop

% Finds coordinates of minimum volume
valueToFind = MIN;
[row, column] = find(Volume_total == valueToFind);
PositionMin_Volume = ...
[row(1) , column(1)];      % In format [x,y] NOT [row, column]

iMIN=imatrix(PositionMin_Volume(1), PositionMin_Volume(2));
jMIN=jmatrix(PositionMin_Volume(1), PositionMin_Volume(2));
kMIN=kmatrix(PositionMin_Volume(1), PositionMin_Volume(2));
mMIN=mmatrix(PositionMin_Volume(1), PositionMin_Volume(2));

clear imatrix jmatrix kmatrix mmatrix

%-----

```

Values to present in command window

```

% Web dimensions
TW=tw(iMIN)*1000;
HW=hw(kMIN)*1000;

% Corrugation dimensions
A1=a1(jMIN)*1000;
A2=a2(mMIN,jMIN)*1000;
A3=a3(mMIN,jMIN)*1000;
A4=a4(mMIN,jMIN)*1000;
ALPHA=alpha(mMIN);

% Flanges dimensions
T1=t1(iMIN)*10^3;
B1=b1(jMIN)*10^3;
T2=t2(kMIN)*10^3;
B2=b2(mMIN)*10^3;

% Shear and moment capacity
VRD=Vrd(PositionMin_Volume(1), PositionMin_Volume(2))/1000000;
MRD=Mrd_ULS(PositionMin_Volume(1), PositionMin_Volume(2))/1000000;

% Utilization ratios
Utilization_Shear=Ut_shear(PositionMin_Volume(1), ...

```

```

    Position_Mn_Volume(2);
    Utilization_Moment_final=Ut_moment_final(Position_Mn_Volume(1),...
    Position_Mn_Volume(2));
    Utilization_Moment_initial=Ut_moment_initial(Position_Mn_Volume(1),...
    Position_Mn_Volume(2));
    Utilization_Moment_LT=Ut_moment_LT(Position_Mn_Volume(1),...
    Position_Mn_Volume(2));
    SLS_RATIO=SLS_ratio(Position_Mn_Volume(1), Position_Mn_Volume(2));

% Reduction factor shear
X_Shear=X_shear(Position_Mn_Volume(1), Position_Mn_Volume(2));

% Volumes
Volume_Web=Volume_shear(Position_Mn_Volume(1), Position_Mn_Volume(2));
Volume_Flange=Volume_moment(Position_Mn_Volume(1), Position_Mn_Volume(2));
Volume_Total=Volume_total(Position_Mn_Volume(1), Position_Mn_Volume(2));
SW_RATIO=swratio(Position_Mn_Volume(1), Position_Mn_Volume(2));

```

[Published with MATLAB® R2017b](#)

Appendix B – FE-results regarding case studies

FE-results for Skulnäs bridge designs

Initial imperfection = 4 mm Hw=1421mm 10 kN					Initial imperfection = 4 mm Hw=2500mm 10 kN				
Increment	LPF	kN	Def	Def+Initial	Increment	LPF	kN	Def	Def+Initial
0	0	0	0	0	0	0	0	0	0
1	0,999994	9,99994	0,00464	4,0046407	1	0,99995	9,9995	0,02043	4,020433
2	1,99997	19,9997	0,0093	4,009297	2	1,99978	19,9978	0,04092	4,040924
3	3,49992	34,9992	0,01631	4,0163105	3	3,49933	34,9933	0,07177	4,071772
4	5,74979	57,4979	0,0269	4,0268969	4	5,74823	57,4823	0,1183	4,1183
5	9,12448	91,2448	0,04293	4,0429281	5	9,1206	91,206	0,18968	4,189679
6	14,1862	141,862	0,06732	4,0673236	6	14,1769	141,769	0,29561	4,295612
7	21,7782	217,782	0,10473	4,10473	7	21,7561	217,561	0,45924	4,459242
8	33,1644	331,644	0,16277	4,162771	8	33,1125	331,125	0,71253	4,71253
9	50,2392	502,392	0,25455	4,25455	9	50,1173	501,173	1,11244	5,11244
10	75,83	758,3	0,40376	4,403759	10	75,5481	755,481	1,76665	5,76665
11	101,367	1013,67	0,56627	4,566274	11	113,334	1133,34	2,903	6,903
12	126,87	1268,7	0,75078	4,750775	12	168,257	1682,57	5,16021	9,16021
13	152,309	1523,09	0,95639	4,956389	13	231,476	2314,76	10,4736	14,4736
14	176,655	1766,55	1,3568	5,3568	14	231,952	2319,52	10,563	14,563
15	179,095	1790,95	8,1504	12,1504	15	232,393	2323,93	10,673	14,673
16	177,635	1776,35	10,1492	14,1492	16	232,96	2329,6	10,9289	14,9289
17	175,831	1758,31	12,307	16,307	17	232,332	2323,32	11,2751	15,2751
18	171,816	1718,16	16,3167	20,3167	18	231,137	2311,37	11,2585	15,2585
19	165,794	1657,94	21,0749	25,0749	19	230,04	2300,4	11,2009	15,2009
20	158,313	1583,13	26,1288	30,1288	20	228,395	2283,95	11,0853	15,0853
21	150,458	1504,58	31,1498	35,1498	21	225,935	2259,35	10,8891	14,8891
22	142,754	1427,54	35,8692	39,8692	22	222,21	2222,1	10,5794	14,5794
23	133,774	1337,74	41,0377	45,0377	23	216,516	2165,16	10,1087	14,1087
24	131,614	1316,14	42,293	46,293	24	205,525	2055,25	9,22081	13,22081
25	129,45	1294,5	43,5648	47,5648	25	190,525	1905,25	8,07899	12,07899
26	126,185	1261,85	45,4979	49,4979	26	187,106	1871,06	7,82992	11,82992
27	121,021	1210,21	48,4085	52,4085	27	183,672	1836,72	7,58356	11,58356
28	111,324	1113,24	50,0718	54,0718	28	178,505	1785,05	7,21877	11,21877
29	104,736	1047,36	49,0799	53,0799	29	175,632	1756,32	7,03654	11,03654
30	103,847	1038,47	48,976	52,976	30	171,252	1712,52	6,82519	10,82519
31	103,104	1031,04	48,9266	52,9266	31	167,338	1673,38	6,65271	10,65271
32	102,293	1022,93	48,9853	52,9853	32	163,723	1637,23	6,48652	10,48652
33	101,798	1017,98	49,3827	53,3827	33	160,776	1607,76	6,34369	10,34369
34	102,184	1021,84	50,4858	54,4858	34	155,937	1559,37	6,10371	10,10371
35	104,168	1041,68	53,3273	57,3273	35	148,683	1486,83	5,74847	9,74847
36	106,847	1068,47	55,5598	59,5598	36	140,953	1409,53	5,40898	9,40898
37	109,464	1094,64	57,3549	61,3549	37	139,716	1397,16	5,36705	9,36705
38	111,869	1118,69	58,8116	62,8116	38	138,651	1386,51	5,33986	9,33986
39	113,747	1137,47	60,1306	64,1306	39	137,451	1374,51	5,32181	9,32181
40	115,627	1156,27	61,7182	65,7182	40	136,64	1366,4	5,34238	9,34238
41	116,541	1165,41	62,8454	66,8454	41	136,418	1364,18	5,4198	9,4198
42	116,977	1169,77	63,7535	67,7535	42	136,548	1365,48	5,48818	9,48818
43	116,565	1165,65	64,0644	68,0644	43	131,717	1317,17	4,2199	8,2199
44	116,002	1160,02	64,4637	68,4637	44	129,996	1299,96	3,85463	7,85463
45	113,493	1134,93	65,5922	69,5922	45	128,618	1286,18	3,53574	7,53574
46	112,77	1127,7	66,2623	70,2623	46	127,056	1270,56	3,1116	7,1116
47	112,107	1121,07	66,8159	70,8159	47	125,616	1256,16	2,54672	6,54672
48	110,91	1109,1	67,4386	71,4386	48	124,989	1249,89	2,23022	6,23022
49	108,331	1083,31	68,2625	72,2625	49	123,715	1237,15	1,62488	5,62488
50	105,394	1053,94	69,2567	73,2567	50	122,189	1221,89	1,19436	5,19436
51	101,582	1015,82	70,3969	74,3969	51	120,287	1202,87	0,77162	4,77162
52	100,663	1006,63	70,6869	74,6869	52	119,022	1190,22	0,42537	4,42537
53	99,7447	997,447	70,986	74,986	53	118,063	1180,63	-0,029	3,970995
54	98,3733	983,733	71,4406	75,4406	54	116,964	1169,64	-0,8742	3,125762
55	96,5208	965,208	72,1335	76,1335	55	116,248	1162,48	-1,5388	2,4612
56	94,9669	949,669	72,8358	76,8358	56	114,568	1145,68	-2,8535	1,14653
57	93,4196	934,196	73,561	77,561	57	113,647	1136,47	-3,4433	0,55673
58	91,7276	917,276	74,2496	78,2496	58	112,563	1125,63	-4,0481	-0,0481
59	90,0985	900,985	74,6726	78,6726	59	110,87	1108,7	-4,8452	-0,84518
60	88,2766	882,766	74,8166	78,8166	60	110,68	1106,8	-4,9243	-0,92431

Shear capacity from Abaqus = 1790,95 kN	Shear capacity from Abaqus = 2329,6 kN
Shear capacity from Matlab = 1530 kN	Shear capacity from Matlab = 1530 kN

FE-results for Nissan bridge designs

Initial imperfection = 11 mm Hw=500mm 10 kN					Initial imperfection = 4 mm Hw=1500mm 10 kN				
Increment	LPF	kN	Def	f+Initial	Increment	LPF	kN	Def	f+Initial
0	0	0	0	11	0	0	0	0	4
1	0,99996	9,99956	0,00312	11,00312	1	0,99999	9,99994	0,01091	4,01091
2	1,9998	19,998	0,00625	11,00625	2	1,99997	19,9997	0,02187	4,02187
3	3,49941	34,9941	0,01094	11,01094	3	3,49992	34,9992	0,03842	4,03842
4	5,74846	57,4846	0,01799	11,01799	4	5,74978	57,4978	0,06347	4,06347
5	9,12121	91,2121	0,02857	11,02857	5	9,12446	91,2446	0,10158	4,10158
6	14,1784	141,784	0,04447	11,04447	6	14,1862	141,862	0,15997	4,15997
7	21,7601	217,601	0,06841	11,06841	7	21,7781	217,781	0,25047	4,25047
8	33,1231	331,231	0,10449	11,10449	8	33,1644	331,644	0,39322	4,39322
9	50,1463	501,463	0,15901	11,15901	9	50,2391	502,391	0,62485	4,62485
10	75,6225	756,225	0,24166	11,24166	10	75,8382	758,382	1,01875	5,01875
11	112,882	1128,82	0,36583	11,36583	11	114,193	1141,93	1,74603	5,74603
12	164,628	1646,28	0,73283	11,73283	12	171,484	1714,84	3,36156	7,36156
13	181,064	1810,64	2,33745	13,33745	13	175,4	1754	13,2032	17,2032
14	187,274	1872,74	4,00964	15,00964	14	172,971	1729,71	16,5162	20,5162
15	190,896	1908,96	5,57947	16,57947	15	170,195	1701,95	20,0036	24,0036
16	194,396	1943,96	7,87449	18,87449	16	167,197	1671,97	23,6398	27,6398
17	197,197	1971,97	11,4787	22,4787	17	162,111	1621,11	29,4933	33,4933
18	198,224	1982,24	17,6089	28,6089	18	156,587	1565,87	35,2998	39,2998
19	190,817	1908,17	31,1293	42,1293	19	151,023	1510,23	40,4025	44,4025
20	187,777	1877,77	34,6055	45,6055	20	149,506	1495,06	41,6674	45,6674
21	185,068	1850,68	37,7937	48,7937	21	148,094	1480,94	42,797	46,797
22	183,406	1834,06	40,5057	51,5057	22	146,704	1467,04	43,8617	47,8617
23	182,59	1825,9	42,8407	53,8407	23	144,605	1446,05	45,4056	49,4056
24	182,304	1823,04	44,8909	55,8909	24	141,43	1414,3	47,6358	51,6358
25	182,318	1823,18	46,6961	57,6961	25	139,628	1396,28	48,8973	52,8973
26	182,573	1825,73	49,0506	60,0506	26	136,897	1368,97	50,8554	54,8554
					27	135,352	1353,52	52,0377	56,0377
					28	132,944	1329,44	54,0399	58,0399
					29	131,628	1316,28	55,2944	59,2944
					30	128,973	1289,73	58,1439	62,1439
					31	126,722	1267,22	60,6467	64,6467
					32	124,871	1248,71	62,9247	66,9247
					33	122,722	1227,22	66,0342	70,0342
					34	120,739	1207,39	69,5963	73,5963
					35	119,362	1193,62	72,3481	76,3481
					36	118,199	1181,99	74,576	78,576
					37	117,072	1170,72	76,3717	80,3717
					38	115,918	1159,18	77,7306	81,7306
					39	115,2	1152	78,088	82,088
					40	114,416	1144,16	77,9218	81,9218
					41	111,743	1117,43	76,9695	80,9695
					42	111,172	1111,72	76,7452	80,7452
					43	110,642	1106,42	76,5076	80,5076
					44	109,967	1099,67	76,0844	80,0844
					45	110,026	1100,26	75,537	79,537
					46	111,275	1112,75	75,1755	79,1755
					47	112,998	1129,98	75,48	79,48
					48	113,889	1138,89	76,8244	80,8244
					49	111,269	1112,69	79,2758	83,2758
					50	110,047	1100,47	79,5347	83,5347
					51	108,525	1085,25	79,7572	83,7572
					52	101,176	1011,76	80,2739	84,2739
					53	98,6701	986,701	80,434	84,434
					54	97,8004	978,004	80,4949	84,4949
					55	96,9315	969,315	80,5603	84,5603
					56	95,5942	955,942	80,6801	84,6801
					57	91,6806	916,806	80,6166	84,6166
					58	90,1592	901,592	80,5884	84,5884
					59	88,6341	886,341	80,5592	84,5592
					60	86,3384	863,384	80,5137	84,5137
Shear capacity from Abaqus = 1982,24 kN					Shear capacity from Abaqus = 1754 kN				
Shear capacity from Matlab = 1530 kN					Shear capacity from Matlab = 1530 kN				

Appendix C – Results from LCC studies

LCC study results for Skulnäs bridge

Original bridge design - Geometry											
	Cross-section [m]	Length [m]	Volume [m3]	Steel class	Density [kg/m3]	Weight [Ton]					
Web			0,5403	S355	7850	4,241					
hw	1,34	33,6									
tw	0,012	33,6									
Top Plate			0,4704	S355	7850	3,693					
t1	0,028	19,6									
	0,028	14									
b1	0,5	19,6									
	0,5	14									
Bottom Plate			0,676368	S420	7850	5,309					
t2	0,033	19,6									
	0,033	14									
b2	0,61	33,6									
Total for 2 beams			3,374			26,487					
Total area for repainting		295,68	m ²								
Cross-section area		0,05021	m ²								
						3% rate					
LCC - 100 years		ADT=10000	ADT=20000	ADT=5000							
Investment cost		1239195	1239195	1239195							
Maintenance and repair		732808	732808	732808							
User cost		184980	370052	92490							
Total		2156983	2342055	2064493							
						ADT 10000					
LCC - 100 years	%	0	1	2	3	4	5	6	7	3	3
Investment cost		1239195	1239195	1239195	1239195	1239195	1239195	1239195	1239195	1239195	1239195
Repair cost		2486400	1387192	836394	538735	365758	258500	188272	140236	538735	538735
Operation and maintenance		626400	393237	267063	194073	148981	119366	98832	83920	194073	194073
User cost		639600	390921	259513	184981	139691	110371	90310	75929	82490	369962
Demolition cost		123920	45814	17105	6448	2454	942	365	143	6448	6448
Total		5115515	3456359	2619270	2163432	1896079	1728374	1616974	1539423	2060941	2348413

Stainless steel flat web bridge design - Geometry											
	Cross-section [m]	Length [m]	Volume [m3]	Steel class	Density [kg/m3]	Weight [Ton]					
Web			0,5248	S355	7850	4,120					
hw	1,42	33,6									
tw	0,011	33,6									
Top Plate			0,4032	S355	7850	3,165					
t1	0,03	19,6									
	0,03	14									
b1	0,4	19,6									
	0,4	14									
Bottom Plate			0,5292	S420	7850	4,154					
t2	0,035	19,6									
	0,035	14									
b2	0,45	33,6									
Total for 2 beams			2,914			22,879					
Total area for re-painting		278,208	m ²								
Cross-section area		0,04337	m ²								
						3% rate					
LCC - 100 years		ADT=10000	ADT=20000	ADT=5000							
Investment cost		1667937	1667937	1667937							
Repair and repainting cost		91693	91693	91693							
User cost		19891	39782	9945							
Total		1779521	1799412	1769575							
						ADT 10000					
LCC - 100 years	%	0	1	2	3	4	5	6	7	3	3
Investment cost		1667937	1667937	1667937	1667937	1667937	1667937	1667937	1667937	1667937	1667937
Repair cost		0	0	0	0	0	0	0	0	0	0
Operation and maintenance		302400	189023	137424	91693	69585	55059	44991	37688	91693	91693
User cost		65600	41005	27642	19891	15095	11944	9760	8176	9945	39782
Demolition cost		166794	61666	23023	8679	3303	1268	492	192	8679	8679
Total		2202731	1959631	1856026	1788200	1755920	1736208	1723180	1713993	1778254	1808091

Stainless steel corrugated web bridge design - 1421mm						
	Cross-section [m]	Length [m]	Volume [m3]	Steel class	Density [kg/m3]	Weight [Ton]
Web			0,2005	1.4162	7800	1,564
hw	1,421	33,6				
tw	0,0042	33,6				
Top Plate			0,3839136	1.4162	7800	2,995
t1	0,029	33,6				
b1	0,394	33,6				
Bottom Plate			0,618408	1.4162	7800	4,824
t2	0,045	33,6				
b2	0,409	33,6				
Total for 2 beams			2,438			19,015
Total area for re-painting		287,707392	m ²			
Effective Cross-section area		0,036276656	m ²			
Geometry-ratio	1,08					
			3% rate			
LCC - 100 years		ADT=10000	ADT=20000	ADT=5000		
Investment cost		1415125	1415125	1415125		
Maintenance and repair		91693	91693	91693		
User cost		19891	39782	9945		
Total		1526709	1546600	1516763		

		ADT 10000							ADT 5000	ADT 20000	
LCC - 100 years	%	0	1	2	3	4	5	6	7	3	3
Investment cost		1415125	1415125	1415125	1415125	1415125	1415125	1415125	1415125	1415125	1415125
Repair cost		0	0	0	0	0	0	0	0	0	0
Operation and maintenance		302400	189023	127424	91693	69585	55059	44991	37688	91693	91693
User cost		65600	41005	27642	19891	15095	11944	9760	8176	9945	39782
Demolition cost		141513	52319	19533	7363	1802	1076	417	163	7363	7363
Total		1924638	1697472	1589724	1534072	1501607	1483204	1470293	1461152	1524126	1553963

Stainless steel corrugated web bridge design - 2500mm						
	Cross-section [m]	Length [m]	Volume [m3]	Steel class	Density [kg/m3]	Weight [Ton]
Web			0,3091	1.4162	7800	2,411
hw	2,5	33,6				
tw	0,00368	33,6				
Top Plate			0,27719328	1.4162	7800	2,162
t1	0,0247	33,6				
b1	0,334	33,6				
Bottom Plate			0,3650304	1.4162	7800	2,847
t2	0,028	33,6				
b2	0,388	33,6				
Total for 2 beams			1,952			15,227
Total area for re-painting		336	m ²			
Effective Cross-section area		0,0290498	m ²			
SW-ratio	1,08					
			3% rate			
LCC - 100 years		ADT=10000	ADT=20000	ADT=5000		
Investment cost		1168905	1168905	1168905		
Maintenance and repair		91693	91693	91693		
User cost		19891	39782	9945		
Total		1280489	1300380	1270543		

		ADT 10000							ADT 5000	ADT 20000	
LCC - 100 years	%	0	1	2	3	4	5	6	7	3	3
Investment cost		1168905	1168905	1168905	1168905	1168905	1168905	1168905	1168905	1168905	1168905
Repair cost		0	0	0	0	0	0	0	0	0	0
Operation and maintenance		302400	189023	127424	91693	69585	55059	44991	37688	91693	91693
User cost		65600	41005	27642	19891	15095	11944	9760	8176	9945	39782
Demolition cost		116891	43216	16135	6082	2314	889	345	135	6082	6082
Total		1653796	1442149	1340106	1286571	1255899	1236797	1224001	1214904	1276625	1306462

LCC study results for Nissan bridge

Original bridge design - Geometry						
	Cross-section [m]	Length [m]	Volume [m3]	Steel class	Density [kg/m3]	Weight [Ton]
Web			0,3133	S355	7850	2,460
hw	0,51	38,4				
tw	0,016					
Top Plate			0,384	S355	7850	3,014
t1	0,025	38,4				
b1	0,4					
Bottom Plate			0,6912	S420	7850	5,426
t2	0,045	38,4				
b2	0,4					
Total for 2 beams			2,777			21,800
Total area for repainting		170,496	m ²			
Cross-section area		0,03616	m ²			
		ADT 5000	ADT 10000	ADT 20000		
LCC - 100 years	%	3	3	3		
Investment cost		1145455	1145455	1145455		
Repair cost		310319	310319	310319		
Operation and maintenance		194073	194073	194073		
User cost		113511	227022	454044		
Demolition cost		5960	5960	5960		
Total		1769318	1882829	2109851		

Stainless steel flat web bridge design - Geometry						
	Cross-section [m]	Length [m]	Volume [m3]	Steel class	Density [kg/m3]	Weight [Ton]
Web			0,2661	1.4166	7800	2,076
hw	0,495	38,4				
tw	0,014					
Top Plate			0,3072	1.4166	7800	2,396
t1	0,02	38,4				
b1	0,4					
Bottom Plate			0,5376	1.4166	7800	4,193
t2	0,035	38,4				
b2	0,4					
Total for 2 beams			2,222			17,330
Total area for re-painting		168,192	m ²			
Cross-section area		0,02893	m ²			
		ADT 5000	ADT 10000	ADT 20000		
LCC - 100 years	%	3	3	3		
Investment cost		1307252	1307252	1307252		
Repair cost		0	0	0		
Operation and maintenance		91693	91693	91693		
User cost		12206	24412	48823		
Demolition cost		6802	6802	6802		
Total		1417953	1430159	1454570		

Stainless steel corrugated web bridge design - 500mm						
	Cross-section [m]	Length [m]	Volume [m3]	Steel class	Density [kg/m3]	Weight [Ton]
Web			0,2260	1.4166	7800	1,763
hw	0,5	38,4				
tw	0,0109					
Top Plate			0,28121472	1.4166	7800	2,193
t1	0,0237	38,4				
b1	0,309					
Bottom Plate			0,6235392	1.4166	7800	4,864
t2	0,046	38,4				
b2	0,353					
Total for 2 beams			2,262			17,640
Total area for re-painting		160,896	m ²			
Effective Cross-section area		0,0294473	m ²			
Geometry-ratio	1,08					
		ADT 5000	ADT 10000	ADT 20000		
LCC - 100 years	%	3	3	3		
Investment cost		1325750	1325750	1325750		
Repair cost		0	0	0		
Operation and maintenance		91693	91693	91693		
User cost		12206	24412	48823		
Demolition cost		6898	6898	6898		
Total		1436547	1448753	1473164		

Stainless steel corrugated web bridge design - 2500mm						
	Cross-section [m]	Length [m]	Volume [m3]	Steel class	Density [kg/m3]	Weight [Ton]
Web			0,2565	1.4162	7800	2,000
hw	1,5	38,4				
tw	0,0041					
Top Plate			0,1919232	1.4162	7800	1,497
t1	0,0245	38,4				
b1	0,204					
Bottom Plate			0,2210688	1.4162	7800	1,724
t2	0,0285	38,4				
b2	0,202					
Total for 2 beams			1,339			10,444
Total area for re-painting		277,0944	m ²			
Effective Cross-section area		0,0174339	m ²			
SW-ratio	1,086					
		ADT 5000	ADT 10000	ADT 20000		
LCC - 100 years	%	3	3	3		
Investment cost		858010	858010	858010		
Repair cost		0	0	0		
Operation and maintenance		91693	91693	91693		
User cost		12206	24412	48823		
Demolition cost		4464	4464	4464		
Total		966373	978579	1002990		

Appendix D – FE-results from parametric studies

FE-results for different flat fold lengths a_1 and different web depths.

Hw=1000mm tw=4mm alpha=32 L/H=2														L=2000	
FEM 1.4162	a1 [mm]	25	50	57	80	100	120	150	200	250	300	320	350		
FEM 1.4162 Imp.=Hw/200	Shear cap. [kN]	728	1170	1218	1211	1123		1147	983	889					
FEM 1.4162 Imp.=Tw		742	1197	1238	1239	1233	1219	1179	1024	918	782	788	743		
	Buckling mode	Global	Global	Global	Inter.	Inter.	Inter.	Inter.	Local	Local	Local	Local	Local		
	Eigenvalue	77	296	394	610	504	445	337	219	140	91	83	69		
FEM S355	a1 [mm]	25	50	80	100	200									
FEM S355 Imp.=Hw/200	Shear cap. [kN]	579	793	799	799	696									
	Buckling mode	Global	Global	Inter.	Inter.	Inter.									
	Eigenvalue	81	311	640	530	230									

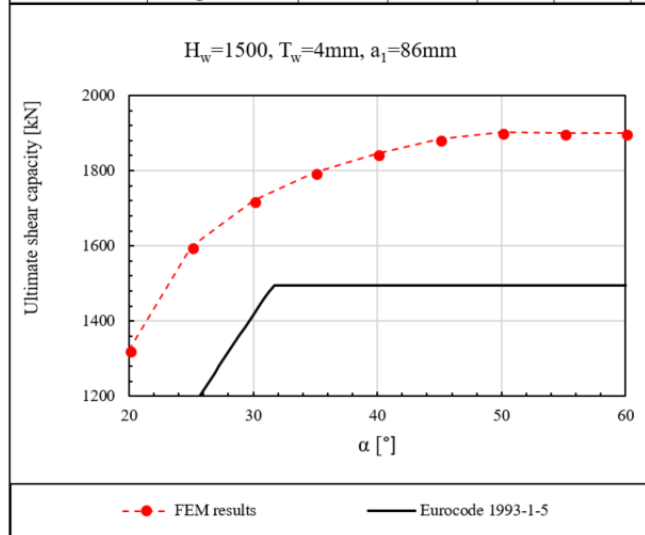
Hw=1500mm tw=4mm alpha=32 L/H=2														L=3000	
FEM 1.4162	a1 [mm]	50	80	86	100	120	150	200	250	300	320	350			
FEM 1.4162 Imp.=Hw/200	Shear cap. [kN]	1177	1728	1754	1803		1511	1346	1160						
FEM 1.4162 Imp.=Tw		1254	1813	1831	1868	1774	1669	1540	1292	1118	1082	1010			
	Buckling mode	Global	Global	Global	Global	Inter.	Inter.	Inter.	Local	Local	Local	Local			
	Eigenvalue	164	439	497	629	532	388	296	196	128	116	95			
FEM S355	a1 [mm]	50	80	100	150										
FEM S355 Imp.=Hw/200	Shear cap. [kN]	961	1166	1191	1059										
	Buckling mode	Global	Global	Global	Inter.										
	Eigenvalue	172	461	660	407										

Hw=2000mm tw=4mm alpha=32 L/H=2														L=4000	
FEM 1.4162	a1 [mm]	50	80	100	120	135	150	175	200	220	250	275	300		
FEM 1.4162 Imp.=Hw/200	Shear cap. [kN]	1021	1793	2121	2267	1713	1616		1586						
FEM 1.4162 Imp.=Tw		1106	2119	2362	2434	2192	2156	2046	2031	1998	1684	1574	1462		
	Buckling mode	Global	Global	Global	Global	Inter.	Inter.	Inter.	Inter.	Inter.	Local	Local	Local		
	Eigenvalue	109	293	446	591	481	439	364	334	313	255	196	165		
FEM S355	a1 [mm]	50	80	120	150										
FEM S355 Imp.=Hw/200	Shear cap. [kN]	859	1369	1527	1254										
	Buckling mode	Global	Global	Global	Inter.										
	Eigenvalue	115	308	621	461										

Hw=2500mm tw=4mm alpha=32 L/H=2														L=5000	
FEM 1.4162	a1 [mm]	50	80	100	120	150	200	220	250	275	300				
FEM 1.4162 Imp.=Hw/200	Shear cap. [kN]	968		2015	2508	1840	1620	1696	1606		1493				
FEM 1.4162 Imp.=Tw		1004	1849	2508	2784	2636	2372	2330	2146	2079	1815				
	Buckling mode	Global	Global	Global	Global	Inter.	Inter.	Inter.	Inter.	Local	Local				
	Eigenvalue	82	214	324	447	498	363	342	302	238	203				
FEM S355	a1 [mm]	50	100	120	150	200									
FEM S355 Imp.=Hw/200	Shear cap. [kN]	802	1653	1806	1478	1400									
	Buckling mode	Global	Global	Global	Inter.	Inter.									
	Eigenvalue	86	341	469	523	381									

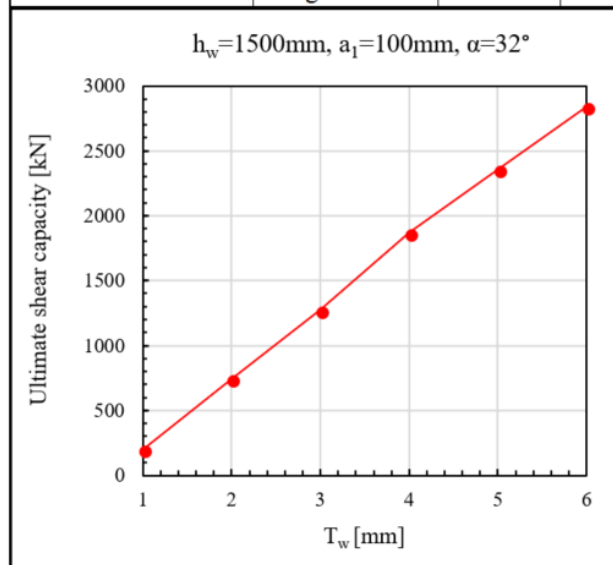
FE-results regarding influence of corrugation angle α on ultimate shear capacity.

		Hw=1500mm, Tw=4mm, a1=86mm								
FEM results	alpha	20	25	30	35	40	45	50	55	60
Initial imp.=Tw	Shear cap.	1324	1599	1721	1796	1846	1884	1903	1901	1900
	Buckling mode	Global	Global	Global	Global	Global	Global	Inter.	Inter.	Inter.
	Eigenvalue	224	331	449	577	708	846	960	1007	1055



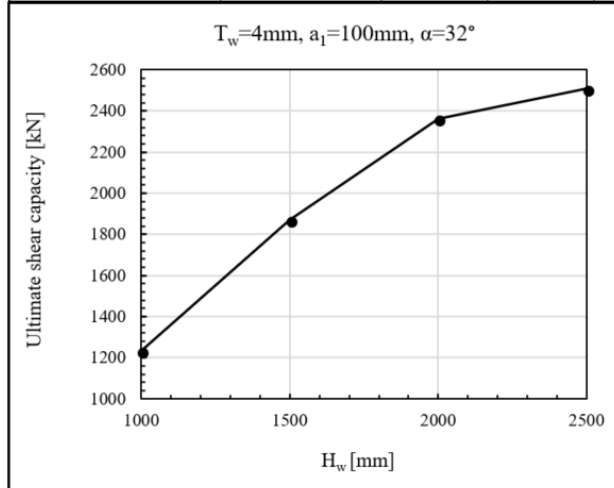
FE-results regarding influence of Tw on ultimate shear capacity

		Hw=1500mm, a1=100mm, alpha=32						
		Tw	1	2	3	4	5	6
FEM Imp.=Hw/200	Shear cap.		156	598	1145	1803	2287	2759
H _w =1500mm			197	741	1273	1868	2357	2836
	Buckling mode		Inter.	Inter.	Inter.	Global	Global	Global
	Eigen value		31	135	330	629	792	945



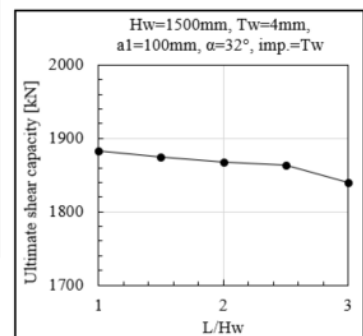
FE-results regarding influence of Hw on ultimate shear capacity.

		Tw=4mm, a1=100, alpha=32				
		Hw [mm]	1000	1500	2000	2500
FEM Imp.=Hw/200	Shear cap		1123	1803	2121	2015
Initial Imp.=Tw			1233	1868	2362	2508
	Buckling mode		Inter.	Global	Global	Global
	Eigenvalue		504	629	446	324

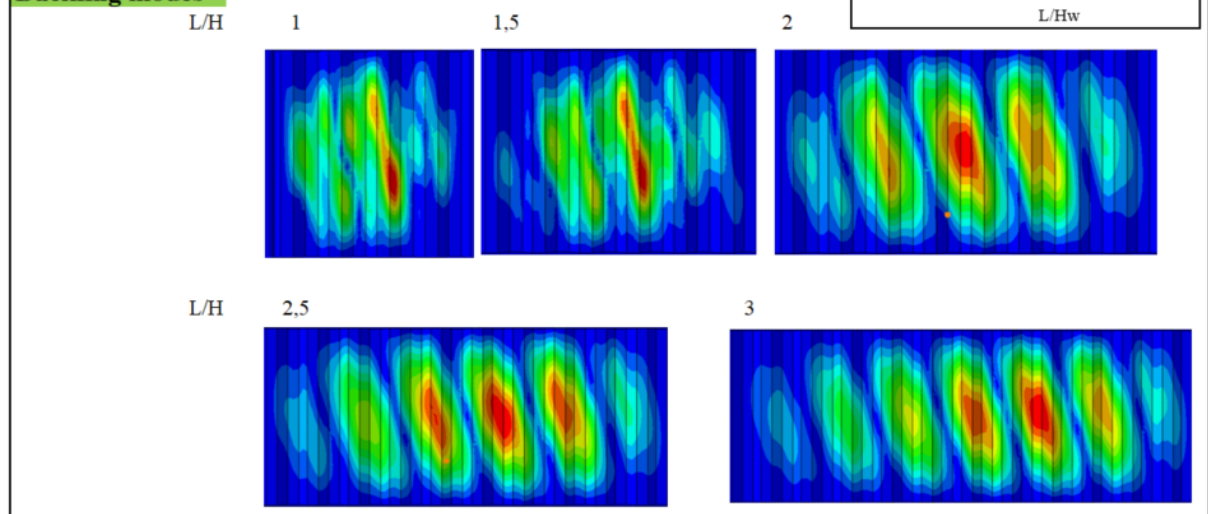


FE-results regarding influence of L-H-ratio on ultimate shear capacity.

		Hw= 1500 mm tw=4mm alpha=32 Corrugation length= 369,6 mm				
		5	7	9	11	13
	L/H	1	1,5	2	2,5	3
	L [mm]	1500	2250	3000	3750	4500
Initial Imp.=Hw/200	Shear cap.	1804	1803	1803	1798	1775
Initial Imp.=Tw		1883	1875	1868	1863	1840
	Buckling mode	Global	Global	Global	Global	Global
	Eigenvalue	656	640	629	620	612
	Real length	1478	2218	2957	3696	4435
	Real ratio	0,99	1,48	1,97	2,46	2,96

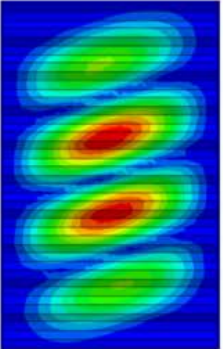
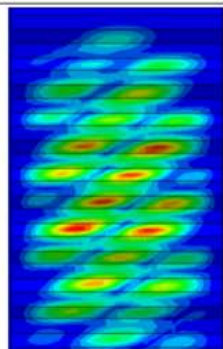
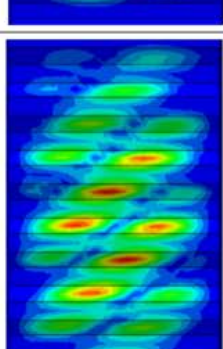
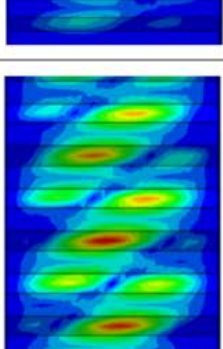
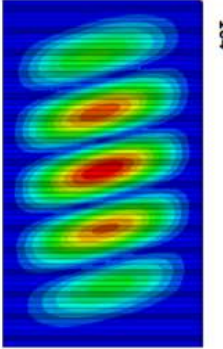
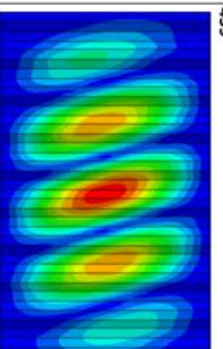
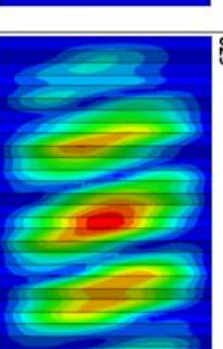
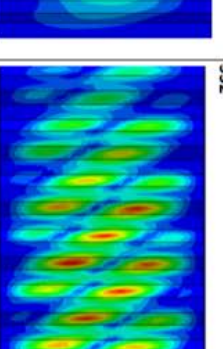
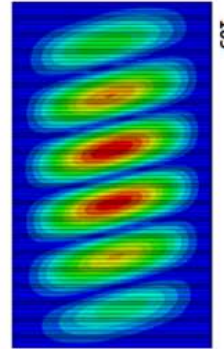
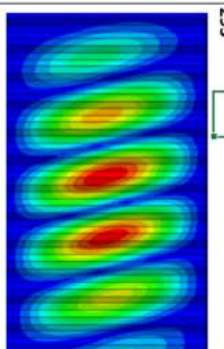
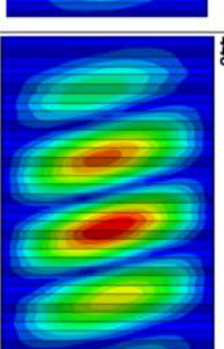
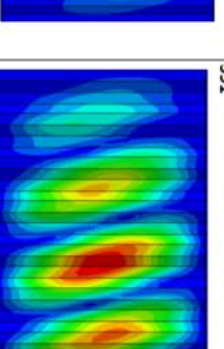
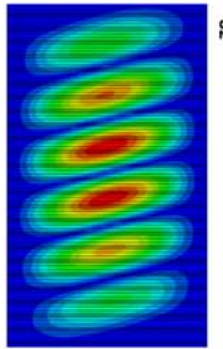
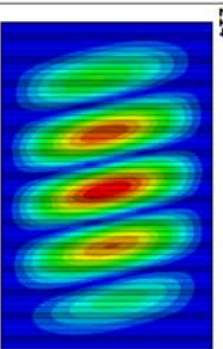
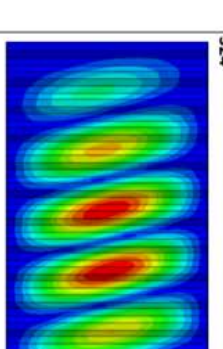


Buckling modes



Appendix E – Shear buckling modes for different a_1

Shear buckling modes and eigenvalues for different a_1 and geometries.

<p>a_1 [mm] Eigenvalue</p> <p>Hw=1000mm tw=4mm alpha=32</p> <p>FEM 1.4162 ABAQUS 6.13</p>	<p>50 296</p> 	<p>80 610</p> 	<p>100 504</p> 	<p>120 445</p> 
<p>a_1 [mm] Eigenvalue</p> <p>Hw=1500mm tw=4mm alpha=32</p> <p>FEM 1.4162 ABAQUS 6.13</p>	<p>50 164</p> 	<p>80 439</p> 	<p>100 629</p> 	<p>120 532</p> 
<p>a_1 [mm] Eigenvalue</p> <p>Hw=2000mm tw=4mm alpha=32</p> <p>FEM 1.4162 ABAQUS 6.13</p>	<p>50 109</p> 	<p>80 293</p> 	<p>100 446</p> 	<p>120 591</p> 
<p>a_1 [mm] Eigenvalue</p> <p>Hw=2500mm tw=4mm alpha=32</p> <p>FEM 1.4162 ABAQUS 6.13</p>	<p>50 82</p> 	<p>80 214</p> 	<p>100 324</p> 	<p>120 447</p> 